SPRINGER BRIEFS IN
APPLIED SCIENCES AND TECHNOLOGY

Jaeyoun (Jay) Kim

Microscale Soft Robotics

Motivations, Progress, and Outlook

Springer

SpringerBriefs in Applied Sciences and Technology

More information about this series at http://www.springer.com/series/8884

Jaeyoun (Jay) Kim

Microscale Soft Robotics

Motivations, Progress, and Outlook

Springer

Jaeyoun (Jay) Kim
Electrical and Computer Engineering
Iowa State University
Ames, IA, USA

ISSN 2191-530X ISSN 2191-5318 (electronic)
SpringerBriefs in Applied Sciences and Technology
ISBN 978-3-319-50285-4 ISBN 978-3-319-50286-1 (eBook)
DOI 10.1007/978-3-319-50286-1

Library of Congress Control Number: 2016959765

Printed on acid-free paper

This Springer imprint is published by Springer Nature
The registered company is Springer International Publishing AG
The registered company address is: Gewerbestrasse 11, 6330 Cham, Switzerland

This book is dedicated to my mother
for her ceaseless encouragement.

Preface

No one tears a piece of cloth from a new garment and uses it to patch an old garment. For then the new garment would be ruined, and the new patch wouldn't even match the old garment.

Luke 5:36

This book was originally intended to be a very brief survey of the history and progress of *microscale soft robotics*, a rapidly evolving subfield of robotics. To the author's dismay, the task of tracking the subfield's technological origin and enabling factors has rapidly become an overwhelming one due primarily to the subfield's *new-wine-in-new-wineskin* nature quoted above. In short, even at the moderate, centimetric to millimetric length scales, the realization and operation of soft robots turned out to require *out-of-the-box* ideas that are far from simple downscaling of their macroscale counterparts. As emphasized in the main text, the subfield owes tremendously to the explorers of the biological world and visionary researchers unafraid of transplanting one type of technology to another.

The author gratefully acknowledges the National Science Foundation for supporting his research projects through its grants CMMI-1265844 and CBET-1605275. The knowledge and experience accumulated along the work have been the main impetus in the conception and writing of this book.

Ames, IA, USA
October 2016

Jaeyoun (Jay) Kim

Contents

Acronyms

2D	Two dimensional
3D	Three dimensional
IR	Infra-red
MEMS	Micro-electromechanical system
RoC	Radius of curvature
S^3	Small, soft, and safe
SRMT	Soft robotic micro-tentacle
UV	Ultraviolet

Chapter 1
Introduction

Why delve into microscale soft robotics? Why now, of all times? An engineer's direct answer would be: Because *now* we can. The need for microscale soft robots and their potential benefits have long been in recognition since the dawn of robotics. In fact, we never stopped making demands for small machines capable of operating in a highly inaccessible, tightly constrained environment, be it an inner organ of the human body undergoing a medical intervention or the gap under the door to a room in a hostage situation. In the former, safety comes first. The robot's body must be soft enough to avoid causing damages to the surrounding tissues. In the latter, the softness can enable the robot to *squeeze* its way through narrower door gaps. Clearly, there exists ample reasons for robots to be small and soft.

The *microscale* portion of the requirement has become gradually satisfied since the 1980s with the advent of micro-electro-mechanical systems (MEMS). Basing themselves on the silicon-based integrated circuit fabrication technologies, however, the conventional MEMS devices and micro-robots were inherently rigid.

The *soft* portion of the requirement had to wait longer for its full satisfaction until the proliferation of soft material-based bio-MEMS provided the corresponding technical solutions during the first decade of the new millennium.

In addition to the advent of the soft bio-MEMS, there have also been some unexpected contributions from *nature*. It is well known that the researchers of microscale soft robotics did not start from scratch even in its early days. Nature is replete with highly optimized model systems for small and soft robots. In fact, they have been up for grabs for thousands of years, waiting for the emergence of biomimetics and bio-inspired engineering to enable their systematic investigation and replication. Its materialization has led to a greatly accelerated progress in microscale soft robotics, starting from the first decade of the millennium.

With the demand, motivation, and the technological building blocks all at the same place at the same time, the researchers in the new field may have expected things no less than an explosion. The detonation, however, seems to have suffered multiple delays due primarily to the highly inter-disciplinary nature of the field.

J. (Jay) Kim, *Microscale Soft Robotics*, SpringerBriefs in Applied Sciences and Technology, DOI 10.1007/978-3-319-50286-1_1

Note that the constituent technologies such as MEMS, soft bio-MEMS, and bio-inspired engineering have been traditionally studied by research groups with little or no overlap in their research interests. Moreover, as noted above, the applications of the completed microscale soft robots often lie in the realm of clinical medicine or security/surveillance/defense which, again, exhibit scant overlap with the developers of the building-block technologies. It took time for the researchers, funding agencies, and entrepreneurs to become aware of each other and recognize the need for cooperation.

In that sense, the venturous, almost speculative, atmosphere of the past decade, which has fostered the inter-disciplinary cross-overs between various fields of studies, encouraging the exploration of highly unconventional concepts and ideas, is truly an unexpected blessing.

It is rather ironic that such a grand convergence was stimulated in part by the downturns in the hi-tech industry in the early 2000s, such as the infamous Telecom Bubble Burst in 2002, which had shuffled the researchers in many fields across the technological borders whether they liked it or not. Surely, the cascade of such seemingly disastrous events would later be remembered as an example of the rare *blessing in disguise* by the historians of technology in the future. Currently, the field is rolling along the path to becoming a mainstream technology, as indicated by the explosive increase in the number of publications in Fig. 1.1.

With microscale soft robotics stably on the road to maturity and their applications thriving in many fields, the demand to survey and catalogue the motivations, enabling technological factors, and achievements has arisen naturally. In accordance, I decided to write this book with its content divided into five chapters, each covering the technological motivations, constituent enabling technologies, an exemplary case study, current progress, and outlooks of microscale soft robots.

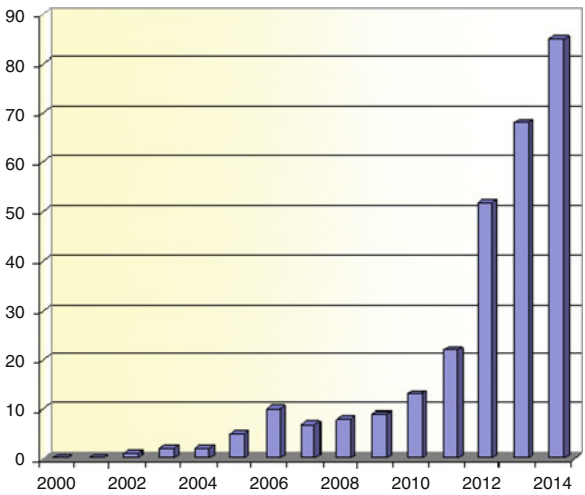

Fig. 1.1 The increase in the number of publications on *soft robots* in recent years

The biggest lessons I have learned while writing this book are twofold. First of all, we still have a lot to learn from our mother nature. Secondly, as quoted in the Preface of this book, many macro-scale structures and functionalities are to be re-designed from the ground up to fit the microscale world. These two aspects will provide a consistent set of viewpoints throughout the book.

Ultimately, this book aims to predict and suggest future research directions for the field of microscale soft robotics. I sincerely believe that its highly inter-disciplinary nature will eventually push the field into a technological platform promoting scientific convergence in near future.

Chapter 2
Motivations

Microscale robots have been around for decades. Soft robots are relatively new to robotics but they have also been on the road to secure their position in the field for at least a decade [1]. So, the fusion of the two in recent years, which gave birth to microscale soft robotics, may seem logical and even inevitable [2]. In the world of technology, however, a mere co-existence of two related fields doesn't necessarily guarantee their marriage. There must be compelling reasons, or motivations, for the researchers to invest their time and effort.

In the case of microscale soft robotics, it is straightforward to see the motivations: the longstanding thrusts to develop robots for clinical interventions and biomedical studies [3]. Over the concerns of safety, those applications impose strict restrictions on both the size and mechanical properties of the devices to be used—The robots must be small and soft, hence engendering the new field of S^3 (*small*, *soft*, and *safe*) robotics [4]. Soon, it became noted that such S^3 robots can bring additional benefits such as polymorphism, re-configurability, and multi-functionality, which immediately constituted another motivation set. This chapter focuses on describing such motivations in a more quantitative detail.

2.1 Small

Conventional robots have been measured in centimeters and meters. Their miniaturization down to millimetric- or sub-millimetric scales, or even towards microscale, has been intensely sought after in robotics for the prospect of hugely widened application scope. Figure 2.1 succinctly illustrates the technological status of "gentle grabbing" of soft objects in robotics. For objects with their dimensions ranging from 1 to 10 μm, such as individual cells, a large variety of devices have been developed and utilized, with the pneumatic micropipette aspirator as the representative example. On the other hand, for objects measured in centimeters and

J. (Jay) Kim, *Microscale Soft Robotics*, SpringerBriefs in Applied Sciences and Technology, DOI 10.1007/978-3-319-50286-1_2

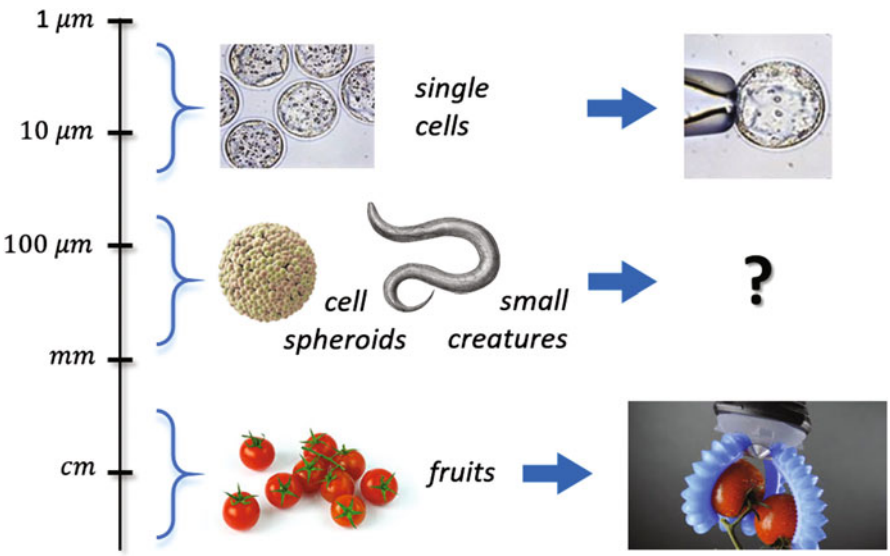

Fig. 2.1 Technological status quo of *gentle* grabbing of soft objects

above, we have started to witness the emergence of various commercial large-scale soft robots. A practical example is the Soft Robotic Gripper from *Soft Robotics Inc.* in Cambridge, Massachusetts, USA, which boasts the capability to handle subtle items such as fruits safely and adaptively as shown in Fig. 2.1. There is, however, a gap in the middle which corresponds to the size range spanning tens of microns to a couple of millimeters. This gap can immediately be recognized as the future battleground for microscale soft robotics.

Traditional examples of other small and delicate objects to be handled gently include small animals, such as the nematode or zebrafish, fish eggs and animal egg cells, and pollens. One important addition to the list in recent years is the cell spheroid. It has stemmed from the realization that neither the conventional, two-dimensionally cultured cells nor the microfluidically isolated single cells can adequately mimic the biological characteristics of the real cells constituting tissues and organs, deterring the intended processes of physiological studies and drug screening. The inadequacy arises from the obvious fact that the cells in truly biological settings are three-dimensionally assembled and networked [5]. In response, many three-dimensional cell culture techniques have been developed over the last decade [6, 7], leading to successful realizations of spheroidal aggregates of cells or cell spheroids. Soon, their efficient and safe handling has emerged as an important issue. The cell spheroids typically measure $<100\,\mu\text{m}$ in diameter and are very fragile and sensitive against externally applied stress and deformation. In fact, their dimensions and delicacy render themselves a perfect target for soft robotic manipulation. Seminal results have already been reported [8, 9] with ample potential for future improvements.

One more important source of impetus for microscale soft robotics is their anticipated roles in future minimally invasive medicine in which the diagnostic and operational procedures must occur in remote, hard-to-reach, and highly constrained locations of human body in a non- or minimally invasive fashion. In those cases, the robotic operator must be delivered to the site through catheters or hollow needles and work on highly fragile and subtle objects, such as thin blood vessels or nerve cell for anastomoses or small pieces of tissues for transplanting operations. There the main limiting factor will be the diameter of the catheter and the needle which is typically below a couple of millimeters. All of these have converged into a strong motivation for the realization of *microscale* soft robots.

2.2 Soft

To robots and devices for medical intervention inside the human body, safety always comes as the top priority. For such devices, damaging the tissues around the point of operation is considered a far more serious issue than failing the mission itself. Adoption of soft materials with their compliance levels matched to those of the surrounding biological tissues as the building material of the devices can eliminate the possibility of such problems from the ground up by practically depriving the devices of the capability to damage their biological environment.

For comparing the compliance of materials, one frequently adopts the elasticity, or Young's modulus, E defined as the ratio between the force per unit cross-sectional area and the fractional length increment

$$E = \frac{F/A}{\Delta/L} \tag{2.1}$$

where F, A, L, and Δ represent the axial loading force, initial area, initial length, and the elongation, respectively. As Majidi has pointed out [10], it is apparent from the mathematical form of the formula that the quantity E is only relevant to a prismatic homogeneous object undergoing an axial deformation which is small with respect to its initial length. Nevertheless, the order-of-magnitude comparisons of E values can provide good insights on the issue of operational tissue safety and the scope of adoptable materials since the contact interface between two materials with greatly different levels of E tends to undergo an uneven distribution of force and concentration of stress, causing damages to the softer side which, typically, is the biological tissues.

Table 2.1 summarizes the measured Young's moduli of a few well-known soft materials and biological environments. It indicates that some common elastomers, such as PDMS, exhibit a Young's modulus very close to that of the biological tissues, rendering themselves compliance-matched to biological environments. It becomes especially true for recently introduced elastomers that are

Table 2.1 Experimentally measured E of various materials

Material	E [MPa]	Notes
PMMA	∼2800	From [11]
Polyurethane	10–1000	www.polyurethanes.basf.de
PDMS, hardened	2.3–2.5	Thermally hardened Sylgard 184 from [12]
PDMS, typical	0.7–1.2	Sylgard 184 [13]
Solaris™	0.17	From [14]
Ecoflex™	0.06	From [14]
Human skin	0.42–0.85	Age-dependent [15]
Organ tissues	∼0.001	Liver and muscle tissues [16]

compliance-matched to biological tissues within only an order of magnitude. Good examples include Ecoflex™($E \sim 60\,\text{kPa}$) and Solaris™($E \sim 170\,\text{kPa}$) from *Smooth-On Inc.* [14].

Along the progress of the microscale soft robots, researchers have come to the realization that the two motivations mentioned above, i.e., the compactness and compliance, can be combined to produce another point of motivation, i.e., the deformability. In fact, the deformability must be deemed a motivation genuinely unique to *microscale* soft robots, not shared by microscale rigid robots or large-scale soft robots. The latter can be made deformable to a certain extent but it requires huge aspect-ratios in their structures and/or high-power actuation. At microscale, on the other hand, both requirements can be bypassed rather easily, as evidenced by the variety in the available shapes and motions in S^3 robots. More specifically for microscale soft robots, the deformability manifests itself as polymorphic adaptability, dynamic re-configurability, and continuum motion.

Polymorphic Adaptability Soft robots and actuators can transform their morphologies to fit themselves to the environment. In fact, such an ability can be found ubiquitously in the biological world. Figure 2.2a shows one example in which the octopus exhibits its exceptional ability to squeeze itself into a highly constrained space for migration and habitation. A notable example of the capability's artificial replication is shown in Fig. 2.2b. The multigait soft robot developed by Harvard researchers in 2011 succeeded in passing through a gap narrower than its original bodily dimensions by pneumatically squeezing its body to fit the narrow opening. Another example is the retinal pigment epithelium sheet transplanter demonstrated by Konishi and co-workers [18]. The otherwise flat and wide micromanipulator can be pneumatically rolled into the form of a thinner cylinder so that it can be inserted through a narrow, hollow needle.

Dynamic Re-configurability With judicious choice of the shape, dimensions, and material composition, the polymorphic adaptability can be pushed to the extreme, to the point of giving not just a new shape but also a new functionality to the robots and actuators. Such a dynamic re-configurability has been highly sought after in soft robots as a prerequisite for realizing on-demand multi-functionality. Regarding this aspect, the soft micromanipulator shown in [18] can be another example since the

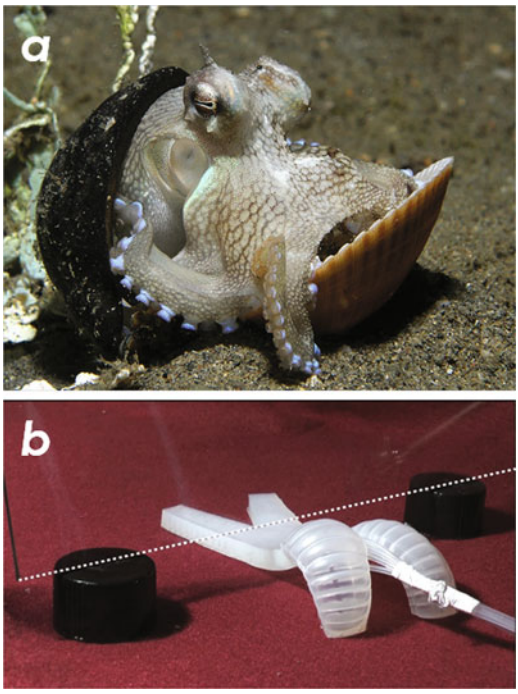

Fig. 2.2 (**a**) An octopus can squeeze itself into a shell much smaller than its body for habitation and migration (Image from *Wikimedia Commons*). (**b**) The *Multigait Soft Robot* from Harvard University [17] can squeeze itself through the narrow gap underneath a glass panel (Photograph courtesy of George Whitesides Laboratory)

cylindrical rolling motion, an extreme case of utilizing the deformability, also allows it to function as a gentle grabber (and also a releaser) of delicate planar structures, such as tissue sheets.

Continuum Motion Beyond the three aspects described above, the adoption of highly deformable and stretchable materials for building robots and actuators can also greatly simplify their design and implementation. It is straightforward to see that most rigid robots and actuators are articulated, with a finite number of bending/twisting joints providing the motion capability. Internally, the joints consist of hinges, fixtures, and friction-mitigation mechanisms meticulously assembled and fitted for proper operation. Such a level of sophistication gets increasingly difficult to achieve or justify as the overall dimensions decrease. Deformable material-based actuation can ease the complication by enabling joint-less, continuum-based motions, as will be described in the following chapters.

2.3 Safe

The compliance of the material also limits the maximum level of force to be exerted by the actuator made of it. According to Shimomura et al. [9], typical biological tissues in the form of multi-cell aggregates can withstand up to 1 mN of force.

For microscale actuators made of highly compliant materials like PDMS, such a force level is hard to achieve since the actuator body itself becomes deformed and recedes before it could exert force exceeding the critical level. For example, the author's own work of microscale PDMS tentacle actuator [19] turned out to apply only sub-mN level force. It became maxed at 0.78 mN under 10 psi pneumatic pressure, which is only one order of magnitude higher than the muscle force of a *C. elegans*, a common nematode [20]. In fact, many of the soft actuators are excessively compliant to the point of frustration for some practical applications, such as intra-vascular navigation, prompting researches to develop switchable schemes for stiffening the actuators.

In recent years, human friendliness has arisen as an extra point of motivation in the field of robotics. It came from the need to make the robots maximally suitable for interaction with humans, especially those who are under/over-aged, handicapped, or undergoing clinical cares. In those situations, the rigid, inorganic look-and-feel of the conventional robots can estrange the potential users, leading to a reduction in their use and effectiveness. In fact, the entertainment community reacted most quickly. For instance, *Pixar Studio* has premiered a highly futuristic, totally soft-bodied robot *Baymax* in 2014.

Chapter 3
Enabling Technologies

The motivations described in the previous chapter have been recognized by researchers in the field of robotics since its early days. Their realization, however, had to wait for a number of key concepts and technological enabling factors to become available. It is interesting to point out that many of these *enabling factors* have been listed as the targets for *future research* in soft robotics in the visionary review paper by Trivedi et al. in as early as 2008 [21]. In fact, the laborious thrusts to overcome the challenges can be viewed as the process of making the enabling technologies available. This chapter reviews five essential ones among them in detail.

3.1 Elastomers

3.1.1 PDMS

Regardless of their dimensions, *soft* robots require soft and flexible materials capable of withstanding high-level deformation for their realization. Various elastomers turned out to fit the description. The invention of synthetic rubber in the early nineteenth century marked the first introduction of artificial elastomers. Their utilization for robotics, especially those related to microscale soft robotics, however, had to await the widespread popularization of elastomers that are compatible with both laboratory-scale rapid prototyping *and* industrial manufacturing. In that sense, the emergence of *poly(dimethylsiloxane)* (PDMS) can be deemed the true starting point of microscale soft robotics from the material point of view [22].

J. (Jay) Kim, *Microscale Soft Robotics*, SpringerBriefs in Applied Sciences and Technology, DOI 10.1007/978-3-319-50286-1_3

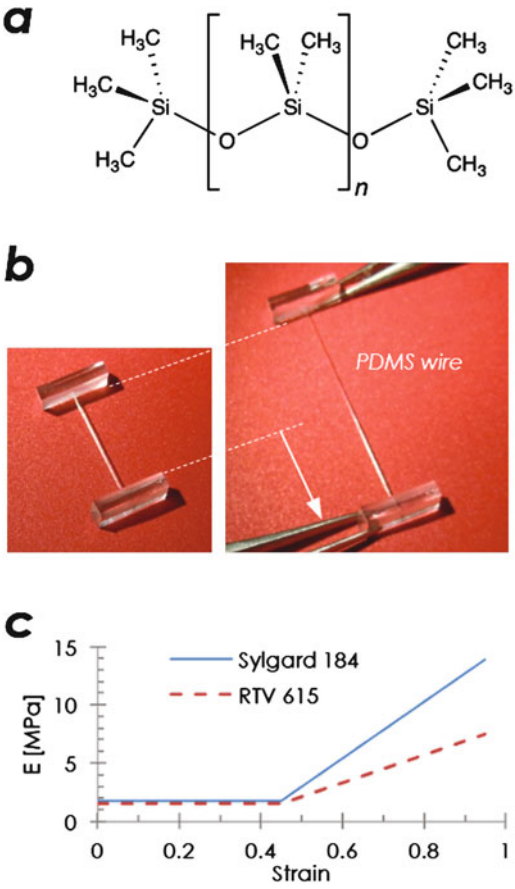

Fig. 3.1 (**a**) The basic chemical structure of PDMS (Image from *Wikimedia Commons*). (**b**) A PDMS microwire exhibits its resilence against stretching by withstanding a 400% elongation repeatedly (Image from the author). (**c**) Young's moduli of representative elastomers as a function of strain

3.1.2 Beneficial Properties

Figure 3.1a shows the basic chemical structure of PDMS. Prior to cross-linking, it exists primarily in liquid form. Application of its cross-linking agent, along with heating, solidifies it in a straightforward fashion. Thanks to this property, PDMS was originally harnessed as a sealing and caulking material with on-site curing advantage in 1960s. Gradual identification of its beneficial properties, however, has rapidly expanded its application scope towards the realms of consumer products and biomedical engineering. This subsection surveys its properties and applications with a special emphasis on how it has acquired its unique position in modern soft robotics.

Mechanical Properties The mechanical properties of PDMS are highly favorable for building soft robots. PDMS exhibits high-level elasticity and deformability which have been observed to persist all the way down to micro- and nano-scale

structure size range. For example, as shown in Fig. 3.1b, one experiment had showed that a 150 µm-thick PDMS microwire can withstand 400% elongation repeatedly without suffering from residual deformation [23].

With its Young's modulus ranging typically from 0.7 to 1.2 MPa, as described in Table 2.1, the material can also give tactile sensations that are very safe and familiar to those attainable from the human body. As described in Sect. 2.2, some variants of PDMS exhibit Young's moduli as low as 125 kPa, almost matching those of biological tissues on an order-of-magnitude basis.

On top of that, typical PDMS materials (e.g., Sylgard 184™and RTV 615™) exhibit Young's modulus nearly constant over a remarkably wide range, up to 45% as shown in Fig. 3.1c, facilitating not only the design and analysis but also guaranteeing stably repeatable operations [24].

Chemical and Surface Properties PDMS is also chemically inert to most materials to the point of becoming bio-compatible and even bio-implantable. In its intrinsic form, the PDMS surface is highly hydrophobic with its typical contact angle in the range of 100∼110°. The surface repels most organic and inorganic materials and exhibits little solubility to various solvents. Prolonged contact with solvent, however, has been reported to cause swelling in the PDMS structures [25].

Optical Properties Optically, PDMS remains transparent over a wide portion of the visible and near-infrared spectral regimes [26]. Molded PDMS surfaces also exhibit nanoscale roughness, ensuring minimal scattering of light. Therefore, most optical loss arises from light scattering within the PDMS bulk. A recent measurement based on PDMS microwires showed < 3 dB/cm loss [27], which may not be extremely low but adequate for many microscale applications. With so many fabrication techniques and functional building blocks already available for PDMS-based microfluidics, the introduction of optical functionalities has immediately engendered the exciting new field of *optofluidics* in which optical functions assist microfluidics by providing a wealth of optical diagnostic schemes [28]. The low auto-fluorescence level of PDMS further enhances its usefulness in that respect [29].

Rapid Prototyping Despite the beneficial properties enumerated above, PDMS could not have achieved such a uniquely dominant position in the field of soft MEMS, had it not been for the rapid, versatile schemes for its shaping, collectively referred to as *soft-lithography*.

Figure 3.2 illustrates the most typical process: *replica-molding*. As mentioned above, PDMS originally exists in liquid-phase (LP) with its viscosity in the range of 3500 cP, which is close to that of the maple syrup. Its solidification can be initiated through the addition of the cross-link agent. Since the mixture solidifies very slowly, sometimes taking several hours, it can easily fill molds with complex shapes. Once settled completely, the solidification can be accelerated through the application of heat. De-molding of the cured PDMS from the mold is straightforward thanks to its chemical inertness. The fidelity of the molding process is usually at nanoscale, guaranteeing optics-quality surfaces to the PDMS replicas.

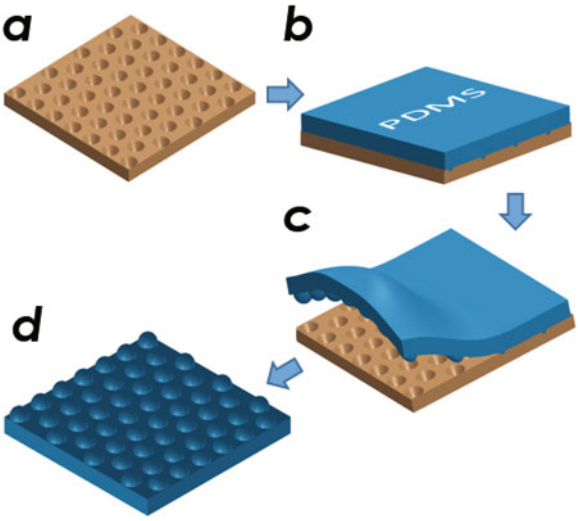

Fig. 3.2 A schematic illustration of the PDMS replica molding process: (**a**) Preparation of a rigid master pattern, (**b**) Pouring of liquid-phase PDMS and settling, (**c**) Peeling-off of the PDMS replica upon curing, (**d**) PDMS replication completed

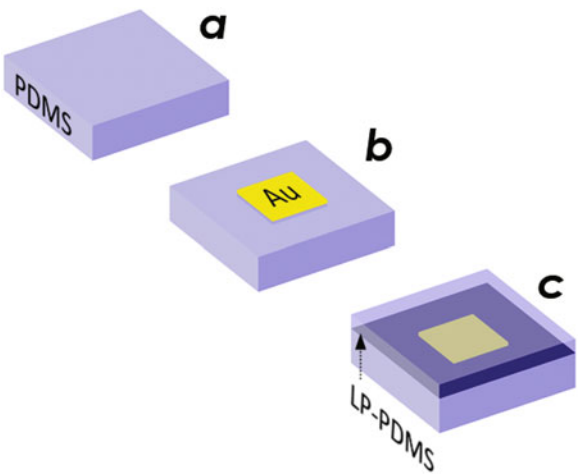

Fig. 3.3 A schematic illustration of the additive PDMS shaping process: (**a**) Preparation of the base PDMS block, (**b**) Installation of objects to be embedded, (**c**) Pouring of liquid-phase PDMS and curing

With a round of plasma treatment, the PDMS surface can be modified to enable irreversible, adhesive-free bonding with glass or silicon surfaces and formation of water-tight channels and chambers. This property is often likened to the silicon's ability to provide natural oxide layers and is deemed a truly significant enabling factor for PDMS in various MEMS and microfluidic applications.

Another interesting and useful property of PDMS is its compatibility with *additive* shaping. Figure 3.3 shows the concept schematically. Basically, it allows the incremental building of complex PDMS structures through layer-by-layer additions of PDMS. It exploits the property that an LP-PDMS poured or spin-coated over an already cured PDMS surface bonds monolithically with the latter, as long as the top surface of the existing PDMS layer is free of impurities and humidity. It is an especially useful property for embedding objects inside bulk PDMS [30].

3.1.3 Shortcomings

The properties of PDMS, however, are not always beneficial to soft MEMS or soft robotics. There certainly are a number of shortcomings which fundamentally limit the utility of PDMS in those technological areas.

Gas Permeability The most notable one is its gas permeability. It is well known that PDMS structures are permeable to molecules of gas such as oxygen and carbon dioxide [31]. Water vapor has also been observed to pass through PDMS structures, causing water loss along microfluidic channels [32, 33].

This gas permeability should not be considered entirely adverse since a number of applications do take advantage of it. The most common use can be found in conjunction with photocurable polymers which require not only the UV light but also inhibition of oxygen for their solidification. To those, the PDMS surface practically acts as an inhibition layer to photocuring. One exemplary use can be found in the fabrication process for the *microfluidic sticker* in which the PDMS surface functions as a non-stick mounting layer for UV-curable polymers [34]. Another example of its use is the stop-flow lithography [35, 36] in which microstructures are continuously fabricated through UV-exposure of liquid-phase photocurable polymer flowing through a PDMS microfluidic channel. There, the UV-solidified photopolymer structures can flow through the channel without sticking to the channel walls thanks to the existence of lubrication layers consisting of the uncured, liquid phase photopolymer near the oxygen-rich PDMS surfaces [37].

The gas permeability of PDMS, however, becomes more detrimental than beneficial beyond those applications. In robots and devices relying on pneumatic or hydraulic actuation, it becomes a major source of gas leak and pressure drop. The situation becomes even more serious as the PDMS structure becomes thinner and the pressure becomes higher. For non-actuation applications, the porosity of PDMS frustrates researchers by causing uptakes of small molecules, such as fluorescent dyes or biomolecules under test, that are critical for biomedical applications [38]. To mitigate the shortcomings, researchers have tried to coat the PDMS surface with less- or non-permeable materials [38, 39]. For deformation-intensive actuator and robot applications, however, the coating material must exhibit elasticity comparable to that of PDMS. The whole consideration, in fact, leads to the adoption of a totally new elastic material for realizing microscale soft robots and actuators. Details will be discussed in the following subsection.

Incompatibility with Subtractive Shaping Another serious technological issue of PDMS is its incompatibility with most subtractive patterning techniques. Due to the material's chemical inertness, it is almost impossible to etch PDMS. Addressing this issue may not be impossible but would require significant modification of the chemical properties of PDMS. Further details will be discussed in later chapters.

3.1.4 Parylene

Poly(p-xylylene), or parylene, is another elastomer also adopted frequently as the structural and/or functional material for building microscale soft devices. Collectively, parylene refers to a group of semi-crystalline, thermoplastic polymers introduced by *Specialty Coating Systems* and commercialized by *Union Carbide Corporation* in 1965 [40]. Thanks to its compatibility with high-yield, room-temperature chemical vapor deposition (CVD) process and the consequential capability to form chemically inert, solvent-resistant thin films in a conformal, pinhole-free fashion, it has seen its initial success as a coating material for electronics and biomedical devices.

The Gorham process for parylene deposition is based on the thermal vaporization and pyrolysis of granular dimer precursor, di-*p*-xylylene (or [2.2] paracyclophane) at a temperature exceeding 550 °C, which eventually cleaves the dimer into reactive radical monomers. Inside a separate deposition chamber which is held at room-temperature, the reactive monomer adsorbs to all exposed surfaces and then polymerizes to realize conformal coating. This room-temperature process greatly facilitates the use of parylene along with thermally sensitive materials [42].

A number of different methods have been developed to pattern and shape the CVD-deposited parylene layer. Due to the material's high-level inertness to solvents, those methods rely primarily on dry, physical processes [43] such as oxygen-based plasma etching [43], reactive ion beam etching [44], and reactive ion etching [45].

3D micro-structures that are essential to fabrication of complex robots and devices have also been developed. Of special interest are facile realization of suspended or high aspect-ratio structures at microscale. Such structures have been implemented primarily through the deposition of parylene onto sacrificial or easily removable molds [46]. Examples of 3D structures realized in such a way include the hemispherical bump electrodes [47] and the 3D micro-electrode arrays [48].

The material's bio-compatibility (FDA-approved, USP class VI grade), excellent transparency across the visible spectrum, high dielectric strength, and mechanical flexibility (Young's modulus at $\sim$4 GPa) further enhance its value for applications in microfluidics, bio-MEMS, and micro-robotics [49].

3.1.5 Parylene C

As mentioned above, parylene is a collective term with more than 10 variations available under the name commercially. Among them, parylene C is most widely adopted for building MEMS devices. In addition to the parylene's common advantages enumerated above, parylene C also exhibits very low intrinsic stress. Thanks to the smoothness of the surface, the film also suffers from little optical scattering, providing high transmittance in the visible regime [50].

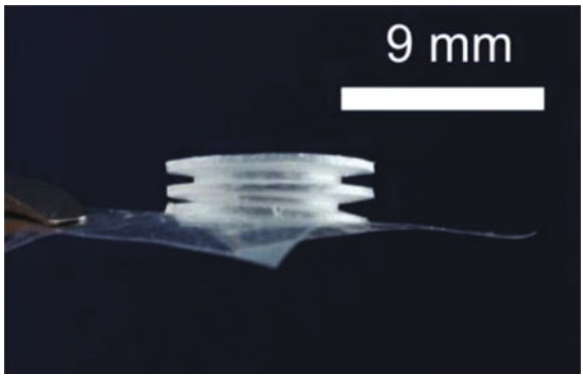

Fig. 3.4 An optical micrograph of parylene C micropump for implanted drug delivery in small animals. Reprinted with permission from [41]. Copyright 2012 Springer

Additional advantages of parylene C include its proven bio-compatibility, both in vitro [51] and in vivo [52], low cytotoxicity, and resistance against hydrolytic degradation [53, 54] that are of special importance to its use for implantable and biomedical MEMS devices.

One prominent example is the parylene-based *bellows*, shown in Fig. 3.4, devised to produce a greatly amplified diaphragm deflections from low-power electrolysis for drug delivery [41, 55]. It is interesting that parylene C has been utilized jointly with PDMS for expanded functionality [56]. There, parylene-metal-parylene electrodes were anchored to a PDMS substrate for strain sensing under severe stretching. Its implementation was based on the use of suspension enabled by sacrificial layer etching mentioned above.

3.1.6 Shortcomings

The material, however, is far from perfect or ideal. Its material properties are highly dependent on the changes in deposition conditions [42]. In particular, faster deposition turned out to increase its surface roughness [57]. Its mechanical characteristics have also been observed to be affected by photo-induced oxidation as well [58].

Parylene C exhibits a particularly low glass transition temperature (60∼90 °C) [59], suffering thermal oxidative degradation and loss of material in oxygen-rich environments with the temperature exceeding 125 °C, necessitating the use of vacuum environment for its thermal annealing.

Above all, the water and vapor permeability, one of the main reasons for choosing parylene over other softer materials, turned out to be not entirely zero [60]. The same limitation applies also to permeability to ion and solvent [61] as well.

3.2 Unconventional Soft Lithography

The beneficial properties of PDMS, especially its compatibility with rapid, on-demand prototyping, have successfully led to an intense popularization of microfluidics during the first decade of the millennium, as evidenced by the explosive increase in the number of publications in Fig. 3.5.

While there have been incessant introductions of new microfluidic devices along the time, the fabrication techniques themselves have been largely unchanged from their original forms in the sense that they still rely primarily on replica molding of patterns on rigid, flat surfaces and their plasma-assisted bonding to another rigid flat substrate, as described in Sect. 3.1.1. Inevitably, those conventional techniques are well suited for making 2D networks of micro-channels on flat, rigid substrates but are not very suitable for realizing actuators and robots that are inherently three-dimensional. For the implementation of S^3 robots in particular, our wish-list for fabrication techniques includes, but is not limited to:

- Three-dimensional, non-planar structures
- High aspect-ratio, vertical structures
- High aspect-ratio, hollow structures
- Thin membranes and tubes
- Completely sealed hollow chambers

Unconventional fabrication techniques for such exotic geometries have begun to emerge only recently thanks to a number of technological motivations and enabling factors. They are itemized and described below. Note that their significantly interlinked nature makes it difficult to describe them as standalone topics. So, the readers are suggested to focus on the connections between the items.

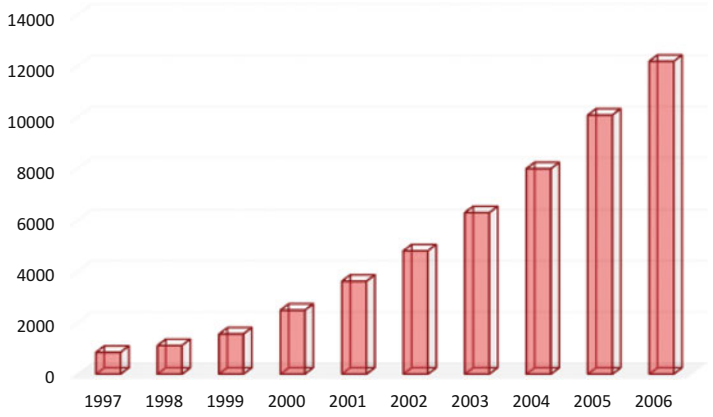

Fig. 3.5 The number of publications on *microfluidics* around the turn of the millennium

Table 3.1 New trends in Bio-MEMS in comparison with the conventional ones

Conventional	New
Static	Dynamic
	Re-configurable
	Deformable
Planar	Three-dimensional
	High aspect-ratio
	Standalone
Artificially organized	Physiologically relevant
	Physiologically realistic
	Organo-morphic

New Trends in Bio-MEMS Be it intended or not, some of the new trends in microfluidics and bio-MEMS have acted as the main impetus to the progress in unconventional fabrication techniques and, hence, in microscale soft robotics, rendering themselves worth mentioning ahead of the techniques. Recently, the fields of bio-MEMS and microfluidics have undergone an overall shift in their research emphasis. Table 3.1 summarizes the new trends by contrasting the features with those of conventional ones. One notable goal of the new research thrusts is the creation of artificial *on-chip organs* for drug discovery and physiological studies [62]. The goal obviates the need for the transitions listed in Table 3.1 and justifies the efforts.

The *lung-on-a-chip* shown in Fig. 3.6a is one representative example [63]. Basically, it is a cell-culture platform equipped with stretchable substrate so that it can emulate the physiological condition of the lung's airway which undergoes incessant stretching–unstretching cycles arising from respiration. As Fig. 3.6a indicates, its realization requires PDMS thin membranes, multi-layer assembly and bonding, and dynamic re-configurability (for the pneumatic actuation), all of which rely critically on unconventional fabrication approaches.

PDMS-Optimized Techniques In accordance, a number of PDMS-optimized, or even PDMS-specific, fabrication techniques have been devised and heavily exploited. The *additive shaping* (also known as *multi-step co-molding* [64]) described in Sect. 3.1.2 and illustrated in Fig. 3.3 is a notable example of the latter. The technique turned out to be useful not only for layer-by-layer fabrication and embedding of heterogeneous elements but also handy for producing tightly sealed structures such as tubes [19] or chambers [64]. A more detailed description of its utilization will be presented in the next chapter.

The chemical inertness and robustness of PDMS has also been exploited extensively, leading to the adoption of various unusual sacrificial materials for replica molding. One prominent example is the use of sucrose, i.e., table sugar, and its derivatives [65–67]. In many aspects, sucrose is ideal as the sacrificial material for PDMS replica molding, as shown schematically in Fig. 3.6b. It is non-toxic and bio-compatible to the point of being edible. Dissolving it requires only a warm water bath, eliminating the need for solvents which tend to get PDMS swollen irreversibly.

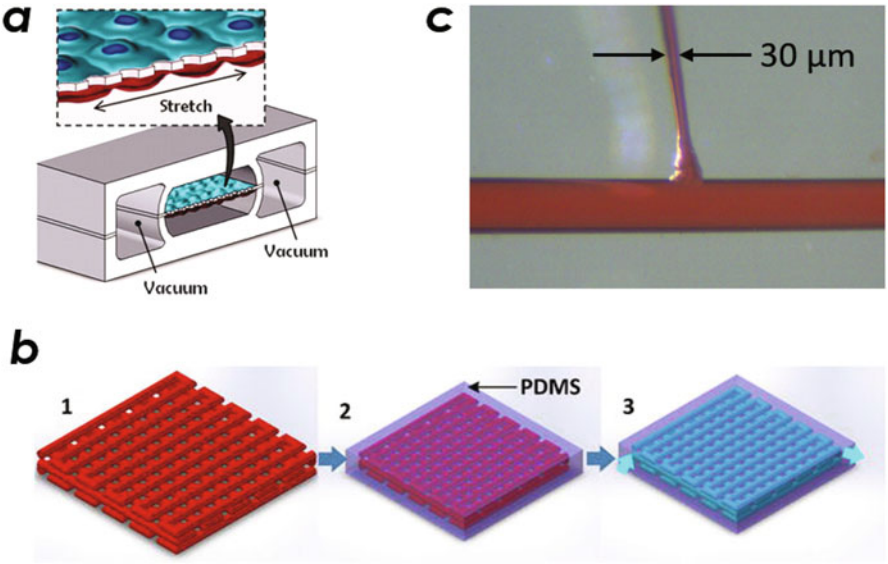

Fig. 3.6 (**a**) A schematic diagram of the *lung-on-a-chip* (Image from *Wikimedia Commons*). (**b**) Typical process for sucrose-molding of PDMS in which the sucrose mold (*red*) is first encapsulated in liquid-phase PDMS (*light blue*) and then dissolved with water to leave empty channels in solidified PDMS (*dark blue*). Reprinted with permission from [65]. Copyright 2015 Springer. (**c**) Optical micrograph of a sucrose-molded PDMS microfluidic channel network with a physiologically realistic, vaso-mimetic junction (Image from the author)

The globe box or chemical fume hood can also be dispensed with. Above all, sucrose can easily be shaped and assembled to form sacrificial molds with surface smooth at nanoscale [66]. Its compatibility with piece-by-piece assembly [66] or 3D-printing [65, 67] has especially facilitated the construction of complex 3D microfluidics. Figure 3.6c shows one such example in which two sucrose-molded microchannels are connected three-dimensionally with a gradual taper, mimicking the junctions in human vasculature [66]. In turn, those capabilities can provide the structural basis for microscale soft robots.

3D-Printing and 3D-Shaping The art of 3D-printing has been rapidly permeating into many facets of human society. The fields of MEMS and bio-MEMS are not exceptions. So far, there have been substantial efforts to build the master molds [65, 68] as shown in Fig. 3.7, or even the microscale devices themselves, through 3D-printing [69–71]. PDMS itself is not amenable to 3D-printing due to its slow curing and inherent softness but it can still be 3D-*shaped* through judicious material preparation and process control.

At this point, presenting a practical example exploiting both the unique properties of PDMS (from Sect. 3.1.1) and unconventional soft lithography (from Sect. 3.2) may further clarify the impact of new enabling technologies. One of the author's own works is chosen.

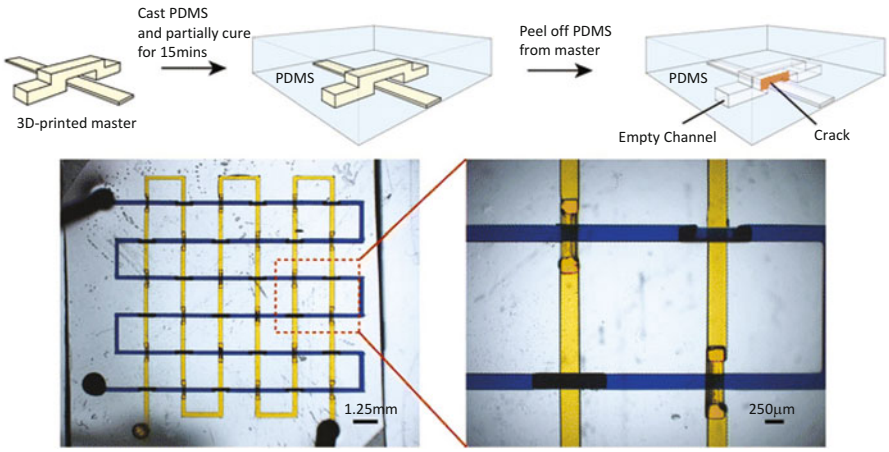

Fig. 3.7 A schematic diagram of 3D-printing-based microfluidic device fabrication. Reprinted with permission from [68]. Copyright 2015 Springer

Case Study 1: Elastomeric Micropillar

Microscale pillars, or micropillars, with very high aspect-ratio, i.e., with the ratio of its height to the diameter exceeding at least 50, have been highly sought after in MEMS for use in various applications. They can function as probes, actuators, and sensors. Especially for applications as the sensing element, compliance of the micropillar also becomes a matter of concern. In fact, high aspect-ratio micropillars made of soft materials must be ideal for detecting subtle mass-flows such as wind. PDMS could have been an ideal material for the purpose for its robustness and stability. However, reports on high aspect-ratio, upright micropillars made of PDMS have been scarce due to two major reasons.

First of all, the fabrication easily becomes greatly challenging to the point of impossibility. As described in Sect. 3.1.2, the conventional process of PDMS shaping depends on replica molding which inevitably necessitates *de*-molding for the release of the completed structure. While the de-molding step can be as simple as manual peeling in the case of planar microfluidics, it can become highly detrimental to 3D structures like micropillars. Another important issue is the inherent softness of PDMS with its Young's modulus E typically under 1 MPa. The resulting compliance makes the realization of upright structures difficult, often inducing irreversible collapses of such structures. Due mainly to these reasons, the height and aspect-ratios of the PDMS micropillars realized through replica-molding have been limited under 0.47 mm and 19 mm, respectively [72].

Recently a new fabrication scheme has been proposed based on a joint utilization of a unique material property of PDMS and a new, unconventional soft lithographic technique. More specifically, on the material side, it exploited the well-known fact that PDMS can be made to exhibit a higher level of rigidity through localized, in

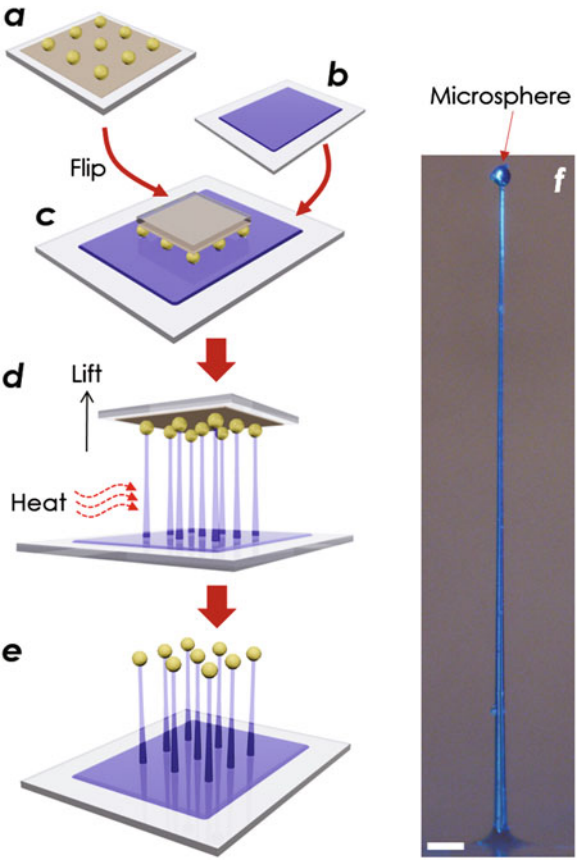

Fig. 3.8 (**a–e**) The fabrication steps for PDMS micropillar: (**a**) Assembly of microspheres on a double-stick tape, (**b**) Spin-coating of a PDMS thin film and its half-curing, (**c**) Flipping of the microsphere/tape assembly and its dipping into the half-cured PDMS thin film, (**d**) Lifting of the microsphere/tape assembly while applying heat, (**e**) Removal of the tape. (**f**) The optical micrograph of the highest PDMS micropillar with its height and aspect-ratio at the unprecedented values of 2.4 mm and 112 mm, respectively (Scale bar: 100 μm)

situ heating. On the fabrication side, it adopted the *direct pulling* soft lithography, as illustrated in Fig. 3.8 [12]. In fact, the direct drawing technique has already been utilized for a number of different materials, such as polystyrene [73], PMMA [74], PTT [75], sucrose [66], polyurethane [76], SU-8 [77], and adhesives [78], for realization of extremely high aspect-ratio structures such as wires and pillars. The greatest advantage of this technique is its total elimination of the need for de-molding, solving the fabrication issue from the ground up. The direct pulling method, however, has not been successfully applied to soft materials like PDMS. Only through the combined use of in situ heating, has it become a viable method for PDMS micropillar fabrication. One representative outcome is shown in Fig. 3.8f. It is in fact the PDMS micropillar with the world's highest aspect-ratio (112) and height (2.4 mm), **signifying the power of combining advantageous features of elastomers and unconventional soft lithography**.

Another important, advantageous feature of the technique is that the microsphere can be *left* on the top of the micropillar at the point of the release (Fig. 3.8e). This feature can enhance the functionality of the micropillar significantly since a large

variety of microspheres are commercially available. For instance, by choosing the magnetic microbead as the microsphere, we can render the micropillar sensitive to and/or manipulable by external magnetic fields.

3.3 Deformable Building Blocks

Joint utilization of the elastomers' unique features and their unconventional processing techniques can greatly facilitate the structuring of microscale soft robots. To realize robotic operations, however, one further needs to implement active functionalities. Above all, the structures must be wired, or interfaced, for the exchange of power and information. Such *interfacing* can be achieved through electrical and/or optical conduits. On top of that, actuators and sensors must be installed for dynamic operations. Granted, such building blocks have been in existence for decades for macroscale, rigid robots in the form of equally rigid components like metal wires, glass optical fibers, and electric motors.

The advent of soft robotics, however, has totally changed the technological scenery by forcing the use of soft and stretchable interfaces, sensors, and actuators. Then the call for miniaturization has kicked in, further complicating their physical realizations. Coping with such a *new-wine-in-new-wineskins* approach has proven a great challenge, both from technological and scientific points of view. Fortunately, there have been parallel streams of research on *soft* versions of the interfacing, sensing, and actuation elements in existence. Even though the research efforts were not exactly intended for microscale soft robotics, their outcomes turned out to be remarkably useful for it. This section will review some of them which contributed directly to the realization of S^3 robots.

3.3.1 Electrical Interface

Metallic wires have long been functioning as the conduit for electrical power and signals in various forms of conventional robots. They have been so robust and reliable that their adoption in large-scale soft robots has almost been taken for granted. Figure 3.9 shows one example of such use. For microscale soft robots, however, the unmodified adoption of metallic wires has become prohibitively difficult and the reasons are almost self-evident.

Clearly, the mechanical loading of the metallic wires becomes increasingly burdensome to the robot as its dimensions shrink. Such an increase in mechanical loading translates directly into complications in the actuator design and power budget allocation. The issue can be addressed only by making the metallic wires thinner by the same proportion, maintaining their length-to-diameter ratios, or *aspect-ratios*. Thinned wires, however, inevitably suffer more from mechanical fatigue and external damages, rendering themselves more vulnerable to failures.

Fig. 3.9 A robotic leg with *air muscles* from *Shadow Robot Company Ltd.* utilizes metallic wires for electrical interfacing (Image from *Wikimedia Commons*)

For S^3 robots made primarily of elastomeric materials, the solution seemed also self-evident: the metallic wires must be *embedded* inside the robots themselves in a highly stretchable fashion, thus achieving effectiveness from both cost and, more importantly, space points of view.

Fortunately for S^3 robotics, a huge technological pool for such flexible, embedded electrical interfaces has been built up. It has actually been established for another hot field of technology, stretchable and/or foldable electronics, but is readily available for tapping from the robotics side. Two major technological approaches exist: *redundant wiring* and *the use of highly deformable conductors*.

In the former, the metallic wires are patterned with redundant length, either through wavy patterning or the addition of spring-like structures, as shown in Fig. 3.10 [79–82]. The latter, on the other side, utilizes two new technological elements, microfluidics and room-temperature liquid metal, in combination. The wires are constructed in the form of microfluidic channels in elastomer sheets. Filling the microfluidic channels with liquid metal, such as EGaIn (Eutectic Gallium-Indium), enables conduction [83–86]. Neither approach is without issues presently since the electrical properties of the wires tend to change inevitably with its shape, to the point of encouraging their use for deformation sensing. Further research and development are required to resolve the issues.

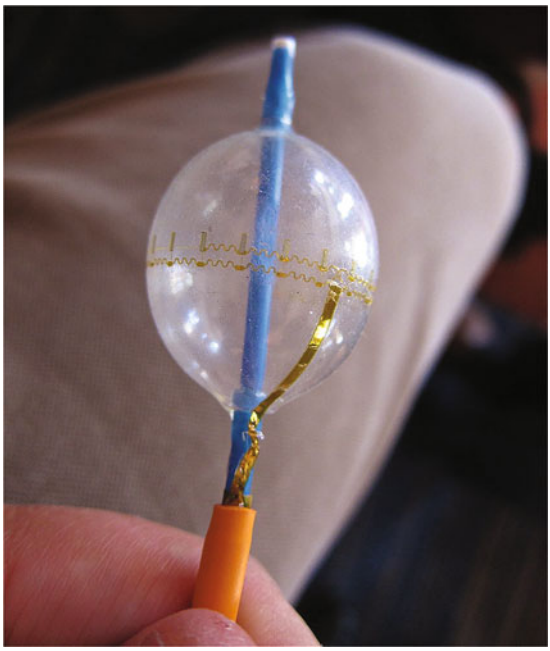

Fig. 3.10 A cardiac balloon catheter equipped with stretchable temperature and EKG sensors (Image from *Wikimedia Commons*)

3.3.2 Optical Interface

For S^3 robotics, optical interface is a very attractive alternative to those based on electrical schemes. Above all, optical interfacing relies on dielectric materials, facilitating the accommodation of elastomeric polymers. In addition, it is inherently immune to electromagnetic interference (EMI) and free from the dangers of spark generation. It also contributes to the accomplishment of *all-dielectric* embodiment of the S^3 robots, which is critical for their operability in magnetic environments such as MRI chambers. Being based on dielectric materials, however, does not directly translate into deformability of the overall structure. Substantial efforts have been paid for the realization of deformable *soft* optics as opposed to *rigid* optics [87].

Historical Overview Centuries of brilliant innovations have shaped rigid optics into its current status of dominance. Over the time, the field has evolved from empirical trial-and-errors, in which even a genius like Galilei had to purchase 200 lenses to find the right combination to realize a normally performing telescope, to modern, on-demand production of various discrete and integrated optics. Discoveries of new design principles and fabrication techniques, along with their computerization, have played essential roles in improving the precision and durability of rigid optics.

The root of soft optics can be traced back to the polymer-based molded optics which entered the world of optics in complete dominance of rigid optics. They were definitely softer than glass-based optics and some of them were even deformable to a certain degree. However, they were meant to be static in terms of their functionality

and could not be categorized as *bona fide* soft or deformable optics. Optical devices proactively exploiting the softness and/or deformability joined the mainstream optics in step with the popularization of elastomer-based microfluidics in MEMS and bio-MEMS communities at the turn of the millennium.

Technological Trichotomy PDMS, introduced in detail in Sect. 3.1.1, and other optically clear elastomers again played the role as the main enabler. It is noteworthy, and interesting, to point out that roughly three different levels, namely the *convenient*, *convergence*, and *critical* levels, can be identified in the progress of soft, deformable optics. In fact, such a trichotomy is not exclusive to soft optics. Similar three-phase development can be observed in many other examples of technological development, especially in those resulting from the fusion of two technologies with very different backgrounds. For instance, Fig. 3.11 shows how the fusion of two fields of study, microfluidics and plasmonics, engendered a new field of *plasmo-fluidics* in those three stages [28].

At the convenience level, the use of elastomer is largely incidental, or even coincidental, with the prospect of co-fabrication with microfluidic devices as the primary motivation. Soon, the advances in the field engender new optical devices with their features greatly enhanced over rigid optics-based ones through full exploitation of the deformability. This proactive exploitation can be referred to as the level of convergence. Recently, there appears a new class of deformable optics seemingly designed from scratch with the use of deformable materials in mind. In those, the amalgamation of the optical functionality and deformability seems *inevitable*. Such a high level of dependence certainly deserves to be labeled as *critical*.

Convergence Level Stretching-based spectral tuning of diffraction gratings and resonators, in which the pitch and cavity length are mechanically controlled, are good examples of convergence-level fusion. The scheme has been extended to control the characteristics of metamaterials and plasmonic nano-antennas through

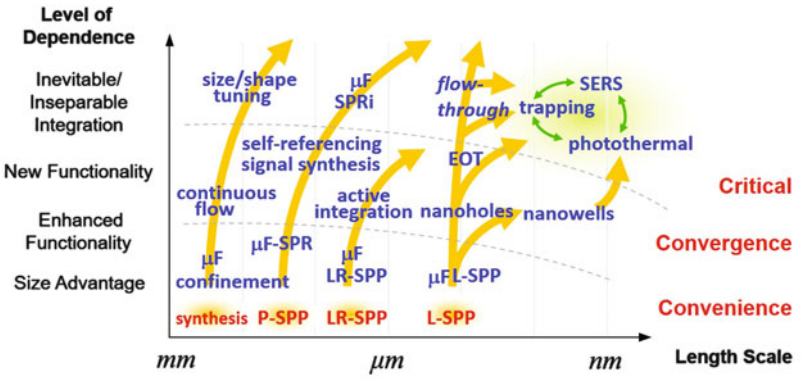

Fig. 3.11 The trichotomy diagram illustrating the advances of *plasmo-fluidics*

modulation of the separation between nanostructures in each unit cell. The use of PDMS may not be indispensible for that purpose but highly beneficial in terms of the performance-to-cost ratio. For example, the thermo-optic spectral tuning of the plasmonic metamaterial in [88] was very efficient with a 150 nm shift resulting from only 45 V but it required the use of an exotic phase-change material. Using PDMS, Pryce et al. demonstrated almost 400 nm peak shift with 50% strain which would require less than 1 mN with sufficiently thin PDMS substrates [27]. Such a relative advantage is the main merit of convergence-level soft optics.

Critical Level Optical Interface In the framework of the trichotomy, the deformable optical interface certainly falls in the category of critical level application. Optical power and signals can be most effectively delivered over the optical waveguide and a large number of schemes have been reported for its deformable realizations [89–95]. The efforts ultimately target a fully functional integration of active and passive optics on a single deformable substrate as envisioned in Fig. 3.12.

Among the reported approaches, the most important ones are those relying solely on PDMS. Since the realization of optical waveguiding requires core and cladding structures with different refractive indices, efforts have been made to locally increase the index without affecting the elastomeric properties of PDMS. To date, such *index contrasting* has been accomplished through the joint use of two different types of PDMS [93, 95] or PDMS mixed with curing agents at two different ratios [92]. Further progress is needed in this specific area not just for S^3 robotics but also for wearable and foldable devices in general.

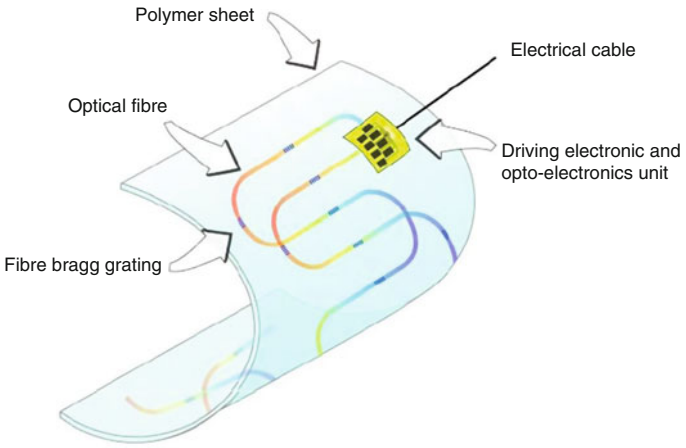

Fig. 3.12 An envisioned deformable active/passive optical integration (Image from *Wikimedia Commons*)

3.3.3 Sensors

Along with the thrusts for deformable interfaces, there also have been a parallel line of effort to realize deformable sensing elements. Initially, it started out as a utilization of the flexible electrical/optical interface schemes introduced in the previous subsections. The sensors were rigid, rather than soft, but they were small in comparison with the area of deployment. With the help of the flexible/stretchable interfacing schemes, they basically formed deformable sensor networks. The *artificial arthropod eye* shown in Fig. 3.13a is one representative example [96] in which multiple vision units, each comprising a microlens and an image sensor pixel, are connected through redundant wiring on an elastomeric membrane. Pneumatic inflation of the membrane thus widens the vision sensor array's field-of-view.

The paradigm is now under transition. The hydrogel-based transparent and flexible touch panel shown in Fig. 3.13b is one prominent example. Rather than relying on a network of stretchable wiring, the touch panel utilizes a single piece of highly deformable functional material [97]. The sensing and estimation of the touch location are accomplished through external signal processing, rather than internal multiplexing. The overall scheme unquestionably leads to a highly simplified yet versatile embodiment.

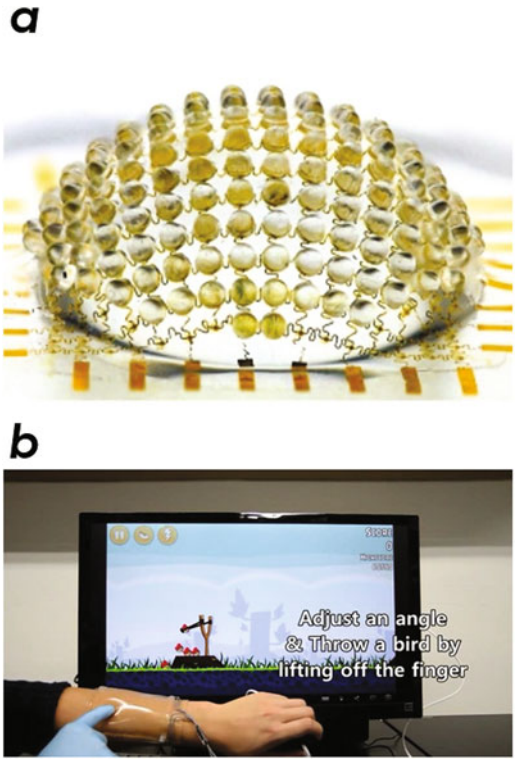

Fig. 3.13 (**a**) Artificial arthropod eye as a deformable sensor network. Reprinted with permission from [96]. Copyright 2013 Nature. (**b**) Hydrogel-based flexible touch panel [97] (Image courtesy of Seoul National University)

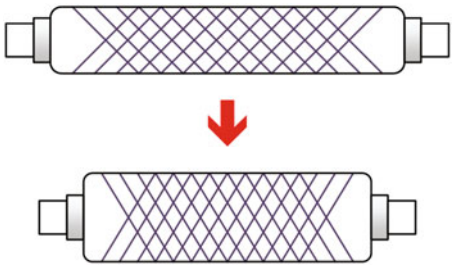

Fig. 3.14 A schematic diagram illustrating the pneumatic operation of the McKibben actuator

3.3.4 Actuators

The deformable actuator is another essential building block for soft robots. Fortunately, soft, pneumatic actuators have been in continuous development and use for both soft and rigid robots at the microscale for decades, constituting a relatively well-established portion of the fields [98, 99]. Figure 3.14 shows the McKibben actuator, often referred to as the McKibben *pneumatic artificial muscle*, which must be the most frequently adopted form among the pneumatic actuators [100, 101]. It is basically an elastic balloon actuator braid-sleeved with wires, typically made of strong polymers like nylon that are less stretchable than the balloon itself is. With compressed air, one can inflate the balloon and expand its volume but the braided wires will lead to a contraction in the axial direction.

The McKibben actuator boasts high strength-to-weight ratio but necessitates additional instruments for air compression and control. Of course, the McKibben actuator is just a starting point. A large number of new pneumatic/hydraulic mechanisms are under development for S^3 robots based on their inherent compatibility with microfluidic channel networks that can help initiation and control of their motions [17, 102, 103]. The two topics to follow, *shape engineering* and *bio-inspiration*, will be of great use for the enhancement and diversification of the S^3 actuator. The current status and future development prospect will be discussed in the following chapters.

3.4 Bio-Inspiration and Bio-Mimicry

In addition to all the tangible enabling factors presented above, there exists one conceptual one that has equally contributed to both microscale robotics and soft robotics: the progress in bio-inspired engineering and bio-mimicry. The effort to acquire new engineering concepts and inspirations from the biological world has been continuous throughout human history, as evidenced by the sketches of the bat-inspired flying machine by Leonardo Da Vinci in Fig. 3.15. Recently, they have become particularly intense fields of research as the techniques for quantitative and systematic analysis of biological functionalities got rapidly rolled out. This section

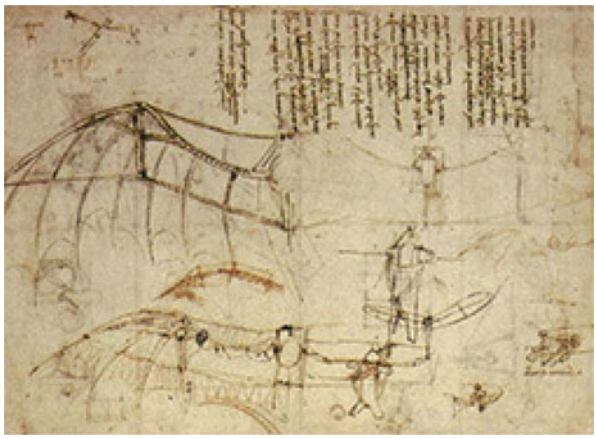

Fig. 3.15 Da Vinci's sketch of bat-inspired flying machine, *ca*. 1488 (Image from *Wikimedia Commons*)

will review how they have influenced the field of microscale soft robotics. How the new microscale soft technologies affect back bio-inspired engineering and biomimetics will be discussed in the later sections.

3.4.1 For Making Small Robots

During the early stage of microscale robotics, the implementation of even the very basic structures and functionalities had been deemed highly challenging. At that time, the remarkably effective anatomy and actuation mechanisms of small living organisms have provided a great deal of breakthrough ideas. Biological surveys have shown that animals at millimeter- to sub-millimeter-scales have evolved unique body structures and mechanisms to perform functionalities essential to their survival and reproduction under severe size limits and the physical constraints arising as their consequence.

Compound Eye for Vision One widely noted example is the compound eye of the insects and crustaceans [104, 105]. The eyes of those small animals are inevitably fixed to the bodies with no effective means for their dynamic rotation. For their survival, therefore, the eyes must be able to cover a wide angular range, or field-of-view, *statically*. Ultimately, an omni-directional vision that can cover 2π steradian (i.e., a hemispherical vision), or wider, is desired. At macroscale, we achieve such a wide field-of-view by cascading a series of lenses meticulously designed, cut, and assembled. The fisheye lens is a good example but such a complex single-aperture optics, however, is prohibitively bulky and alignment-sensitive to be adopted by small animals.

Nature has successfully harmonized the conflicting needs using a totally new type of imaging system called the *compound eye*. As shown in Fig. 3.16a, b, the structure of the compound eye is very different from the camera eyes found in most

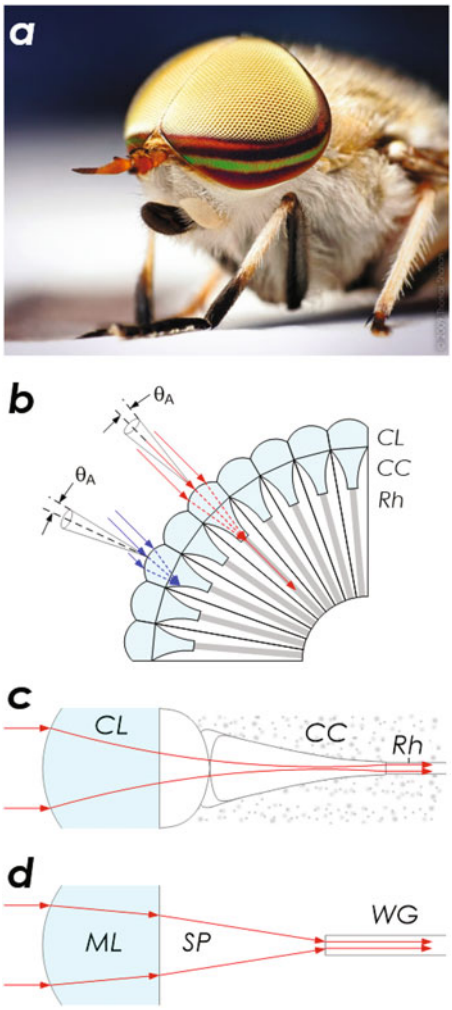

Fig. 3.16 (**a**) The compound eye of *Tabanus lineola*. (Image from *Wikimedia Commons*), (**b**) A schematic diagram of the compound eye's basic structure, (**c**) A functional diagram of an ommatidium (*CL*: Corneal Lens, *CC*: Crystalline Cone, *Rh*: Rhabdom), (**d**) An optical analogy of an ommatidium (*ML*: Microlens, *SP*: Spacer, *WG*: Waveguide)

macroscale animals. It consists of a large number of vision units called *ommatidia*. As shown in Fig. 3.16c, each ommatidium consists of one corneal lens (*CL*), one crystalline cone (*CC*), and one rhabdom (*Rh*) which function as a microlens (*ML*), a spacer (*SP*), and a waveguide (*WG*), respectively, as shown in Fig. 3.16d.

Collectively, they operate as a lens-waveguide light-coupling system, which is ubiquitous in the field of fiber optics and integrated optics, and function as one pixel of the compound eye. A mosaic vision covering a wide field-of-view can be obtained by hemispherically deploying a large number of ommatidia in a radial fashion as shown in Fig. 3.16b. In fact, the compound eyes of many insects provide fields-of-view exceeding 2π steradian.

The key enabling mechanism is the extreme sensitivity of the light-coupling process on the incidence angle. As illustrated in Fig. 3.16b, any light impinging on the corneal lens with its incidence angle deviating even slightly from the center axis will not be coupled into the waveguiding structure of the rhabdom, resulting in its exclusion from image formation. This incidence angle discrimination ensures a narrow acceptance angle θ_c and, hence, minimization of cross-talks between neighboring ommatidia.

There have been multiple attempts to artificially replicate this compound eye structure since it still remains the only scheme to realize a large field-of-view in an extremely small form-factor. So far, the effort has been only partially successful, resulting in satisfying only the size requirement [107, 108] or only the field-of-view [96] requirement but not both of them simultaneously. They have been, however, successful in assuring us the value and potential of bio-mimetic approaches for microscale robotics.

Filiform Hair for Mechanoreception For their survival and reproduction, insects need to detect and process a variety of mechanical stimuli such as touch, impact, and air-flows from wind and sound. To cope with these demands, small animals and insects rely on a largely common sensing platform comprising a high aspect-ratio micropillar fixed inside a socket [106, 109–112].

Figure 3.17a, b, and c shows a cricket, its cerci, and the schematic structure of the filiform hair mechanoreceptor, respectively. Basically the filiform hair functions as a cantilever which amplifies the mechano-stimulus and transduces it towards the nerve underneath. Similar *cantilever-in-a-socket* configurations as the mechanoreception platform can be found in many other species. For example, the lateral line water-flow receptor found in fish and even the hair cell receptor in human cochlea also rely on the same mechanism. Such a *convergence* in the structure and functionality indicates that this configuration is a highly optimized one for mechanoreception in extremely space-constrained environments and, more importantly, a good model for accomplishing the same goal in artificial microscale robots. The sheer number of artificial replication attempts on the filiform hair mechanoreceptor and its variants support the claim [113–117].

To summarize, the examples described above must have given the readers strong assurance that we can learn a lot from nature about how to *squeeze* things and functionalities into a tiny space for the realization of microscale robots. The effort is on-going, as it has always been, and looking up. More details will be given in the following chapters.

3.4.2 For Small and Soft Robots

Not all small animals are soft. It is, however, not difficult to find small and soft animals either and those can provide invaluable knowledge for advancing the design and realization of microscale soft robots. Insects unarguably constitute the best

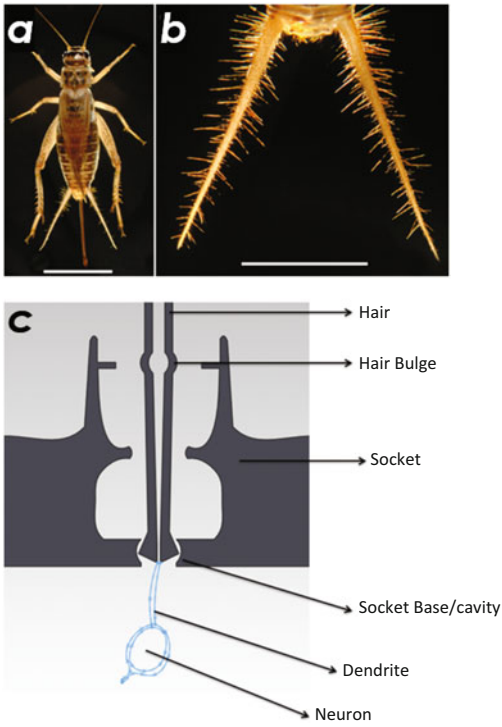

Fig. 3.17 (**a**) An optical micrograph of *Acheta domesticus*, a house cricket, (**b**) A close-up view of the cricket's two *cerci*, (**c**) A schematic diagram of the filiform hair mechanoreceptor's inner structure (Images from Public Library of Science [106])

model for S^3, robots. In fact, almost all parts of their small and soft body structures are under study with the intention of artificial replication [118]. Among them, of special relevance is their locomotion strategies. Two major lines of mimicry effort exist, one for the *actuation mechanism* and the other for the *locomotive strategy*.

For the former, the most prominent example is the microscale hydraulic actuator inspired by the leg-expanding mechanism of the spider [119]. As outlined in Fig. 3.18, spider legs are attached directly to the main body (*prosoma*). Its muscles can act as a pump and increase the fluid pressure [120]. Then the fluid, pressurized up to 10 kPa inside the *prosoma*, extends the joints of the spider's legs, generating an exertion force in the range of 10∼100 mN [119]. By cascading this simple yet effective actuation mechanism, Menon and coworkers have demonstrated the Smart Stick actuator for future space use [119]. Its unit actuator exploits AKEMA Poly Block Ammide (PeBax 6333) mini-tubes (1.0/0.5 mm in OD/ID and 276 MPa in *E*) as the balloon actuators. In the experimental characterization, one unit joint demonstrated up to 2° of rotation at 1 MPa of applied pressure. In the experimental characterization, one unit joint demonstrated up to 2° of rotation at 1 MPa of applied pressure.

In terms of the locomotive strategy, the crawling scheme of the caterpillar, especially those at the larval stages of the butterfly and moth, has been most intensely sought after. Even with an extremely simple body structure lacking the support

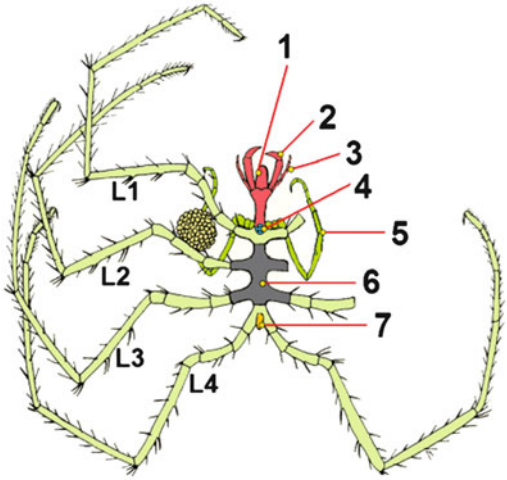

Fig. 3.18 External anatomy of Nymphon sea spider. *6*: *prosoma*, *L1–L4*: legs (G. O. Sars (1895), Image from *Wikimedia Commons*)

of the circumferential muscles, the caterpillar achieves its remarkably efficient locomotion by simultaneously exploiting three elements: highly deformable body, soft actuators, and reliable gripping mechanisms [121]. This observation, followed by soft-MEMS-based implementations, has led to a family of caterpillar-inspired robots [121, 122].

Case Study 2: Micropillar Wind Sensor

As stated in Sect. 3.4.1 with the cricket's filiform hair as an example, mechanoreceptors based on pillar-like structures are ubiquitous in nature [106, 109, 110]. Extensive biomimetic efforts have been invested to fabricate highly flexible micropillars using MEMS technology, but constructing such high aspect-ratio, upright structures with soft, easy-to-bend material had remained a great challenge. The recent success in the realization of the upright PDMS micropillars with extremely high aspect-ratios, described in Case Study 1, has opened a new avenue of research for the implementation of the *artificial* filiform hair mechanoreceptor. The operation principle and embodiment, to be described below, will ascertain that it is a good model system for joint utilization of both the deformable building blocks and bio-inspiration.

The work described in [12] shows how the PDMS micropillar was configured into an artificial filiform hair mechanoreceptor for sensing dynamic air-flows, or winds. An optical interrogation method was chosen to maximally exploit the high-level transparency of PDMS and also other advantages of lightwave-based operation listed in Sect. 3.3.2.

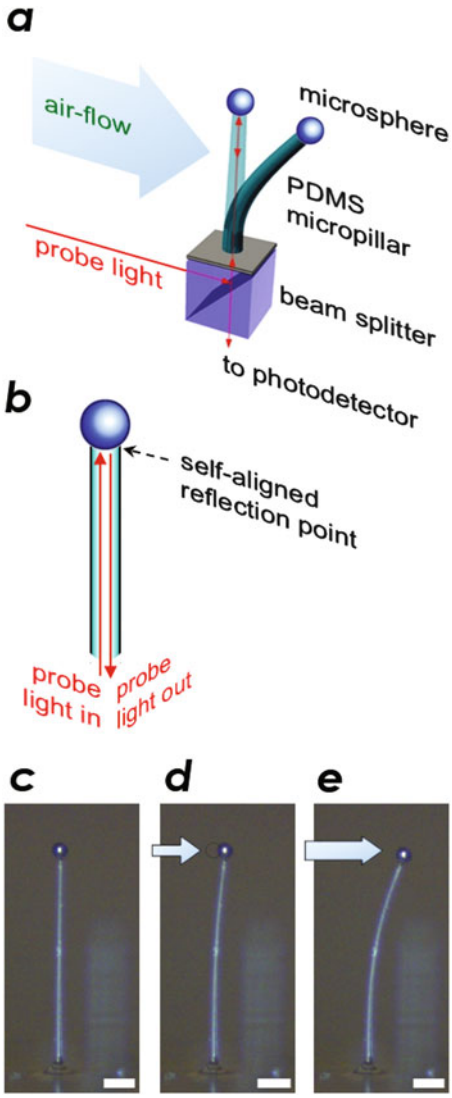

Fig. 3.19 (**a**) The optical interrogation configuration for the PDMS micropillar-based wind sensor, (**b**) A schematic diagram illustrating how the microsphere functions as the self-aligned reflector to the light guided through the PDMS micropillar, (**c**)–(**e**) Optical micrographs of the PDMS micropillar under 0 m/s, 0.12 m/s, and 0.20 m/s air-flows, respectively

Figure 3.19a shows the basic configuration. Basically the PDMS micropillar is set to function as a flexible optical waveguide which deforms under air-flows. On the other hand, the microsphere, which has already been utilized for direct pulling of the micropillar itself, has been set to play the role of a reflector as shown in Fig. 3.19b. The probe laser light impinges on the setup from the side and then re-directed by the beam splitter cube. The portion sent up towards the tip of the PDMS micropillar gets reflected back upon hitting the bottom surface of the microsphere.

Attentive readers may remember that the microsphere was predicted to assume multiple roles other than the pulling itself in Case Study 1. In this setup, the

Table 3.2 Structural parameters of the two PDMS micropillars under test

Micropillar	Height (μm)	Average diameter (μm)	Aspect-ratio	f_{reson} (Hz)
S	1600	22	72.7	102
L	2000	23	86.9	93

microsphere was deliberately chosen to be a hollow glass microbead coated with Ag so that it can function effectively as a reflector to the probe beam. One important advantage is that the microsphere is intrinsically *self*-aligned to the PDMS micropillar waveguide, eliminating the need for the difficult, labor-intensive alignment process. This feature is one of the most useful enablers for the sensor realization.

The validation of the concept and realization was accomplished through elaborate experiments in which multiple micropillar-based sensors were put under artificially generated winds at various flow-rates. For comparative studies, two different PDMS micropillars, shown in Table 3.2, have been realized and tested. Figure 3.19c, d, and e shows the PDMS micropillar gradually deforming under an air-flow with increasing flow-rate. In the absence of the air-flow, the micropillar stays straight, producing maximal reflection. Upon contact with a constant air-flow, it bends due to the fluidic drag force, leading to a decrease in the reflection.

Figure 3.20a shows the results. For both PDMS micropillars, the results indicate that the reflectance is a good measure of the air-flow rate, or the wind speed. The slope of the quasi-linear response region, right beyond the starting point of the *knee*, are approximately 17.8 s/m and 27.7 s/m for micropillars S and L, respectively. In Fig. 3.20b, the measurement results from the experiments using time-varying air-flows, i.e., sound waves, as the excitation source indicate that the reflection waveform can provide accurate information on the frequency of the acoustic excitation, although it does not follow the excitation pattern exactly.

As is evident from the comparison of the upper and lower panels of Fig. 3.20b, the PDMS micropillar's dynamic response also exhibits a strong and clear frequency dependence, which becomes clearer when the modulation depth of the temporal response is plotted as a function of the frequency as shown in Fig. 3.20c. Apparently, the PDMS micropillar cantilever is governed by the second-order dynamics, as evidenced by the highly accurate curve-fitting results shown as the superimposed solid lines. The retrieved peak resonance frequencies are 102 Hz and 93 Hz for S and L micropillars, respectively. It is noteworthy to point out that such a low resonance frequency, in the realm of sub-kHz regime, is a welcome characteristic for some specific applications. One notable example is the cantilever-based harvesting of mechanical energy from human motions for which the biggest challenge has been matching the resonance frequency of the harvester to that of the human motion.

To summarize, the PDMS micropillar-based wind sensing system described above in two installments is an interesting embodiment of many aspects of the recently emerged enabling technologies for microscale soft robotics. The same type of devices will eventually form the technological pool from which the researchers of S^3 robots can tap concepts and building blocks in near future.

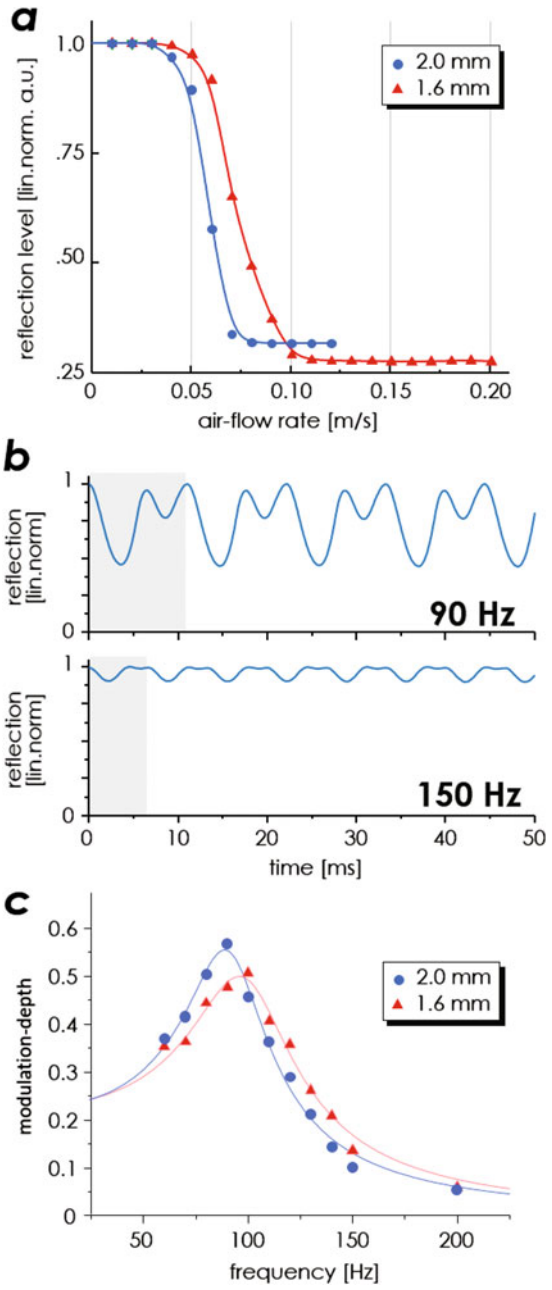

Fig. 3.20 (**a**) The change in the optical power of the reflected probe beam due to the wind-induced bending of the PDMS pillars, (**b**) The temporal changes in the reflectance of the *L* micropillar due to time-varying acoustic excitation, (**c**) The modulation depth of the time-varying excitation response (*symbols*) exhibits clear dependence on the excitation frequency that can be modeled as second-order systems (*solid lines*)

3.5 Shape Engineering

The concept of shape engineering is new even in the already new field of microscale soft robotics. In fact, it is difficult to find publications with explicit use of the term *shape engineering* or review papers or monographs dedicated to it. The study of shape engineering itself, however, has been carried out continuously and unwittingly since the dawn of large-scale soft robotics. It originates from the realization that in soft materials, such as the elastomers, the mechanical response can become highly nonlinear, allowing large changes to occur from small modifications to the environmental or structural parameters.

One prominent example is the *snap-through instability* which refers to the metastable regime in the stress–strain relation in which even an insignificant amount of excess stress can induce a large change in the strain [123]. Buckling, shown in Fig. 3.21 is one manifestation.

In nature, biological creatures have long been exploiting such effects to their advantage [124]. It was already revealed that the fast motion of the Venus flytrap is enabled by that mechanism. It has actually been artificially replicated with PDMS structures for possible sensing applications in future [125]. In engineering, it has been utilized to induce a giant inflation in elastomeric membranes [126, 127]. It has also been conjectured to be the hidden enabler behind the unusually rapid response from a soft robotic tentacle [128].

Currently in the field of soft robotics, there are many parallel shape engineering efforts in progress, either by the specific name or under more general categorizations. May it be the thrust to speed up the motion of the soft robot through optimization of the actuator shape [129] or the study to tailor the cross-sectional shape of elastomeric tubes for better curling performance [130, 131], the ultimate target is common: finding the universal set of the design rules for future soft robots. Present studies rely mainly on computational modeling but, given the intensity of the research interest, one can expect the emergence of semi- or fully analytical design rules in near future. More details will be presented in the following chapters.

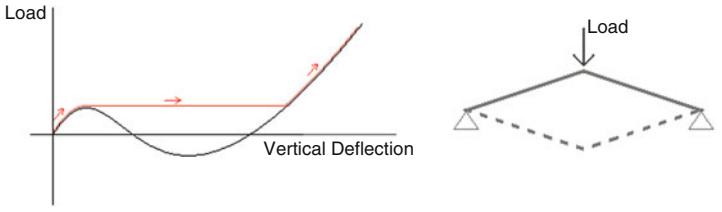

Fig. 3.21 The highly nonlinear relation between stress (loading) and strain (vertical deflection) during *buckling* (Image from *Wikimedia Commons*)

Chapter 4
Soft Robotic Micro-Tentacle: A Case Study

Previous chapters have reviewed the motivations towards microscale soft robots, or S^3 robots, and the technological advances leading to their practical realizations. Now the survey of the current progress in the field is in order. It begins with a case study on a representative S^3 robot in this chapter and then introduces top-of-the-line outcomes from the mainstream research efforts in recent years in the following one.

The *soft robotic micro-tentacle* (SRMT), reported by the author in 2015 [19], has been chosen as the model system for this introductory Case Study since it embodies the majority of the enabling technologies described in Chap. 3 and tries to address most motivations for S^3 robots shown in Chap. 2.

4.1 Overview

Soft robots have been evolving fast [10, 132, 133]. So have robots at the microscale [24, 134]. The time has gotten ripe for the new field of microscale soft robotics to which each can contribute its own set of advantages. Soft robots can offer their life-like look-and-feel and high-level compliance closely matched to those of biological tissues. Micro-robots can provide access to hard-to-reach areas. Small blood vessels and airways in human body constitute good examples.

When integrated synergistically, the resulting microscale soft robot will be especially useful for minimally invasive clinical operations, such as diagnosis, localized drug administration, and surgery, in which the ability to work in remote areas of the human body *without* damaging the surrounding tissues commands the highest priority. In that sense, the microscale soft robots possess the full potential to play the main role in future medicine.

There is, however, much to be done to make microscale soft robots more widely available. First of all, their physical realization is highly challenging. A variety of fabrication methods have been developed for macroscale soft robots. The same

J. (Jay) Kim, *Microscale Soft Robotics*, SpringerBriefs in Applied Sciences and Technology, DOI 10.1007/978-3-319-50286-1_4

applies to microscale rigid robots. But the reports get scarce when it comes to microscale soft robots. Blind application of the methods originally developed for large and/or rigid robots turned out to be utterly inefficient, if not ineffective. For example, typical PDMS shaping techniques such as the sacrificial layer-based de-molding or oxygen plasma-assisted anodic bonding become unusable in the microscale world. We need fundamentally new fabrication techniques for microscale soft robots.

The current scarcity in efficient microscale mechanisms for soft actuation is also an issue. The choice becomes even narrower for microscale soft robots intended to be used in human body because they must not utilize high voltage/current or potentially harmful chemicals such as electro-rheological fluids. In fact, it is strongly encouraged not to include any conductor at all in the robot to render them maximally compatible with magnetic environments such as the MRI-chamber which is essential for visually guiding the robot [101, 135].

There also is the fundamental question: Will the manipulation modes developed for macroscale robots stay effective for microscale soft robots? One example is given in Fig. 4.1. The *two-finger gripping* motion shown in Fig. 4.1a is very effective for picking up relatively rigid objects at macroscale. The action, however, requires fingernails or similarly rigid supporting structures that are not only difficult to implement in microscale soft robots but also potentially harmful for handling soft, fragile objects in delicate clinical environments. As indicated in Fig. 4.1a, the motion inevitably deforms the target object to a certain degree as well.

In short, sustaining innovations in microscale soft robotics clearly requires simultaneous paradigm shifts in fabrication, actuation, and motion control.

SRMT is a new microscale soft robot capable of addressing the issues in a totally different yet efficient way. Its conception and realization are firmly based on the motivations and technological enabling factors discussed in the previous chapters and worth an item-by-item examination.

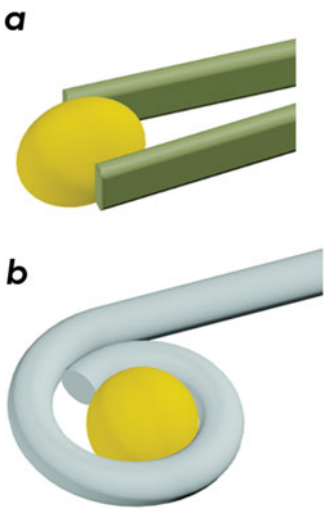

Fig. 4.1 (**a**) Typical *two-finger gripping* motion which inevitably squeezes and deforms the target objects at varying degrees. (**b**) The spiraling tentacle motion that can be much gentler in comparison

4.2 Conception by Bio-Inspiration

The SRMT avoided reliance on the potentially harmful pinching motion shown in Fig. 4.1a through the adoption of the tentacular *wrap-around motion* shown in Fig. 4.1b. Its conception was clearly inspired by the biological world which is replete with tentacles with multi-turn spiraling capability. The examples include:

- Octopus Tentacle
- Elephant's Trunk (Fig. 4.2a, also called *proboscis*)
- Spider Monkey Tail (Fig. 4.2b)
- Plant Tendrils (Fig. 4.2c)

Such a tentacular motion can provide an inherently gentler mode of grabbing and manipulation of objects. First of all, the motion increases the contact area. Thanks to that, the force and stress applied to the object can be reduced. Especially for highly soft tentacles, the wrap-around motion can be conformal, rendering itself gentler and safer. For objects to which the effect of gravity dominates over other forces, such as those from winds or water flows, the tentacles can become an even less intrusive grabber by functioning as a *scoop* which only touches the object around its bottom circumference.

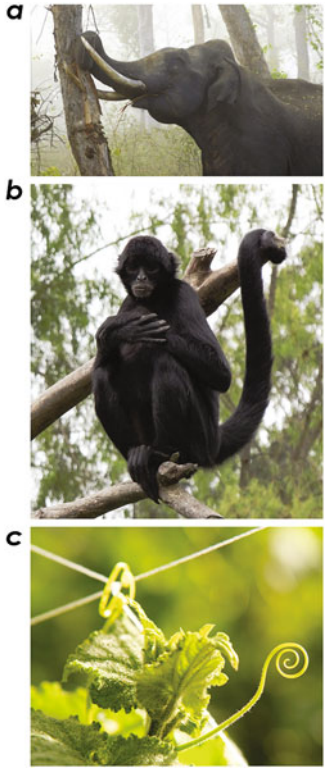

Fig. 4.2 (**a**) An elephant using its tentacle to debark a tree (Image from *Wikimedia Commons*), (**b**) A black-headed spider monkey (*Ateles fusciceps*) utilizing the tentacular motion with its tail (Image from *Wikimedia Commons*), (**c**) The coiled tendril of squash vine (Image courtesy of USDA NRCS)

For these reasons, there have been multiple attempts to artificially replicate the tentacle using elastomers [128, 136–138]. Reports on its *microscale* implementation, however, have been scarce due to the technological challenges for the miniaturization of the basic structure and functionalities.

4.3 Realization by Unconventional Shaping of PDMS

The scheme for the tube-based realization of SRMT is illustrated in Fig. 4.3a. It basically relies on the unequal elongation of a highly flexible tube with its thickness distribution asymmetric as shown in Fig. 4.3b. Pneumatic inflation of the tube will elongate the thinner side further, eventually bending it towards the thicker side.

For physical implementation of such a highly deformable tube with an asymmetric cross-section, the advantageous properties of PDMS (Sect. 3.1.1) and unique capabilities of unconventional fabrication techniques derived from them (Sect. 3.2) have been heavily utilized.

Adoption of Standard PDMS For the choice of the material, the adoption of PDMS seemed almost unavoidable. One distinguishing feature was the use of the standard PDMS (Sylgard 184^{TM}) rather than its more flexible cousins such as Ecoflex^{TM} [14] that have actually been adopted for the realization of macroscale tentacular soft robots [128]. The decision was based on the trial-and-error observations that the standard PDMS itself can provide sufficient level of deformability for the intended actuation at sub-millimetric or micrometer-scales. The higher-level robustness of the standard PDMS will also be an important enabling factor in the following fabrication step.

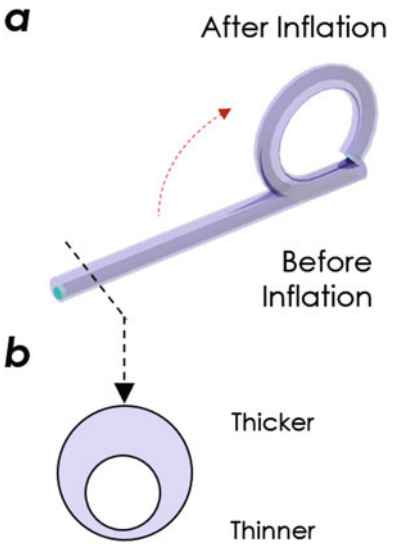

Fig. 4.3 Schematic diagrams for (**a**) deformable tube-based realization of the tentacular action and (**b**) the tube's non-uniform thickness distribution as the enabling factor

Template-Aided Tube Forming Pneumatic actuation suits microscale soft robotics well for its simplicity and efficiency already proven in large-scale soft robotics [128, 129, 139]. Its microscale realization, however, turned out to be very challenging [101, 135].

Above all, current soft lithography-based microfabrication techniques, developed mainly for building planar elastomer structures with low aspect-ratio patterns such as microfluidic channels, are not always suitable for constructing 3D, hermetically sealed cavities required for pneumatic actuation. They may still be built through the bonding of two planar structures [9, 18, 140, 141] or the use of dissolvable templates [131]. The strength and yield of bonding inevitably decrease with the length-scale. Dissolving templates often becomes an equally complex process at microscale.

This work has avoided such complications by constructing a tube, which will function as the pneumatic cavity, by dip-coating liquid-phase PDMS around a cylindrical template and then directly peeling it off after curing, eliminating the need for bonding or de-molding. Figure 4.4a, b shows the process schematically.

More specifically, short sections of a $\sim$100 µm-diameter polyamide wire and 125 µm-diameter fused silica optical fibers were used as the cylindrical template. The former, with its smaller final radius of curvature, proved more suitable for realizing SRMT when compared with the latter. The surfactant sodium dodecyl sulfate (SDS), mixed with water at 1:10 weight ratio, was used to coat the cylindrical templates to facilitate the template removal process. Computer-controlled micromanipulators have been utilized for precise dipping and lifting of the samples.

In Situ Curing and Gravity-Assisted Shaping Many reports published so far have testified that the one of the biggest issues in using liquid-phase PDMS for building long and thin structures, such as pillars or wires, is its tendency to bead [142]. In the fabrication of the ultra-high aspect-ratio PDMS micropillars described in the previous chapter as the Case Study, the beading was suppressed with the help of pre-curing and in situ thermal solidification [12]. The techniques applied to the dip-coated liquid-phase PDMS around the cylindrical template to facilitate the realization of the PDMS microtube with very thin walls without bonding is shown in Fig. 4.4b.

The solidification process can also be controlled for additional tailoring of the microtube's cross-sectional shape. Slowing it down prolongs gravitational impact on the coating, resulting in an increase in the tube's cross-sectional asymmetry, as shown in Fig. 4.5. For example, the 10 samples fabricated in [19] with the 100 µm-diameter template exhibited t_1 and t_2 of 31.8$\pm$4.9 µm and 7.9$\pm$1.0 µm, respectively. As stated above such an asymmetry is essential to induce bending for SRMT. The coating thickness can also be made uniform by rotating the template during curing with a motorized stage.

Release by Direct Peeling As shown in Fig. 4.4c, d, the completely cured PDMS microtube is robust enough to be peeled directly from the template with an optical fiber polymer jacket remover which is a standard tool in most optics laboratories. The process is simpler, cleaner, and faster than those requiring dissolvable templates [23, 66].

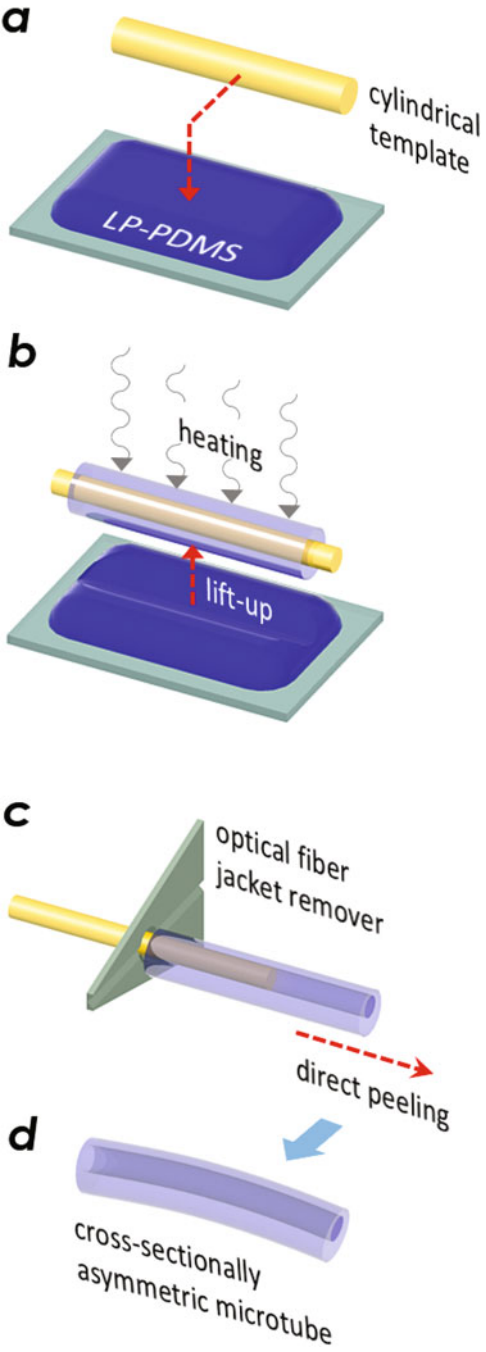

Fig. 4.4 (**a**) To achieve bonding-free fabrication of extremely thin-walled microtubes, liquid-phase PDMS was first dip-coated around a cylindrical template. (**b**) Heat was applied in situ for time-controlled curing of the PDMS coating. (**c**) The resulting microtube is robust enough to be directly peeled from the template with a simple polymer jacket remover. This process is simpler and faster than those relying on dissolvable templates. (**d**) The completed microtube exhibits asymmetric cross-section

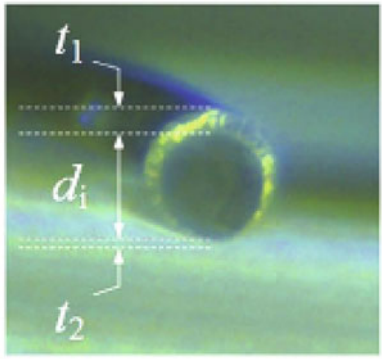

Fig. 4.5 An optical micrograph showing the thinness and cross-sectional asymmetry of the completed PDMS microtube. In this particular one: $d_i \sim 104\,\mu m$, $t_1 \sim 35.6\,\mu m$, $t_2 \sim 7.7\,\mu m$

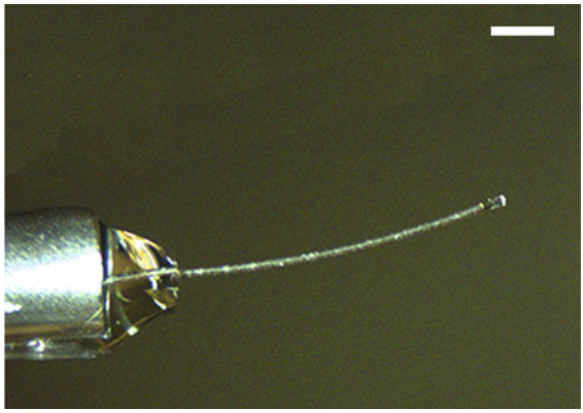

Fig. 4.6 An optical micrograph showing the robustness of the released PDMS microtube. The cylinder on the *left-hand side* is a blunt syringe needle with 2.1 mm outer diameter. Its cross-section was already shown in Fig. 4.5. Scale bar: 1 mm

With polyamide wires and glass optical fibers as the template, microtubes with their length L reaching 5∼8 mm have been fabricated. The main factor limiting the maximum achievable L was the inevitable increase in the friction and wrinkling during the peeling process. Despite their high aspect-ratios (typically exceeding 50) and thinness of the microtube itself and its wall, the peeled-off tubes did not sag or collapse, even when no air pressure was applied, as shown in Fig. 4.6.

Tailoring by Additive Co-Molding The unconventional fabrication technique exploiting the additive co-molding compatibility of PDMS, described in Sect. 3.1.2, becomes especially advantageous when one tries to modify the microtube's geometry and add structures to its exterior. One such task with equal importance to any type of application is the *mounting* of the standalone microtube (Fig. 4.4d) to a bigger PDMS structure for more convenient handling and utilization. The process is illustrated in Fig. 4.7a, b.

For microtubes to be used as the structural platform of SRMT in particular, the process can also be utilized to close the open end with a drop of liquid-phase PDMS to form a hermetic sealing, as shown in Fig. 4.7c. Such sealing is critical to pneumatic actuation and the ability to achieve it without the use of cumbersome

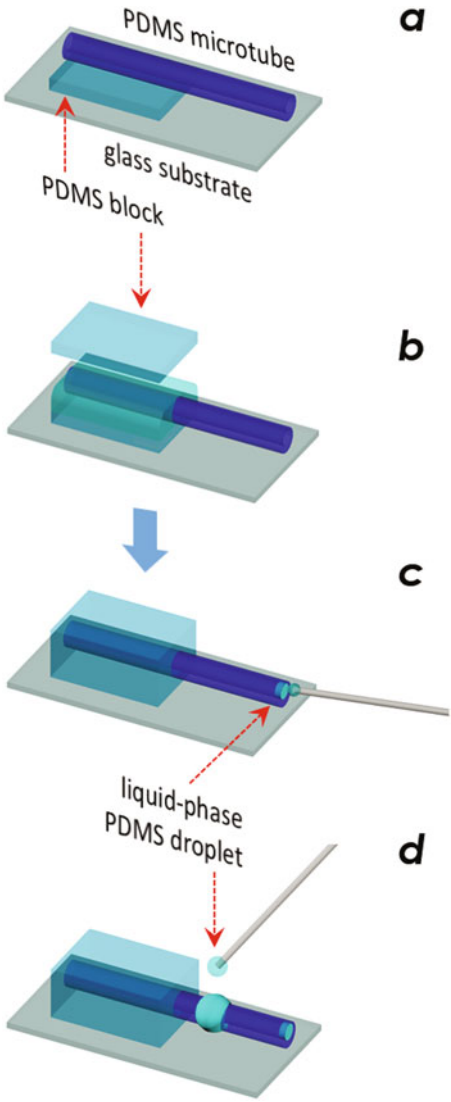

Fig. 4.7 Examples of additive co-molding operations applied to the PDMS microtube: (**a**) Mounting on a PDMS supporting block, (**b**) Adding of a PDMS reinforcement block, (**c**) Sealing of one opening, (**d**) Adding a hump

bonding processes can greatly contribute to the popularity of PDMS SRMT. The same process can be utilized to form a *hump*, which will play an important role in its actuation, on the PDMS microtube as shown in Fig. 4.7d.

4.4 Spiraling by Shape Engineering

The PDMS microtube shown in Fig. 4.6 is an example of the *plain* microtube which exhibits no cross-sectional shape change in the axial direction. The outcomes of multiple experiments have indicated that regardless of the pressure or cross-sectional asymmetry, the plain microtube fails to achieve spiraling. Bending only up to a single turn, shown in Fig. 4.3a and repeated as the inset of Fig. 4.8 for convenience, has been observed so far.

To *amplify* such insufficient bending motions into the multi-turn spiraling motion, much effort has been invested. Conventional solutions include the use of bi-material composite structures [128] or bellows-like surface corrugations [143, 144] which promote the mismatch in the elongation capabilities. They are, however, very complex to implement at microscale. A more simplified, easier-to-realize solution has been intensely sought after by the researchers in soft robotics.

4.4.1 Hump-Enabled Spiraling

A new approach, named the *hump-enabled spiraling* has been introduced and demonstrated in [19] to accomplish the spiraling motion in the PDMS microtube. As shown in Fig. 4.8, the corresponding requirement is as simple as adding a protrusion, or a *hump* to the PDMS microtube. In the fabrication point of view, this approach is highly advantageous since it requires access only to the microtube's exterior and, hence, can be executed after the microtube is completely fabricated and validated through tests.

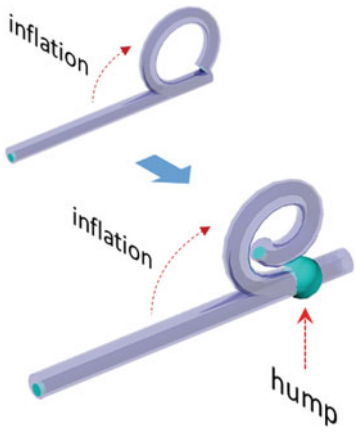

Fig. 4.8 The basic structure and working principle of the humped SRMT. By adding a hump to the plain microtube shown in Fig. 4.3, we can amplify the bending motion into a much more complex, multi-turn spiraling motion

4.4.2 *Theoretical Framework*

The Euler-Bernoulli beam theory can function greatly as the theoretical framework to analyze and predict the hump's role in promoting the spiraling motion [131, 145]. At the instant when the microtube nearly forms a ring shape, the coordinates (x, y) of the deformed base curve can be given through an integration:

$$u(s) = \int_0^s f\left(\int_0^{s'} \frac{M_o}{E \cdot I(\eta)}\, d\eta\right) ds' \tag{4.1}$$

where

s: The natural coordinate of the beam of length L ($s \in [0, L]$),
f: A *cosine* (*sine*) function for $u = x$ ($u = y$),
E: The material's Young's modulus,
I: The second moment of area.

At this specific instant, it is feasible to assume that a plain microtube has a constant I along its length, and that a humped microtube has a step-wise distribution of I, as shown in Fig. 4.9.

In this section, the analysis is restricted to the qualitative investigation of the elastic regime at an instant with a fixed pressure. The full evolution of I with increasing pressure would call for analyses of hyperelastic deformations and plasticity at extreme cases. The bending moment

$$M_o \equiv \pi \cdot r^2 \cdot p \cdot d_e \tag{4.2}$$

where

r: Radius,
p: Current pressure,
d_e: Distance between the microtube's neutral axis and void hole's center.

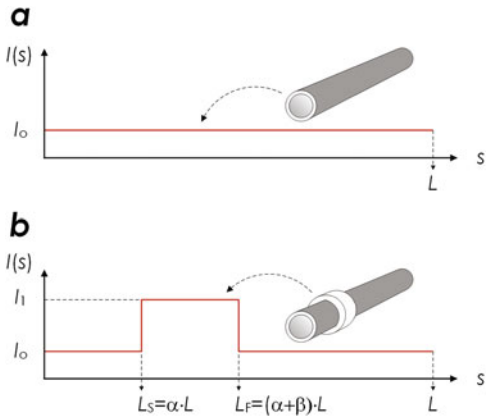

Fig. 4.9 Axial I distribution in (**a**) plain and (**b**) humped PDMS microtubes

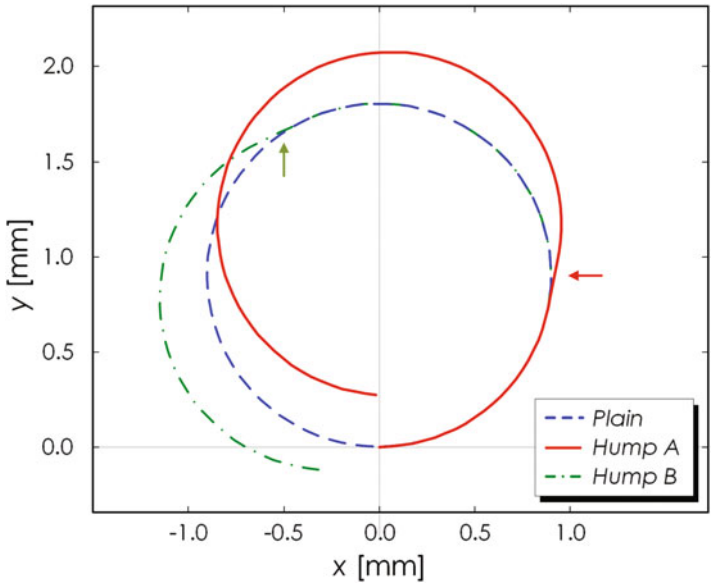

Fig. 4.10 Integration results of Eq. (4.1) for various hump configurations. The *arrows* point to the hump locations in Hump A and Hump B configurations, respectively

The blue dotted curve in Fig. 4.10 shows the result of integrating Eq. (4.1) for the plain microtube. The resultant curve, a perfect circle, indicates that the microtube will bend gradually to form a ring but will not achieve spiraling. It is clear from the plot that the realization of *inward* bending, a prerequisite for spiraling, requires re-entry of the end-point into the first quadrant with its $y > 0$. In light of the simple harmonic functions in Eq. (4.1), the integration over a full cycle will always set both x and y to 0, thereby impeding the desired spiraling.

4.4.3 Analysis of Hump Action

Adding a hump will modulate the microtube's geometry and, hence, the values of I as shown in Fig. 4.9b. In particular for the step-wise distribution of I, the integration in Eq. (4.1) will split into three, each covering the pre-hump, hump, and post-hump sections as:

$$u(s < L_s) = \int_0^s f\left(\frac{M_o \cdot s'}{E \cdot I_o}\right) ds' \tag{4.3}$$

$$u(L_s \leq s < L_f) = \int_0^s f\left(\frac{M_o \cdot s'}{E \cdot I_1} + \frac{M_o \alpha L}{E} \cdot \left(\frac{1}{I_o} - \frac{1}{I_1}\right)\right) ds' \tag{4.4}$$

$$u(L_f \leq s < L) = \int_0^s f\left(\frac{M_o \cdot s'}{E \cdot I_o} + \frac{M_o \beta L}{E} \cdot \left(\frac{1}{I_o} - \frac{1}{I_1}\right)\right) ds' \tag{4.5}$$

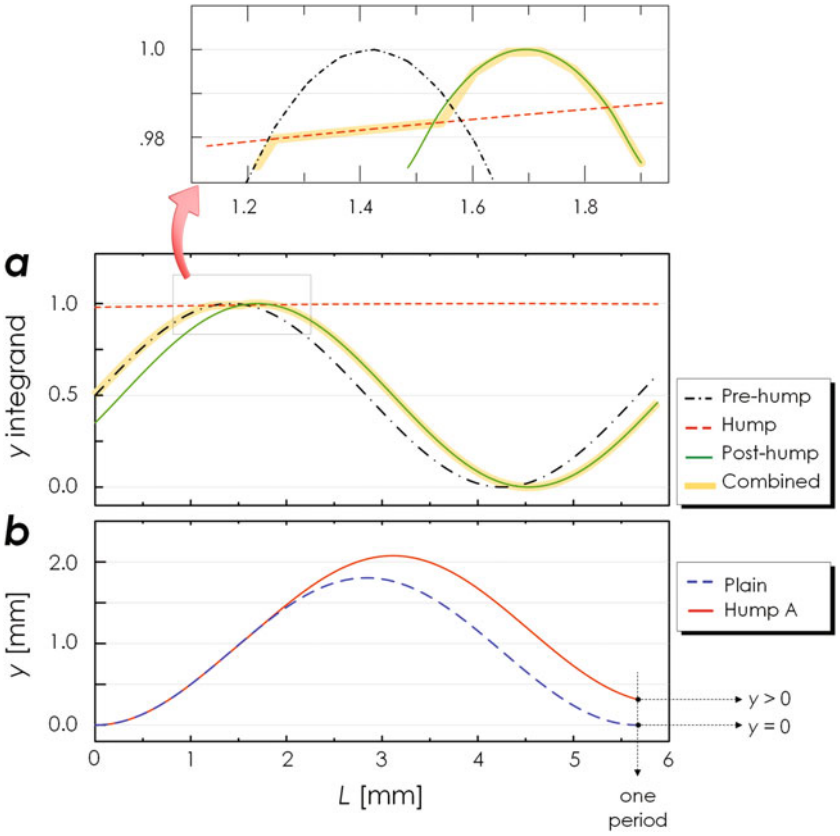

Fig. 4.11 (**a**) The changes in the y-integrands for the pre-hump, hump, and post-hump sections specified in Eqs. (4.3)–(4.5), respectively. (**b**) The integration results for the plain, un-humped microtube (*blue, dashed*) and the humped one (*red, solid*)

where I_1 and I_o are the values of I in the hump and non-hump sections, respectively, as shown in Fig. 4.9b. The position and length of the hump are also specified through α and β in Fig. 4.9b. Equations (4.3)–(4.5) and the integration results in Fig. 4.11a show that the sinusoidal functions in the integrands will obtain abrupt phase shifts when $I_o < I_1$.

Figure 4.11a shows the changes in the y-integrands for the pre-hump, hump, and post-hump sections calculated from Eqs. (4.3)–(4.5), respectively. For the humped microtube, the integration must be performed along the highlighted *combined* route, i.e., first along the pre-hump curve (black, dash-dot), then the hump curve (red, dashed), and then the post-hump curve (green, solid). For the un-humped one, it suffices to integrate along the pre-hump curve.

Figure 4.11b shows the integration results for the plain, un-humped microtube (blue, dashed) and the humped one (red, solid), with the impact of the abrupt

phase-shift taken into consideration. For the integration over a full cycle, the purely sinusoidal integrand of the former ended up $y = 0$. In contrast, with $I_1 \gg I_o$, the hump section curve changes much more slowly than those in other sections and can function as a phase-shift between them (as shown in the inset in detail), eventually altering the integration result to a non-zero, positive value. This enables the inward spiraling of the micro-tentacle.

By adjusting the levels of the phase-shifts to x and y, we can control re-entry point to the first quadrant. A simple criterion can be derived by assuming

$$L \cdot \beta \cdot (I_1 - I_o)/I_1 \ll L/4. \tag{4.6}$$

In that case, spiraling can be ensured with

$$\beta \cdot \frac{I_1 - I_o}{2 \cdot I_1} < \alpha < 0.5 + \beta \cdot \frac{I_1 - I_o}{2 \cdot I_1}. \tag{4.7}$$

Figure 4.12, in combination with Fig. 4.10, shows how a hump (length $= 0.05 \cdot L$) affects the level of bending as a function of its position. For the calculation, a microtube model with its characteristics approximately matching those of the pilot sample named MT1 (shown in Figs. 4.5 and 4.6). With I_o and I_1 at $5.1 \cdot 10^{-16}$ m^4 and $8.6 \cdot 10^{-15}$ m^4, respectively, the inward spiraling can be obtained when $0.024 < \alpha < 0.524$. We set the α value of Hump B at an improper value of 0.55 while setting that of Hump A to the proper value of 0.21, as indicated by arrows in Figs. 4.10 and 4.12. Despite their identical size and shape, the two humps impacted the microtube's bending very differently. As predicted, Hump A did achieve inward spiraling with the final $y > 0$. Hump B, on the other hand, performed even worse than the plain, un-humped microtube, resulting in $y < 0$.

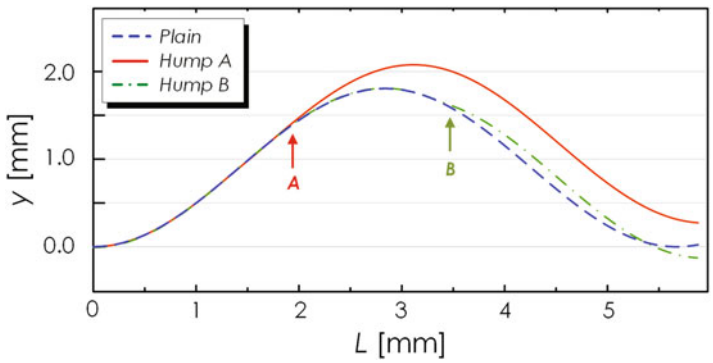

Fig. 4.12 Calculated y-values of three microtubes with different hump configurations. Plain: no axial change in cross-sectional shape, Hump A: with a properly positioned hump ($L_s = 0.21 \cdot L$), and Hump B: with an improperly positioned hump ($L_s = 0.55 \cdot L$). Hump A re-entered the first quadrant with $y > 0$, achieving an inward spiraling. Hump B, on the other hand, actually rendered the bending worse than that of the non-humped Plain

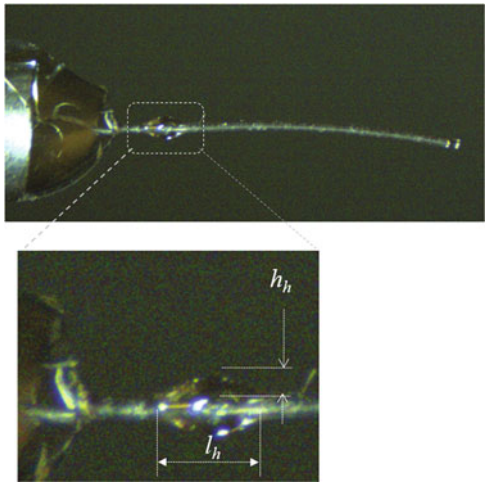

Fig. 4.13 Optical micrograph of the PDMS hump added to the microtube MT1 shown in Figs. 4.5 and 4.6. $h_h = 96\,\mu m$ and $l_h = 610\,\mu m$

4.4.4 Experimental Validation

To experimentally validate the predictions made above, a hump was installed at the proper position on the pilot sample microtube MT1, as shown in Fig. 4.13, the change in the degree of spiraling has been investigated.

Figure 4.14a, b contrasts MT1's pneumatic actuation results before and after adding a 610 µm-long, 96 µm-high hump. It clearly exhibited spiraling with the minimum RoC reduced to 500 µm. This straightforwardly validates the impact of adding a hump at a proper position to the spiraling capability.

To further validate the predictions made above about the adverse impact of the improperly installed hump, a PDMS microtube with structural characteristics very similar to those of MT1 with L, d_i, t_1, and t_2 at 5800 µm, 104 µm, 33 µm, and 7.4 µm, respectively, and compared its bending behaviors before and after adding a hump at an obviously improper position of $0.78 \cdot L$. Figure 4.15a shows the results. In good agreement with the theoretical prediction, the improperly positioned hump resulted in bending radius even greater than that of its non-humped prototype.

On the other hand, Fig. 4.15b shows one of the best spiraling results observed so far. As shown in the optical micrograph, the optimized microtube actuator, with L, d_i, t_1, and t_2 at 5470 µm, 105 µm, 34.6 µm, and 8.2 µm, respectively, and its hump installed at $0.17 \cdot L$ point exhibited spiraling with two full turns, achieving the final RoC of 210 µm. RoC as low as 185 µm has been obtained.

To summarize, all of these results support the validity of both the theoretical and physical realization aspects of the hump-based shape engineering in SRMT.

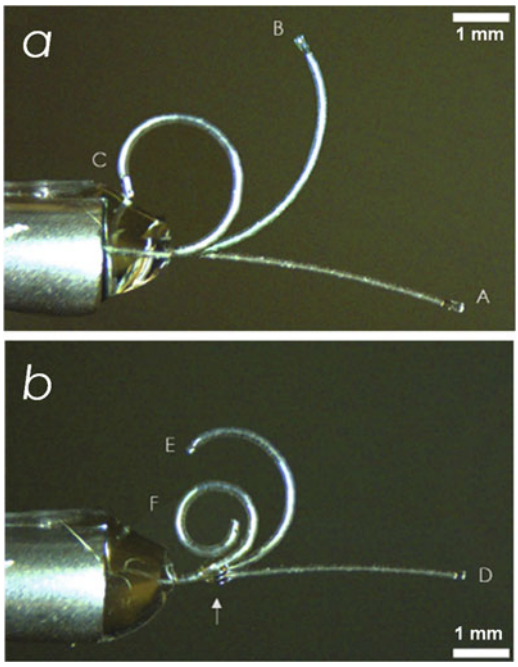

Fig. 4.14 Superimposed images of pneumatically actuated PDMS microtube MT1. Labels *A–C* and *D–F* indicate increasing pressure levels, respectively. (**a**) No hump: Its bending did not develop into spiraling. (**b**) Adding a hump at the arrow point amplified MT1's bending into spiraling

4.5 Addressing Motivations

4.5.1 S^1: Small

As shown in Fig. 4.4, our fabrication method does not require bonding or demolding, the two most challenging processes in soft MEMS fabrication at microscale. Thanks to the *self-adhesive* nature of PDMS in its uncured state, it is also easy to fabricate the microtube structure and add functional modules to it after it was completely tested. All of these render our fabrication process simple and modular, facilitating the realization of smaller devices.

The fabricated microtubes themselves support the claim, with their length L and aspect-ratio reaching 5∼8 mm and >50 while the tube diameter and wall thickness were limited to ∼150 μm and 8∼25 μm, respectively. With further refinements in fabrication techniques, the overall dimensions of the PDMS microtube structure are expected to shrink, rendering themselves increasingly more suitable for operations in highly confined environments.

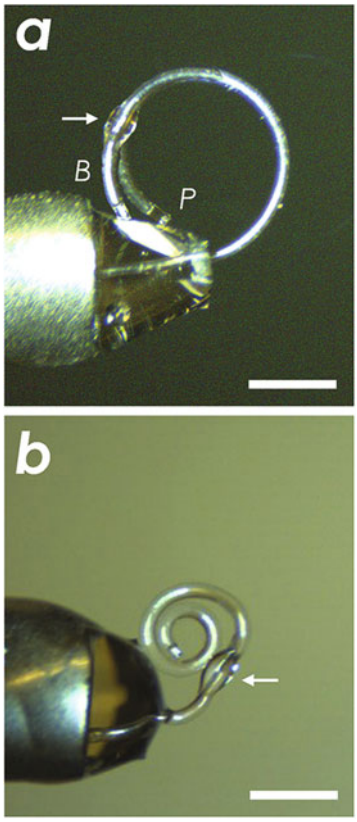

Fig. 4.15 (**a**) Overlapped images of microtube actuations before (*P*) and after (*B*) installing an improperly positioned hump (*arrow-marked*). The RoC got bigger even with the hump. (**b**) Micrograph of a micro-tentacle with a hump (*arrow-marked*) capable of achieving a 2-turn spiraling with the final RoC of 210 μm (Scale bars: 1 mm)

4.5.2 S^2: Soft

The experimental results in Fig. 4.16 confirm that SRMT has extensively exploited the compliance of the material, i.e., PDMS, for its realization and operation. In return, the SRMT actually turned out to provide a highly compliant body to be utilized.

Figure 4.16a shows the levels of its axial elongation and radial expansion at different pressure levels. Clearly, the two morphological changes occurred with a common threshold in the applied pressure ($\sim$ 4.7 psi) below which they became negligible. Beyond the threshold, both the length and radius changed rapidly, eventually getting increased by 5% and 18%, respectively. Such large deformations caused the cross-sectionally asymmetric microtube to bend.

Figure 4.16b and its inset show the decrease in MT1's RoC which also changed abruptly as the pressure surpassed the threshold value. The RoC of MT1 saturated at 1.3 mm at 8.3 psi, forming a ring as shown in Fig. 4.14a.

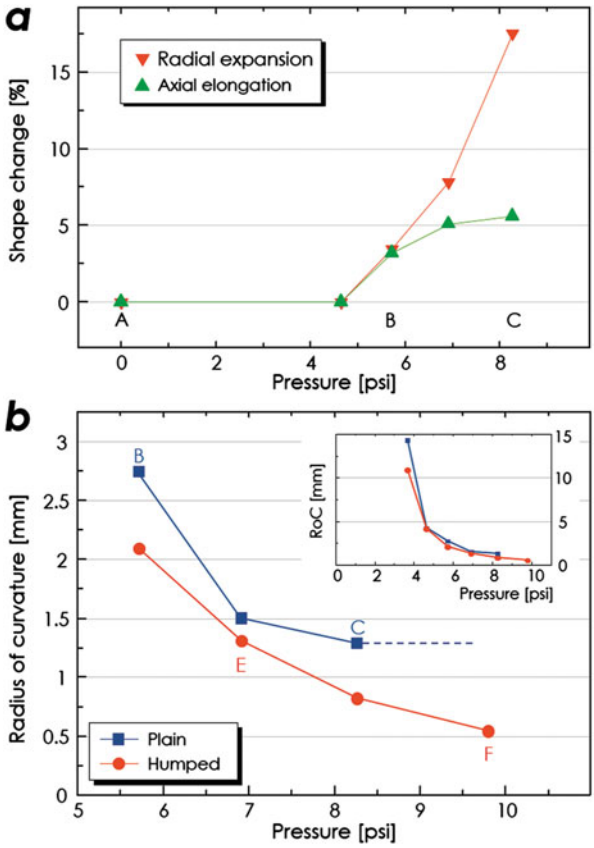

Fig. 4.16 (**a**) Axial and radial shape changes observed in MT1 (before adding the hump) as a function of pressure. (**b**) Changes in MT1's RoC. Without the hump, it saturated at ∼1.3 mm. The hump reduced it to ∼500 µm. The *inset* shows that the RoC decreased rapidly once the pressure surpassed the threshold value at ∼4.7 psi

4.5.3 S^3: Safe

Owing to the use of highly soft PDMS, the de facto standard elastomer for soft MEMS, and its minute form-factor, measured mostly in µms, the SRMT matches the description of the S^3 robot line-by-line, making itself ideal for safe handling of fragile microscale objects.

Experimental Characterization For validation of the claim of safety through experimental measurement of the SRMT's grabbing force, it was configured into a cantilever deflection setup as shown in Fig. 4.17. As the cantilever, a 15 mm-long section of 125 µm-diameter fused silica optical fiber was used. In addition, a rigid, 155 µm-diameter metal wire was installed in parallel with the fiber. Their surface-to-surface separation was 290 µm. Then, the SRMT was set to wrap around both the metal wire and optical fiber so that its grabbing force can function as a point load at h_g to the optical fiber cantilever. The standard beam deflection theory relates the force F and the deflection δc at h_g as:

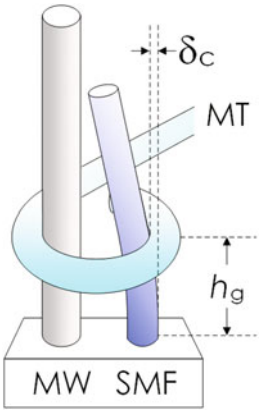

Fig. 4.17 Experimental setup for cantilever deflection measurement
MW metal wire, *SMF* glass optical fiber, *MT* micro-tentacle

$$\delta_c = \frac{F \cdot h_g^3}{3 \cdot E \cdot I} \tag{4.8}$$

$$I = \frac{\pi r^4}{4} \tag{4.9}$$

where

r: Radius of the optical fiber cantilever
E: The material's Young's modulus.

For the measurement, an SRMT with L, d_i, t_1, and t_2 at 5000 µm, 107 µm, 39.1 µm, and 7.2 µm, respectively, was utilized. Its minimum spiraling diameter was 370 µm and the corresponding maximum achievable deflection $\delta_{c,\max}$ was 200 µm. Figure 4.18 shows the measured values of δ_c as a function of h_g at the pressure level of 9.8 psi. Each represents the average of five measurements. The error bar was omitted since the standard deviations were less than 1% of the average values. The force F, estimated through curve-fitting, was approximately 0.78 mN. Only the first four points in the curve-fitting were retained since δ_c approached its maximum possible value and began to saturate beyond $h_g \sim 7.5$ mm.

Novel Safe Grabbing Modality Thanks to the softness of PDMS and the spiraling motion, the SRMT can function as a gentle grabber of microscale objects that can easily be deformed or damaged under rigid grippers. Trial grabbing of biological objects has been performed using a micro-tentacle with L, d_i, t_1, and t_2 at 5000 µm, 104 µm, 31.5 µm, and 6.9 µm, respectively.

The first target was the egg of *Mallotus villosus* which deforms and bursts easily when manipulated with hard tweezers. The optical micrographs in Fig. 4.19a, b were obtained while the egg was being held up by the micro-tentacle. In particular, Fig. 4.19b shows that the micro-tentacle conformally wound itself around the irregularly shaped egg, giving it minimal mechanical stress. No sign of deformation was observed in the released egg. As shown in Fig. 4.19c, we also grabbed and held an ant (approximately 400 µm across the waist) without damaging its body.

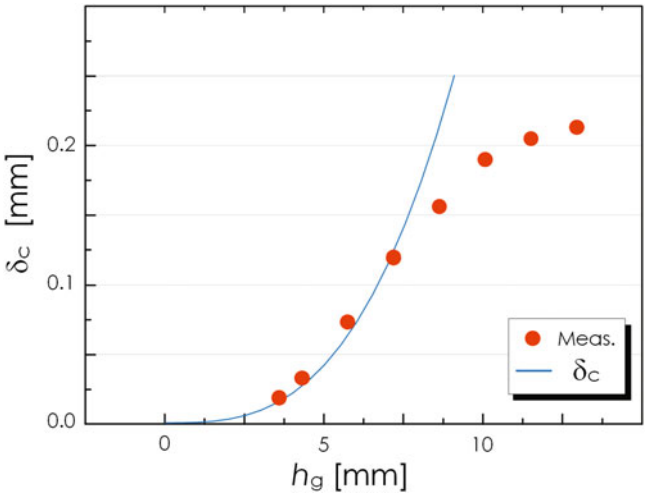

Fig. 4.18 Measured deflection of the cantilever due to the PDMS SRMT's grabbing force. The *solid line* represents δ_c, the deflection at the grabbing point (h_g), calculated based on the standard beam deflection theory with the point-loaded force of 0.78 mN. The measured δ_c begins to deviate from the theory after it exceeds 90 μm, the maximum stroke achievable with the current setup

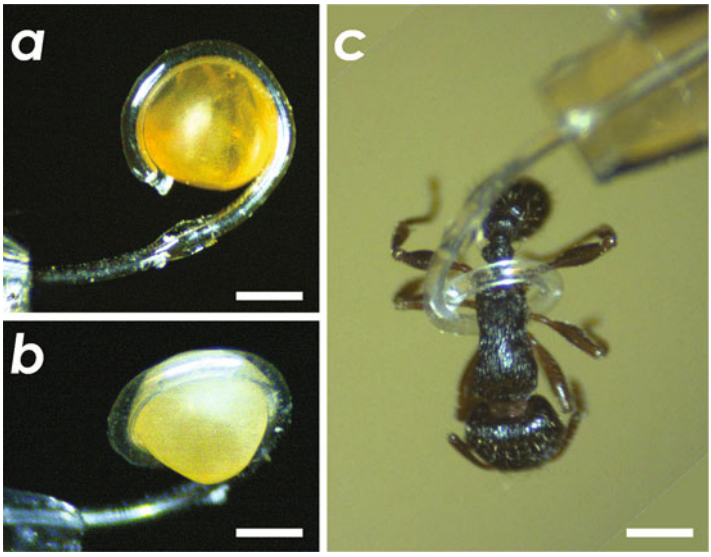

Fig. 4.19 (**a**) and (**b**) Optical micrographs showing the micro-tentacle's ability to grab and hold a *M. villosus* egg by winding around it conformally. (**c**) Optical micrograph of another micro-tentacle grabbing and holding an ant (Scale bars: 500 μm)

The cantilever deflection measurement revealed that the spiraling SRMT's grabbing force is in the vicinity of 0.78 mN at 9.8 psi pneumatic pressure. It indicates that the SRMT produced force very efficiently with a simple and small structure. In fact, the SRMT can be regarded as the bridge between the conventional, larger micro-actuators producing mN-level force and biological micro-organisms such as *C. elegans* capable of producing 62 μN of force [20]. Given that multi-cell aggregates exhibit resilience against force at least up to 1 mN [9], the sub-mN force level of the micro-tentacle can be highly useful for biomedical cellular manipulation.

4.6 Conclusion on Case Study

To conclude, it has been demonstrated that elastomer-based soft-robotic micro-tentacles capable of winding around and holding microscale objects is feasible. The realization of the thin, highly deformable microtubes requires a new fabrication technique based on in situ thermal solidification of PDMS dip-coated around a cylindrical template and direct peeling of the cured structure. Its capability to asymmetrize the microtube's cross-sectional shape enabled the microtube to bend up to a single turn. It is also demonstrated that it is possible to amplify the bending into a life-like, multi-turn spiraling motion through shape engineering. The optimized micro-tentacle exhibited a spiraling motion with two full turns and $\sim$200 μm inner radius, which is ideal for grabbing micro-objects.

Chapter 5
Current Progress

The case study in the previous chapter showed that the motivations and enabling technologies, introduced in the preceding chapters, can function as a good *framework* for assessing the progress in microscale soft robotics and making predictions on its future. The SRMT, however, represents only one facet of the fast-growing field. There are a number of functional building blocks, both static and dynamic, to be perfected for facile realization of S^3 robots. On the other hand, such building blocks must be integrated properly and creatively to step up the ladder of utilization towards the top rung of standalone, autonomous S^3 robotics.

As if reflecting the transitory nature of the field, the levels of progress in the building blocks or utilization are highly diverse. This chapter will first identify major building blocks and utilization levels and their recent progress. Those in their nascent or fledgling stages, however, will be set aside for the subsequent chapter.

5.1 Overview

Similarly to the fields of smartphone or drone research, soft robotics has been showing the signs of becoming an inter-disciplinary, convergent field of study. As the spin-off of the mainstream soft robotics, microscale soft robotics has also been in the path of incorporating technological elements with different flavors. A few of them, such as the microscale actuators, sensors, and interfaces, have already established strong footholds in the field, rendering themselves worthy of separate reviews in this chapter. Their full-scale integration, on the other hand, is also in its due course of progress to achieve the technologically mature forms of microscale autonomous soft machines and microscale soft robots. They all deserve their respective surveys as well. As is frequent in the world of technology, however, the progress is not always direct or streamlined. In fact, the path has been laced with setbacks, detours, and serendipitous breakthroughs. Particularly for the microscale

J. (Jay) Kim, *Microscale Soft Robotics*, SpringerBriefs in Applied Sciences and Technology, DOI 10.1007/978-3-319-50286-1_5

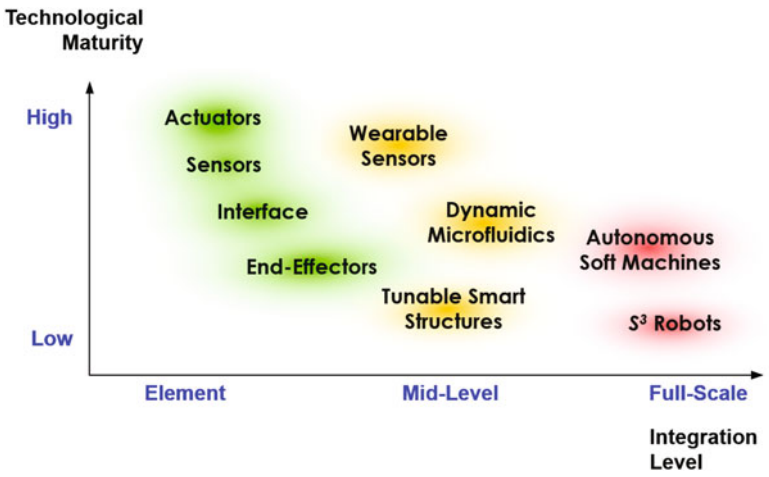

Fig. 5.1 Taxonomy graph on the technological progress in microscale soft robotics

soft robotic technology, a large fraction of its progress has been spawned through its adoption in other standalone, yet not robotic, devices and systems. Good examples include wearable soft sensors, organ-on-a-chip devices, and mechanically tunable smart structures. Those mid-level integrations are also worthy of a brief survey in the sense that they form a cycle of mutual benefit with the mainstream microscale soft robotics, bridging the technological elements and their full-scale integration. Figure 5.1 summarizes the taxonomy. The rest of the chapter will present the survey results on the technological elements, mid-level integrations, and full-scale integrations, in that specific order.

5.2 Building Blocks

Basic concepts and approaches are already described in Sect. 3.3. This section will focus on introducing representative examples of progress in the field ideal for extracting the technological trends in the field.

5.2.1 Actuators

Currently, the progress in the soft actuators can be categorized roughly in two groups, one based on PDMS or related elastomers and the other relying on new materials that are more functional than structural, capable of producing mechanical motion and morphological changes by themselves. Among them, of special interest for soft robotics, and microscale soft robotics in particular, are hydrogels, photo-responsive polymers, and ionic polymers.

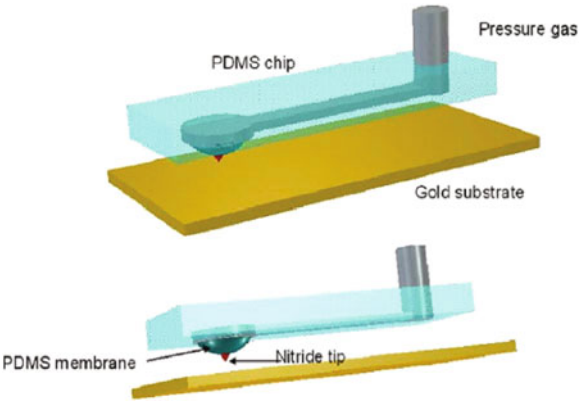

Fig. 5.2 A PDMS-based pneumatic actuator utilized for surface nano-patterning. Reprinted with permission from [147]. Copyright 2007 American Institute of Physics

PDMS-Based Actuators Pneumatic and hydraulic actuators have long been the actuator of choice for soft robotics and the trend has persisted in microscale soft robotics as well. The history and key issues of microscale pneumatic (and also hydraulic) actuators are well-documented in the excellent review of De Volder et al. [146]. During the past decade, the research efforts have been focused on tailoring the miniaturized soft actuators for efficient realization of microscale actuation. In the process, the lessons acquired from biological organisms have played important roles. Again, the spider-inspired actuator for active articulation is a representative example [119]. Contrary to the common consensus that soft actuators are unrefined and/or inaccurate, Li et al. demonstrated that pneumatically actuated elastomeric devices can achieve nanoscale accuracy with the aid of proper control [147]. The soft actuator shown in Fig. 5.2 has been utilized for surface nano-patterning with 200–600 nm feature sizes.

Another major stream of research in the subfield of microscale soft actuator is the quest for new mechanisms to power the actuators. The use of conventional air or hydraulic pumps, which has been taken almost for granted in research and prototyping phases, is in fact against the purpose of S^3 robotics in its requirement for bulky external instruments. A number of physical and chemical mechanisms have been proposed and demonstrated so far. The exploitation of electro-chemical effects, such as electrolysis of various reagents, has turned out to be useful especially when combined with PDMS-based microfluidic structures [148, 149]. There, the process of electrolysis generates bubbles inside microfluidic chambers with at least one side sealed with elastic membranes. The pneumatic force resulting from the inflation has been directly utilized [148] or delivered to other parts of the system through *hydraulic pressure transfer* [149] as shown in Fig. 5.3.

In fact, the bubbles are just a means to induce volume increase inside the confinement chamber and can be replaced by any other volume changing mechanism such as the microspheres made of magnetically responsive elastomer/nanoparticle composite [150] or sound waves in underwater environment [151].

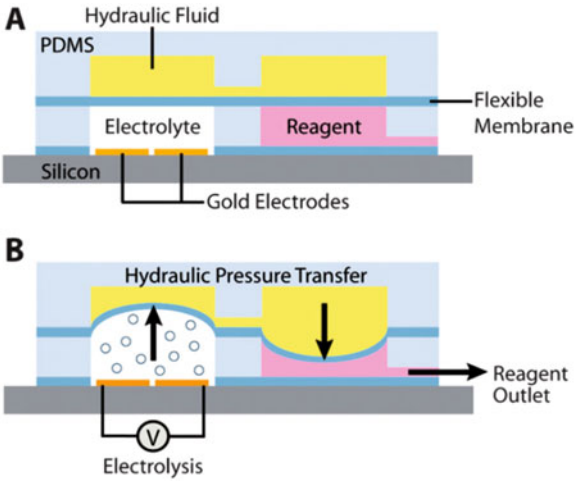

Fig. 5.3 (**a**) A schematic diagram of the electro-hydraulic pump adopting the hydraulic pressure transfer mechanism. (**b**) The bubble pressure formed through the electrolysis is transferred across the flexible membrane to the hydraulic fluid chamber. Reprinted with permission from [149]. Copyright 2010 Royal Society of Chemistry

There have also been continuous efforts to improve and enhance the actuation diversity of pneumatic actuators. Notable examples in the field include the *soft contractile actuator* demonstrated by Walsh and co-workers [64] and the bending-controlled pneumatic actuator by Tekeuchi and co-workers [152]. The former aimed to maximize the degree of freedom in the motion achievable with the conventional McKibben actuator by embedding a number of them in a bigger hosting structure through co-molding. By selectively activating the constituent McKibben actuators, the composite actuator could achieve various forms of deformation. Based on the configuration, Walsh and co-workers realized a pneumatic artificial muscle that can mimic the motions of the ventricle structure of the human heart. On the other hand, Takeuchi and co-workers tried to control the shape of bending in the conventional balloon pneumatic actuator through localized embedding of *stiffness control elements*. In the practical embodiment, the localized stiffness control was achieved with low melting temperature alloy embedded in PDMS and a nichromewire for its heating.

The role of PDMS or other elastomers in soft actuators, however, has not been restricted to that as the structural material for realizing pneumatic chambers. In a series of reports [153–155] Bergbreiter and co-workers have shown that elastomeric structure can be hybridized with silicon-based rigid MEMS to form the energy storage and/or quick-release actuators. The PDMS portion practically functioned as the *rubber string*, contributing eventually to the realization of *jumping* microrobots.

Hydrogel-Based Actuators Hydrogels have been receiving especially intense research interests from the field of soft robotics for their proven usefulness in realizing bio-mimetic and/or programmable actuators structures [156]. Conventionally, they have been utilized as a part of large-scale microfluidic [157] devices. Recently, their application has been expanded into the implementation of full-scale *aquabots* [158] and *microgrippers* for intra-vascular use [159]. Recently, a special form of

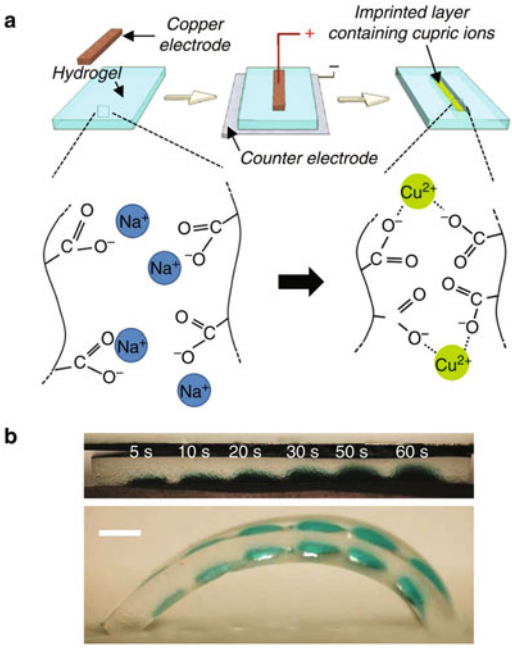

Fig. 5.4 (**a**) A schematic diagram illustrating the electro-chemical process within the hydrogel actuator demonstrated by Palleau et al. (**b**) Side views of an ionoprinted pNaAc gel at differing temporal points under 5 V (scale bar: 3 mm). Reprinted with permission from [161]. Copyright 2013 Nature

hydrogel has carried out the role of the stretchable electrode material for a dielectric elastomeric actuator [160], as shown in Fig. 5.4, re-confirming the versatility of the hydrogel. The difficulties in their small-scale patterning and shaping have been the challenges to overcome for their wider adoption but recent progress in various patterning and printing technologies is indicative of their imminent conquest [161].

Ionic Polymers Ionic polymers, capable of generating morphological changes and mechanical motion in response to applied electric field through migration of ions, are of great interest for microscale soft robotics as well. On top of the lightness and flexibility, they also offer mechanical robustness, another important factor to the utility of the completed device. Frequently adopted ionic polymers include those based on poly(vinylidene fluoride) (PVdF) [162, 163], π-conjugated polymers [164], and Nafion [165].

Photoresponsive Polymers The main hurdle to the adoption of the ionic polymers in microscale soft robots may be the need for electrical interfacing elements, such as wires, that are flexible and stretchable for their actuation and control. In that regard, actuation based on photoresponsive polymers or composite materials is highly attractive [166]. In many cases, they do not require physical connections, providing wireless access to the actuators. Even in the case of wired access, it can be achieved through optical waveguides that can be realized with flexible materials in a much more easily than the electrical counterparts.

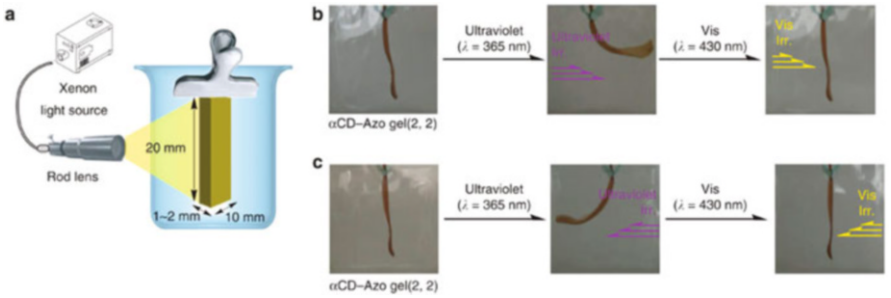

Fig. 5.5 Light irradiation experiments with the setup in (**a**) confirmed that the new composite hydrogel can produce reversible bending in directions opposite to that of the incoming light (**b**) and (**c**). Reprinted with permission from [167]. Copyright 2012 Nature

One example is shown in Fig. 5.5 [167]. In that work, hydrogel becomes mechanically photoresponsive through the introduction of host and guest materials that are also photoresponsive. Upon irradiation with light, such compositions typically lead to formation/dissociation of an inclusion complex which, in turn, leads to sol-gel phase transitions. Through judicious choices for the host (α-cyclodextrin) and guest (azobenzene derivative) materials, however, it has been converted into reversible expansion–contraction behaviors that can directly be utilized for light-driven actuation. Figure 5.5b and c shows that a plate made of the photoresponsive hydrogel can bend repeatedly and reversibly with alternating applications of UV (365 nm) and visible (430 nm) lights.

Another important type of mechanically photoresponsive soft material is the liquid crystal elastomer (LCE) [168–170]. LCEs are unique in exhibiting the entropic elasticity of the elastomer and self-aligning capability of the liquid crystal simultaneously. Figure 5.6a shows the basic principle of the light-driven actuation. It is based on two effects. First, due to the 3D cross-linking inside the LCE, the liquid-crystal molecules must undergo shape or alignment changes collectively, not individually. Second, the actinic light cannot penetrate deeply into the LCE due to the high attenuation at the surface. When combined, these two effects lead to macroscopic volume changes and bending either towards or away from the actinic light, depending on whether their initial molecular orientation was homogenous or homeotropic [168].

Such a volume change is highly useful for many *soft actuation* applications. One notable example is the light-controlled tactile display pixel (or *taxel*) shown in Fig. 5.6b [171]. It is worth pointing out the fact that the configuration has reinforced the usual expansion–contraction cycle of LCE with the inclusion of thermal effect by adopting CNT-mixed LCE instead of plain LCE.

Other types of mechanically stimulus-responsive polymers have been continuously emerging from the research and development phases for clever adoptions in soft robotics. One interesting example is the porous polymer actuator activated by solvent molecules [172]. In practice, the actuator exhibited sub-second response,

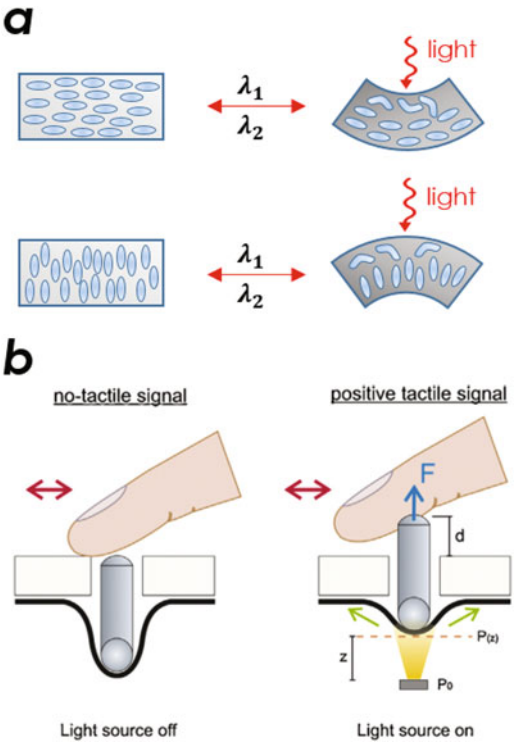

Fig. 5.6 (**a**) The basic principle of the light-driven LCE actuation. (**b**) A schematic illustration of the *U-shaped* LCE-CNT ribbon actuator and its application for tactile signal generation. Reprinted with permission from [171]. Copyright 2014 Elsevier

which will be useful for many grabbing operations in the future. Also of further interest is the hybridization of the mechanical actuation and optical functionalities such as the *color-tunable photonic actuator* [173] that can change both the shape and color simultaneously in response to chemical signals.

5.2.2 Sensors

The fields of microscale soft robotics and transducers/sensors share an interesting history of mutual interaction. The outcome of their interaction first came in the form of miniature force/contact sensors based on compliant mechanics [174–177]. One notable configuration is shown schematically in Fig. 5.7. There, the force sensing structure is made typically of highly deformable materials, such as PDMS. The two paired vertical bars, attached to the horizontal bar within the rectangular bracket, are initially parallel to each other. Any mechanical perturbation to the horizontal bar, due to the probing tip's contact with an external object, however, will tilt them and widen their separation. Depending on the length of the vertical bar, even a minute displacement in the horizontal bar side can be greatly amplified at the terminal tips of the vertical bars. The *lever displacement amplifier* action generates

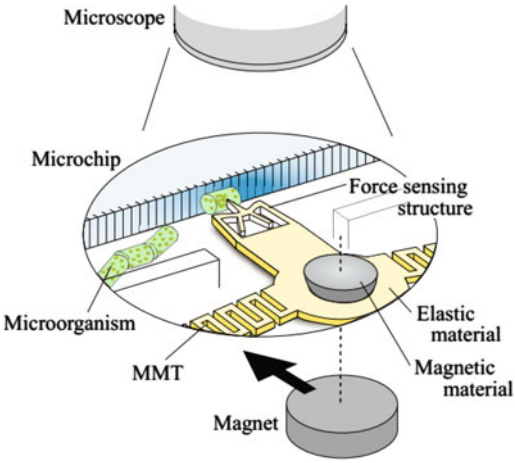

Fig. 5.7 One example of compliant mechanics-based force sensor. Reprinted with permission from [177]. Copyright 2017 Springer

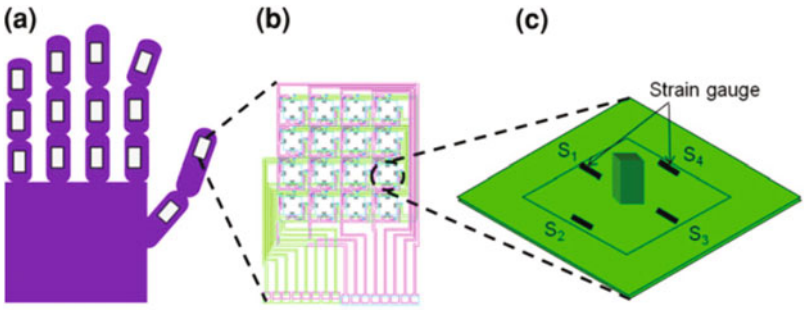

Fig. 5.8 Diagram illustrating the tactile sensor array at (**a**) device, (**b**) taxel, and (**c**) strain transducer levels. Reprinted with permission from [178]. Copyright 2011 Springer

deformations easily detectable with the help of optical microscopes, facilitating its use in biomedical applications. It has demonstrated μN-level force sensitivity [175] and got integrated as a part of a microscale robot as well [176].

The compliant mechanics-based sensing schemes, interesting and useful as they are for under-the-microscope operations, are not well-suited for microscale soft robots that are intended for un-guided, standalone operations. In fact, there has been a separate line of research on such integrated, elastomer-compatible sensors with the main goal of realizing wearable, body-comfortable force/tactile sensors [178–182]. Figure 5.8 shows one example [178]. The concepts and fabrication techniques developed for such sensors have definitely proven helpful to the progress of sensors for microscale soft robots. However, their heavy reliance on metallic elements, arising from their inherent exploitation of resistive [178], capacitive [179, 181], inductive [180], or transistor-action [182], has long been recognized as the challenges to small-scale integration.

As described in Sect. 3.3 briefly, the use of non-metallic, intrinsically flexible/stretchable materials, such as graphene or conducting fluid, in a totally embedded fashion can be more promising for microscale soft robotic integration [183–185]. Initially, the trend began as an attempt to replace the metallic part with non-metallic ones. Currently, the configurations have evolved to produce their own unique features through proactive embracing of technologies derived from microfluidics and/or 3D-printing. The 3D-printed strain sensor in [183] is a good example of such combined exploitation. In the work, the sensing element is made of filaments of conducting fluid directly injected into the bulk of the uncured elastomer through the syringe needle. The void created by the motion of the needle gets eliminated by the influx of the liquid-phase filler which eventually coagulates with the main elastomer body.

The flexible, non-metallic conducting materials, however, haven't been implemented in planar forms as shown above all the time. Again, concepts can be borrowed from the biological world. One example is the flexible/compliant sensor mimicking the cupula receptors [186]. There, a composite material comprising piezo-resistive elements and elastomeric hosting matrix are formed into pillar arrays with molded top-cups, as shown in Fig. 5.9.

Among all of these rapidly progressing fields of soft material-based sensor technology, two new developments are of particular interest to microscale soft robotics. One is the adoption of optical, rather than electrical, transduction mechanisms. Optical transduction schemes can be advantageous over electrical ones by offering immunity to electromagnetic interference (EMI), spark-free operation, and inherent compatibility with stretchable all-dielectric elements for sensing and information delivery. Figure 5.10a shows one example in which the external pressure-induced deformation of the light path becomes transduced into changes in optical transmission [189]. Its flexible substrate-based implementation renders it highly suitable for integration with microscale soft robots.

The other is the direct utilization of the deformation-induced fluid flow inside a microfluidic channel network as the transduction element [188], as illustrated

Fig. 5.9 Completed artificial cupular receptor. Reprinted with permission from [186]. Copyright 2010 Elsevier

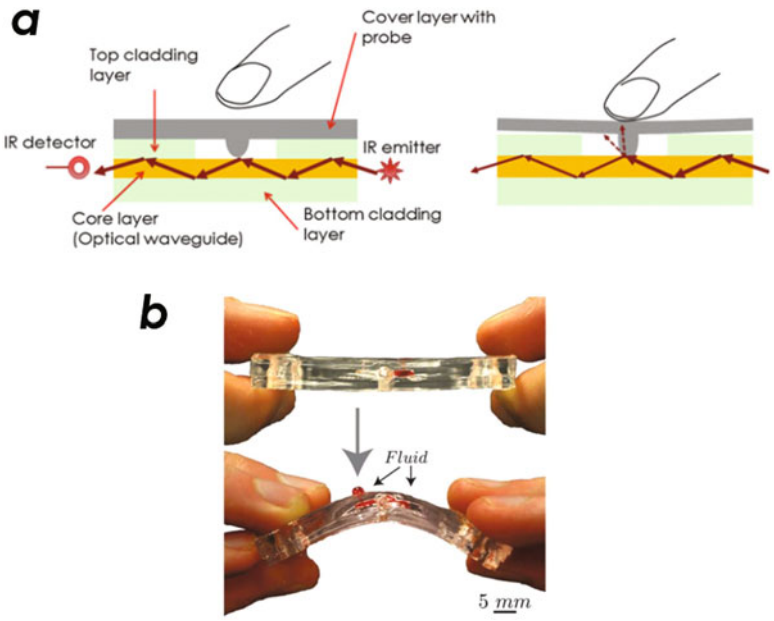

Fig. 5.10 Schematic illustrations of promising future sensing mechanisms based on (**a**) optical waveguiding (Reprinted with permission from [187]. Copyright 2015 Springer.) and (**b**) deformation-induced flows in microfluidic channels (Reprinted with permission from [188]. Copyright 2013 Royal Society of Chemistry)

in Fig. 5.10b. Although it is in its nascent phase, the concept has high potential for future realization of all-microfluidic, autonomous sensing/control hybrids which mimic the architectures and working principles of insects and small animals.

5.2.3 End-Effectors

The *end-effector* refers to the specific portion of a robot which acts directly on the object. The use of the term is especially frequent in biomedical robotics in which the robots are expected to perform various delicate operations to small, highly confined objects such as blood vessels or organs.

In microscale soft robotics, it is common to see their whole body functioning as the end-effector. For some specific tasks, however, only a small portion of the whole body is reserved to the given task while the rest only provides structural support and interface. In either case, the importance of the end-effector cannot be overemphasized. This section reviews the current progress in microscale soft robotics with special emphases on

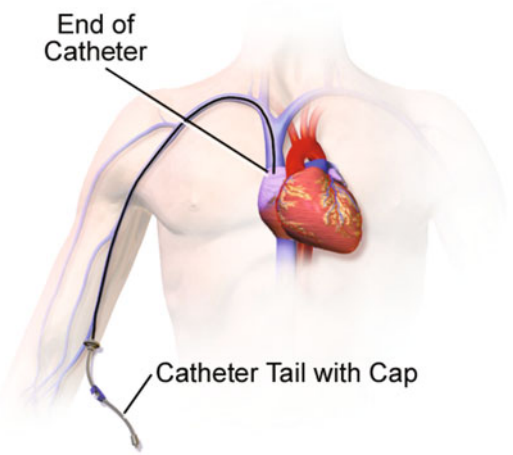

Fig. 5.11 At the branches or highly curved portions of vasculature, the catheter must be able to re-orient itself (Image from *Wikimedia Commons*)

- Intra-vascular Navigation
- Grabbing
- Manipulation
- Sensing and Probing
- Stimulation
- Machining

It is straightforward to see that most end-effector tasks are biomedically oriented. It is, however, not entirely impossible to find non-biomedical end-effectors [147].

Intra-Vascular Navigation Catheters are ubiquitous in clinical practices, intra-vascular interventions in particular. At the branches or highly curved portions of vasculature, the catheter must be able to re-orient itself to reach the intended destination, as shown in Fig. 5.11 [190]. In fact, such a need for re-orientation also occurs for endoscopes that are generally bigger than catheters.

The intra-vascular *navigation* tasks are highly challenging due to the space constraint and, more importantly, the extreme safety concerns over the possibility of damaging the biological environment, such as puncturing the blood vessel wall. Thanks to their S^3 nature, microscale soft robots are regarded as the best candidate for the task. Of the highest level of interest among them are the microtube-based robots and actuators, such as the SRMT introduced in Chap. 4. They fit the blood vessel naturally and can be made with bio-compatible materials.

A large number of tube-shaped, catheter-compatible soft robotic devices, either intended for end-effector uses or just exhibiting inherent compatibility with the intra-vascular navigation tasks, have already been demonstrated [140, 191–194]. One notable example is the navigator exploiting a *Membrane Micro Embossed* microtube made of the bio-compatible polymer PLA (polylactic acid) [193]. Upon pneumatic actuation, the PLA microtube with 300 μm in diameter bends towards the thinner side, rendering itself ideal for navigation in thin blood vessels.

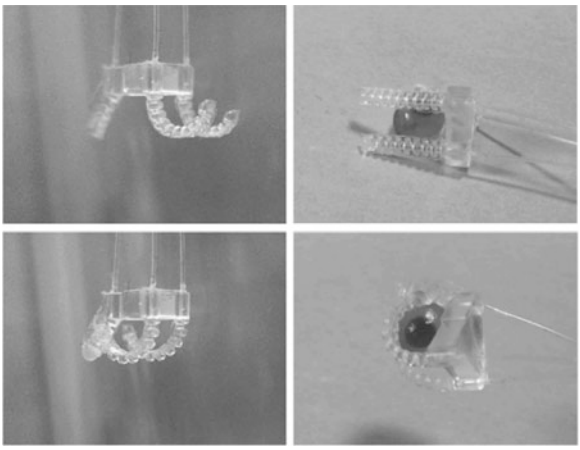

Fig. 5.12 A soft microhand based on miniature pneumatic curling rubber actuator holding a 5 mm-diameter fish egg. Reprinted with permission from [140]. Copyright 2011 Taylor and Francis

Object Grabbing and Manipulation Another important end-effector task is grabbing and manipulation of microscale objects. Again, they can be greatly challenging since the objects are usually soft, delicate, and fragile. Biological tissues, animal eggs, plant pollen, and cell spheroids are good examples. The microtube-based actuators introduced above have exhibited excellency in grabbing and manipulation as well in general. One example is shown in Fig. 5.12. There, two microtube-based pneumatic actuators, with its curling capability enhanced through the adoption of bellows-like single-side corrugation, are configured into a *soft hand* capable of grabbing and holding a fish egg [140]. Individual *fingers* are only 300 μm thin.

Such a *finger-like* grabbing motion has been achieved in many other types of microscale soft actuators as well. Pneumatically expanding chambers can be paired to produce grabbing [195], pinching [9], and gripping [196] motions that are useful, even essential, to various biomedical and clinical operations.

The end-effector motions for grabbing and manipulation, however, are not limited to the hand-like two-fingered motion. In Fig. 4.1 in the previous chapter, it was already suggested that the tentacle-like wrapping-around motion can be advantageous over those based on two-fingered gripping. The rolling-based polymorphism described in Chap. 2 is also a unique one with great potential for intra-body operations [18]. The deformability of the elastomer, one of the main motivations for microscale soft robotics, enables facile realization of new grabbing and manipulation modalities. One recent example is the pneumatic planar actuator that can turn bending into twisting through the use of tilted surface corrugation [141] (Fig. 5.13) that can easily be extended into unique grabbing and holding modalities.

Sensing, Probing, and Stimulation Biological structures, all the way from singles cells to tissues and organs, are designed to take mechanical cues from their environment for proper operation. The endothelial cells lining the inner wall of blood vessels have been the focus of intense research for years. It did not take a long time for the researchers to be convinced that the endothelial cells cultured

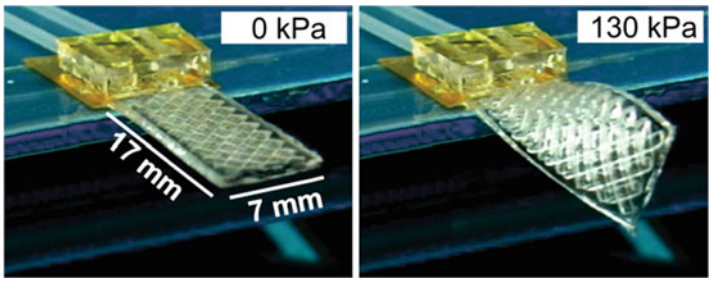

Fig. 5.13 A flexible pneumatic twisting actuator. Reprinted with permission from [141]. Copyright 2014 Elsevier

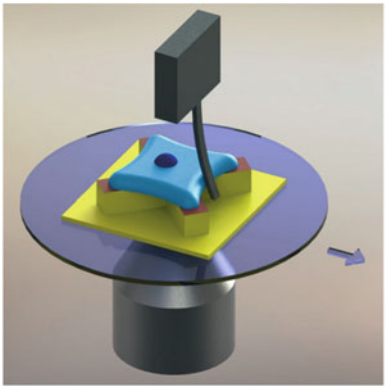

Fig. 5.14 A sketch of *ultra-soft* cantilever for mechanical stimulation and characterization of a single cell (*blue*) mounted on an x-shaped microstructure (*yellow*). Reprinted with permission from [197]. Copyright 2014 Royal Society of Chemistry

under static condition do not faithfully reproduce the physiological conditions they exhibit in natural situations. In reality, blood vessels, along with their endothelial cells, are under constant strain due to pulsatile blood flow. Missing the mechanical cues could render many in vitro experiments physiologically irrelevant. Due to this aspect, the mechanical stimulation of biological organisms has become a major task for MEMS devices from their early days [198].

On the other hand, the mechanical response of the biological structures, again from single cells to organs, has also been attracting significant research interests from a variety of fields [199]. The interesting point is that the two lines operations, with Stimulation on one side and Sensing on the other side, can be handled with the same type of end-effector. Again, microscale soft end-effectors are preferred for size and safety considerations.

One good example has already been introduced in Fig. 5.7 in the previous section. The setup was used as an example of force sensor but Kawahara et al. have also utilized the same setup for stimulation of cells with the help of the magnet [200]. Examples of such dualism in functionality are abundant in the field of bio-MEMS. For instance, Vianay and co-workers have implemented *ultra-soft* cantilevers to investigate the contractile bundle tension of a single cell [197]. As shown in Fig. 5.14, the ultra-soft cantilever made of SU-8 has been utilized for both stimulation and characterization simultaneously.

5.3 Mid-Level Integration

As stated in Sect. 5.1 and also in Fig. 5.1, the mid-level integration does not directly lead to microscale soft robots or similar standalone devices. It, however, is important since it completes a circle of mutual benefit with other academically important fields such as microfluidics and optics. The dynamic and re-configurable aspects of microsystems developed for S^3 robots can be applied to bio-MEMS and micro-optics while the cross-disciplinary functionalities can be adopted back in robotics to enrich the utility of the S^3 robots. Such a cycle of mutual benefit is in continuous motion.

5.3.1 Integration with Microfluidics/Bio-MEMS

Incorporation of dynamically re-shapable and/or re-configurable elements, typically made of highly deformable material, into microfluidic and bio-MEMS devices has been carried out in two major streams. The first one is the thrust to reproduce the physiological environment on chip, which was briefly introduced in Sect. 3.2. The most important factor to S^3 robotics is the technological elements developed for providing mechanical cues to the cells in the device, which was faithfully realized in the *lung-on-a-chip* shown in Fig. 3.6 with the help of a stretchable PDMS membrane, which is also an essential element in S^3 robotics.

The work has also been extended to the replication of vasculature along with its periodic expansion–contraction cycle (also known as *vasomimetics*) [201] and goes beyond the planar regime towards the 3D-printed replication of the cylindrical blood vessels themselves [202] as shown in Fig. 5.15. Given the importance of the 3D tube-like structures in microscale robotics, the vasomimetic outcomes confirm the existence of the cycle of mutual benefit mentioned above.

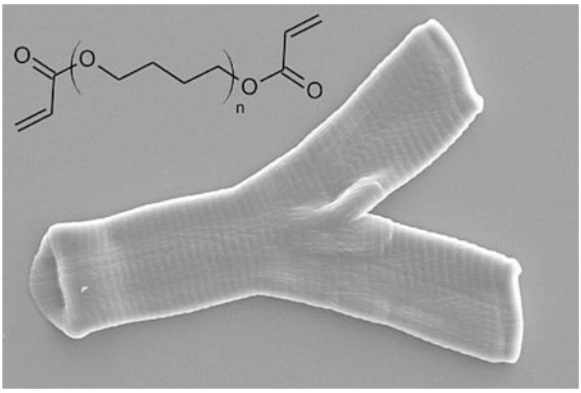

Fig. 5.15 A scanning electron micrograph of a 3D-printed artificial blood vessel with a physiologically realistic branching point. Reprinted with permission from [202]. Copyright 2012 MDPI

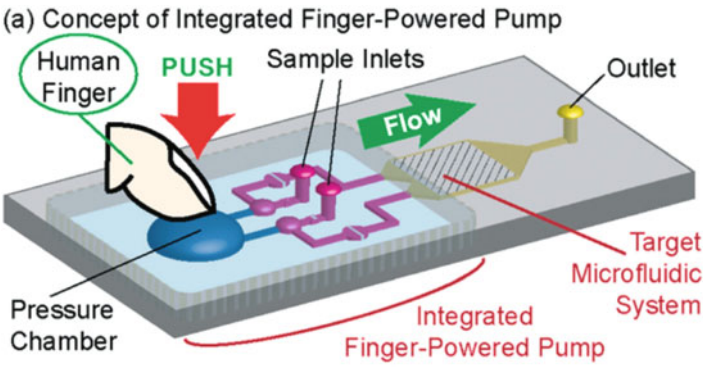

Fig. 5.16 A schematic diagram of *finger-powered* microfluidics based on thin membrane-capped pressure chamber (*blue*). Reprinted with permission from [206]. Copyright 2014 Royal Society of Chemistry

In parallel, the deformable elements have also been endowing dynamic re-configurability to microfluidic and bio-MEMS devices. Examples are abundant [203–207]. In the work described in [203], the microfluidic chip itself was mechanically stretched and un-stretched so that the pitch of the micropillar array inside the microfluidic channel can be modulated. Since the pillar-to-pillar distance affects the propagation direction of the particles inside the micro-flow, the overall structure eventually functioned as a tunable particle sorter or filter.

In another line of the effort, the deformability of the elastomeric microfluidic device has been exploited to enable manual, even *finger-powered*, actuation of the device. In most cases, those schemes utilize thin membrane-capped chambers with check-valves, or fluidic diodes, to induce the desired one-directional microscale flows, as shown in Fig. 5.16. These efforts originally aim to free microfluidic devices from bulky and/or cumbersome external apparatus so that they can be used in resource-limited areas such as the third world. On the microscale robotics side, this line of research has potential to open new avenues of possibilities to power and control microscale soft robots and devices manually.

5.3.2 Integration with Optics

Integration of the elastomeric structure's deformability and re-configurability with optical functionalities for the purpose of producing *mechanically tunable smart optics* has been performed since the dawn of optics-quality elastomers. In fact, some early reports of elastomer-based actively tunable optics date all the way back to 1970s [208].

In the trichonomy chart in Fig. 3.11, such an effort falls in the category of *convergence*-level integration. However, it did not take a long time for the integration effort

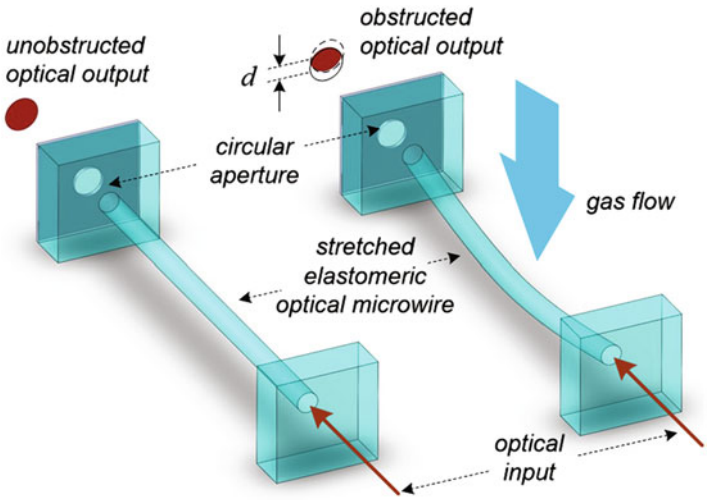

Fig. 5.17 A schematic diagram showing the operational principle of the PDMS microwire-based optical gas-flow sensor

to evolve into the level of *critical* integration in which the structural deformability and the optical functionality become inseparable and their co-existence inevitable.

One good example of such a critical level integration is shown in Fig. 5.17 [23]. In fact, the setup utilizes the PDMS microwire introduced in Fig. 3.1b as the example of the excellent stretchability of PDMS-based structures. Thanks to the optical transparency of PDMS, the microwire can function as a lightguide as shown in the left panel of Fig. 5.17. The transmission, of course, is the maximum when the lightguide remains straight. Any gas-flow that can bend the lightguide due to fluidic drag, however, can alter the light path and reduce the transmission, as illustrated in the right panel of Fig. 5.17. This type of configuration enables all-optical monitoring of gas-flow that can be extremely useful thanks to the spark-free, EMI-immune nature of optical sensing.

A more important aspect of the system in Fig. 5.17 is that it has been conceived from scratch with the availability of highly stretchable, easy-to-bend, optically clear microwire in mind. In that sense, the integration qualifies for the critical level title.

Figure 5.18 shows another example of such critical level-integrated, mechanically tunable smart optical structure [209]. It consists of a PDMS block randomly embedded with transparent microbeads. Under no strain, the composite structure maintains transparency. Under lateral stretch, however, ellipsoidal voids start to appear around individual microbeads, producing anisotropic light deflection that can change the light transmission depending on both the color and angle.

It should be categorized as another example of the critical level integration due primarily to the existence and exploitation of the ellipsoidal void. Stretching-based displacement of internally embedded inner structure has seen widespread adoptions

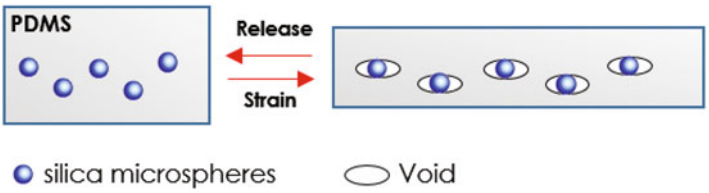

Fig. 5.18 The operational principle of the mechanically tunable display that can be reversibly switched from high transparency to angle-independent structural color [209]

for many applications. This one, however, relies on the specific effect that can only be obtained through the combination of a rigid embed and elastomeric hosting structure. Again in the light of microscale soft robotics, this type of *embedded smartness* is expected to add values and functionalities to future S^3 robots.

5.4 Microscale Autonomous Soft Machines

As indicated in Fig. 5.1, the category of microscale *autonomous soft machine* straddles mid-level and full-level integration, positioning itself between enabling technologies and fully fledged S^3 robots. They are, however, important for their potential to become the inner working components of autonomous, smart robots in future. This section will briefly survey the technological preparedness in that aspect.

5.4.1 Microfludic Feedback and Autonomy

Feedback is the principal basis for self-regulation and autonomy. For the past few years, researchers in bio-MEMS have begun to embrace the analogy between microfluidic and electronic networks and started to build things that can be best described as *electronics-inspired microfluidics*. Given the fact that the analogy between passive components, shown in Fig. 5.19a has been known since the nineteenth century, at the heart of the newly popular analogy is the correspondence between the transistor and the pneumatic valve in Fig. 5.19b. The basic operation of the pneumatic valve is very simple as shown in Fig. 5.19c and d.

Based on these straightforward analogies, a variety of microfluidic networks with feedback, autonomy, self-regulation, frequency discrimination, cascaded logic, and instability have been created [210–214]. This type of *microfluidic autonomy* is as promising as exciting owing to their all-microfluidic implementation. Further research will push the topic towards the realization of totally autonomous network which will be of great value for future microscale soft robotics as well. Of possible help to the development will be the current research on *nonlinear* microfluidics which aims to exploit the inherent nonlinearity of the microfluidic channels made of easily deformable, elastic materials such as PDMS [215–217].

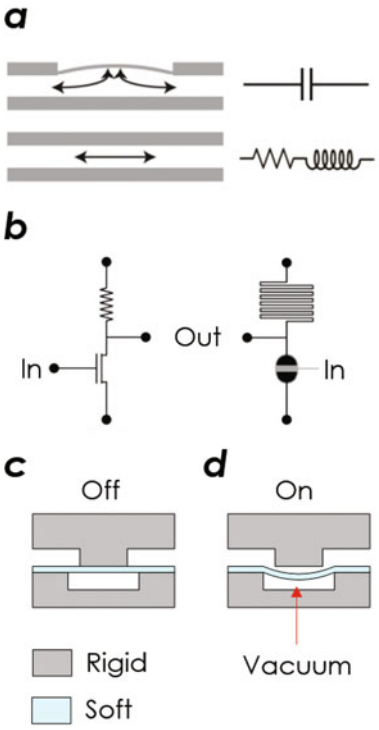

Fig. 5.19
(**a**) Electronic-fluidic analogy for passive elements. (**b**) Transistor-pneumatic valve analogy. (**c**, **d**) Operating principle of the pneumatic valve

5.4.2 Opto-Mechanical Feedback

Another type of autonomous soft machine can be found in the relatively unexpected field of photovoltaics. The corresponding key issue is solar tracking [218–221]. Due to the continuous change in daily and annual solar paths, the solar panels are in need of active sun-tracking. The issue becomes especially serious for edge-installed solar panels illustrated in Fig. 5.20a. There, the incoming sunlight must be re-directed into a lateral propagation to reach the photovoltaic devices installed along the edge. This configuration helps increase the overall efficiency of energy conversion but has the downside of necessitating the light re-direction process. Typically, it has been accomplished by collecting the light with a lens array with each lens paired to a light re-directing element, such as a prismatic reflector, as shown in Fig. 5.20b. It turned out to be an effective process but bound to be invalidated by the change in incidence angle due to the solar movement, as shown in Fig. 5.20c. Installing extra light re-direction elements, however, has not been recommended since they tend to scatter the light already captured inside the panel, reducing the photovoltaic conversion efficiency.

The scheme illustrated in Fig. 5.20d is an autonomous, self-regulating solution based on the use of phase-change material (PCM) [218]. In the setup, the bottom of the panel, made of think elastomeric membrane, is originally flat, guaranteeing

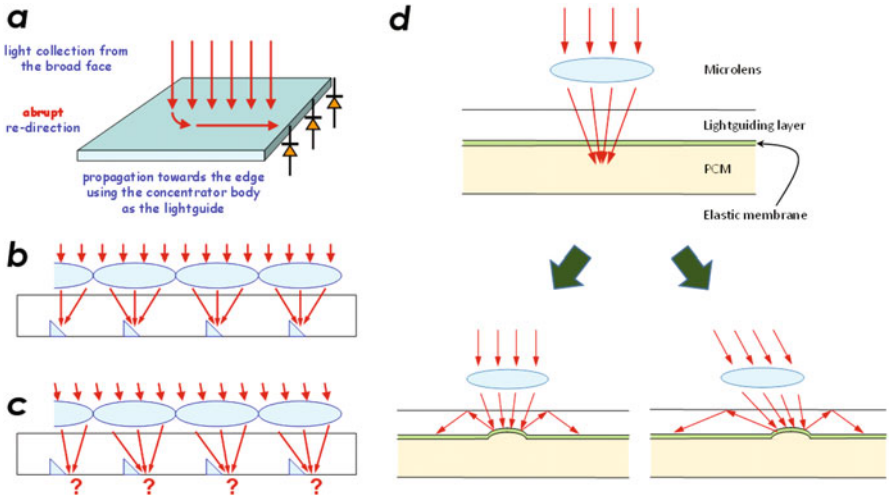

Fig. 5.20 (**a**) A schematic diagram of edge-installed type solar panel. (**b**) A microlens and light re-director pair can trap light within the panel until (**c**) the incidence angle change spoils the re-direction effect. (**d**) The schematic view of a phase-change material (PCM)-based autonomous light re-direction scheme [218]

minimal level of scattering to the captured light. The re-direction of the incoming light is handled by the PCM which expands in volume under heating. The microlenses are designed to put the focal spots on the bottom plane, right into the PCM, so that bulges can be formed along the illumination. The bulge, clearly shown in 5.20d, functions as the light re-direction element. In this way, the light re-direction element can be formed *on-demand*, rather than in a fixed fashion, increasing the overall light re-direction efficiency.

The adoption of PCM, a variant of paraffin wax in many cases, can be significant to microscale soft robotics at least in two aspects. Above all, it indicates that a new, active modality based on elastomeric, highly deformable structure has been added to the arsenal of microscale soft robotics. Secondly, the sunlight can be a good and widely available source of power for microscale soft robots to be deployed outdoors in a standalone, isolated fashion. More research must be provided to push the current status to maturity, of course.

The system shown in Fig. 5.21a shows one example of such effort [221]. It consists of one main, rigid lightguide and one *branching*, flexible lightguide separated by a spacer. They are both mounted on a PDMS block containing a chamber filled with PCM (paraffin wax) and covered by a thin PDMS membrane. The main goal of the setup is to regulate the level of light throughput that passes through the main lightguide in an standalone, autonomous fashion. An opto-mechanical feedback is realized for that purpose.

As shown in Fig. 5.21b, a small portion of the incoming light will be fed into the PCM chamber to induce optothermal excitation. The increase in the PCM volume

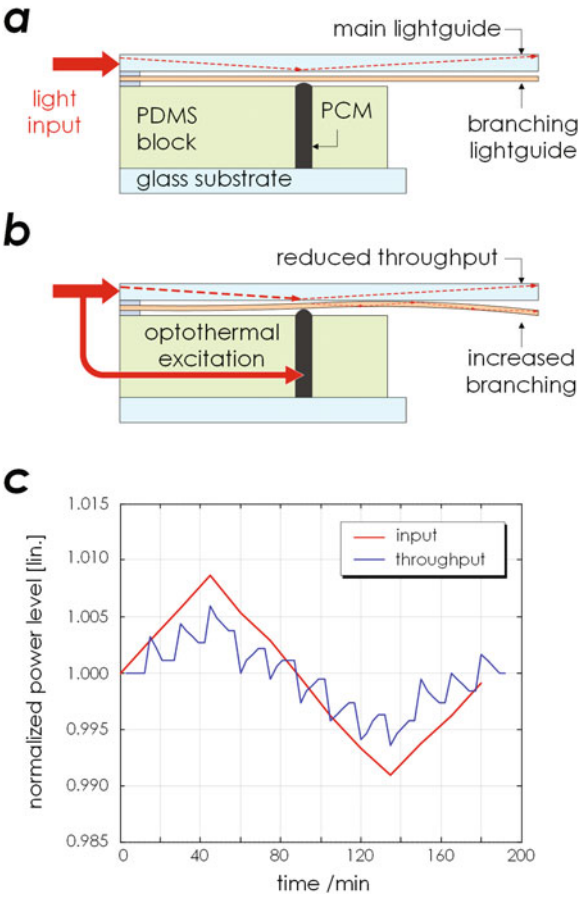

Fig. 5.21 Schematic diagrams of (**a**) the PCM-based light-level regulator and (**b**) its operation principle. (**c**) The experimentally measured optical throughput under opto-mechanical feedback

will make a bulge towards the PDMS membrane and eventually push the branching lightguide towards the main one. Since the lightguide confines the throughput using total internal reflection based on index contrast, the approach and contact of the branching lightguide will inevitably cause escape of the light into it, reducing the throughput and completing the opto-mechanical feedback.

Figure 5.21c shows the measured results. The initial position of the branching lightguide was set to the midpoint between the spacer so that the PCM actuator can function both positively and negatively. The throughput level shows that while the light input increases linearly, the throughput repeats up-and-down fluctuations repeatedly, tying to return to its initially set value. It reacts in the same fashion towards the linear decrease of the light input, confirming the action of the opto-mechanical feedback.

Chapter 6
Towards Full-Scale Integration and Beyond

The previous chapters surveyed the progress made in various sub-fields of microscale soft robotics in recent years. The field is undeniably undergoing rapid changes and expansions, making their survey quite challenging yet exciting. By the time of publication, it is also very probable that the state of the art of the field has already evolved into something very different from a simple sum of the technological building blocks surveyed in the previous chapters. In accordance, this final chapter will review some of the important long-term, essential agendas in microscale soft robotics which will surely stay valid for a longer period of time. Beyond a brief overview, the topics will be discussed by their order in the implementation steps in general, with the materials and fabrication aspects reviewed first and the application of the completed units later.

6.1 Fully Integrated Microscale Soft Robots

Having to start the final chapter of a book dedicated to the microscale soft robot with the declaration on its absence may seem strange and even ironic but also inevitable given the current status of the technology. To qualify as a microscale soft robot in a strict sense, the robot must be made mostly of soft, biologically compliance-matched materials, at least sub-centimetric in dimensions, and able to maneuver and perform given tasks autonomously in an untethered fashion, without relying on externally supplied power or control. Despite all the progress made in the field, and also the availability of so many technological building blocks in soft and/or smart forms, such a fully standalone microscale soft robot has not been reported yet.

Figure 6.1 shows one soft robot, nicknamed *Octobot*, demonstrated by researchers of Harvard University and Cornell University that matches the description given above most closely [222]. It is the outcome of a joint effort by specialists from many fields including microfluidics, mechanical engineering,

J. (Jay) Kim, *Microscale Soft Robotics*, SpringerBriefs in Applied Sciences and Technology, DOI 10.1007/978-3-319-50286-1_6

material science, and 3D-printing. The robot is significant, above all, in achieving the basic control and actuation in an *all-soft* body, without using any rigid material, for the first time in this field of study. The two main sources of the demand for rigid components, i.e., energy-storage and control, are entirely implemented in soft format through the adoption of chemical reaction-based pneumatic actuation and microfluidic logic (surveyed in Sect. 5.4.1), respectively. In particular, Octobot was fueled and powered through hydrogen peroxide and its platinum-catalyzed decomposition into water and oxygen:

$$2H_2O_2\,(\mathrm{l}) \rightarrow 2H_2O\,(\mathrm{l,g}) + O_2\,(\mathrm{g}) \tag{6.1}$$

which results in 250× volume expansion [223]. As the result, the completed Octobot could sustain periodically alternating actuation of its leg sets for 4–8 min autonomously.

The entire work must be praised as the great first step towards the fully S^3 robot. The size requirement, however, still needs to be addressed. As shown in Fig. 6.1, Octobot is centimetric, rather than millimetric. Also, Octobot is not equipped with sensory elements that are indispensable for autonomous operations. The temporal extent of operation is also too limited to perform any practical task. The achievable motion set itself is limited to relatively simple ones as well. These issues can be remedied through adoption of more sophisticated actuation and control mechanisms.

The *autonomous soft robotic fish* demonstrated by MIT researchers is a good example [224, 225]. In practice, the soft fish robot even reproduced the escape maneuver of the biological fish in a very life-like fashion. Such features, however, were obtained by trading off the total softness (through adoption of a compressed gas-based actuator and on-board micro-controller) and size (>10 cm in length) for higher level functionalities.

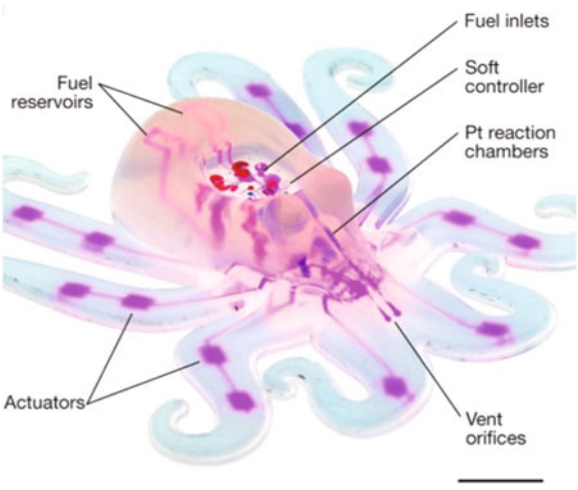

Fig. 6.1 *Octobot*, the first self-contained, totally autonomous soft robot (scale bar: 10 mm). Reprinted with permission from [222]. Copyright 2016 Nature

With no other rivaling robot closer to the rank of the microscale soft robot than those surveyed above, it can be safely assumed that a microscale soft robot in the strict sense is still missing as of the time of writing. A careful examination of currently existing soft robots will reveal that they fall short of becoming true microscale soft robots in strict sense in two major aspects:

- Miniaturization
- Full-scale Integration

Many tasks can be, and need to be, done to address the two issues. Near the top of the list, assuming that the tasks were listed in the order of importance, must be three agendas:

- Get More from Nature
- Achieve Self-Sufficiency
- Refine Material and Fabrication Technologies

Surveying recent progresses on these technological agendas in the light of the two deficiency factors will further enlighten the development roadmap for microscale soft robotics.

6.2 Agenda 1: Get More from Nature

In a sense, the apparent absence of the strict-sense microscale soft robot may seem almost awkward given the fact that the world we are living in is replete with examples of such a fully integrated microscale soft robot—small animals such as the insect, in particular. In another sense, however, it can be a blessing in disguise since it also points to a vast source of useful information still left to be mined.

The related topics of bio-mimetics and bio-inspired engineering have already been surveyed in Sect. 3.4. While the former emphasizes artificial reproduction of advanced biological functionalities and development of fabrication technologies to back up the replication efforts, the latter urges us to exploit the lessons from nature in combination with human technology to produce functionalities capable of surpassing their biological prototypes. In that sense, the bio-inspired engineering process can be regarded as an *artificially accelerated* evolution. There are countless candidate systems to take advantage of. A few of them stand out in particular.

Actuation and Motion For their extreme efficiency and compactness, biological actuation and motion remain the top-of-the-list target for bio-inspired engineering. The potential is so great that the record of bio-inspired outcomes in the area accumulated over the past few decades is extensive but not exhaustive.

Of recent interest is the search for new and effective ways of displacement for small robots. A number of bi-pedal and multi-pedal locomotive modalities have been demonstrated so far as surveyed in Sect. 3.4.2. Many of them, however, could be invalidated once the robots were removed from the idealized lab and deployed in

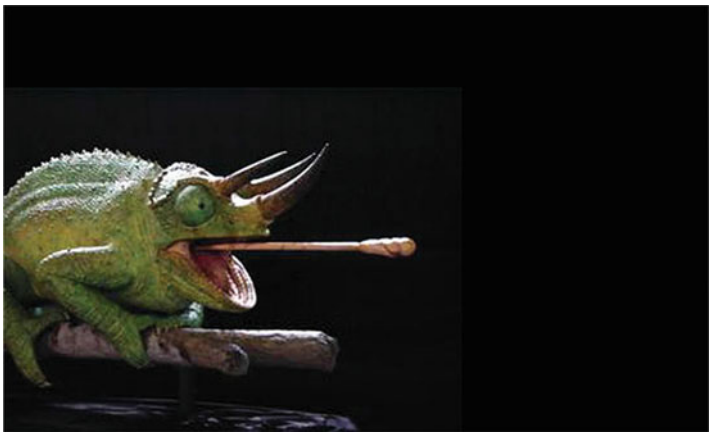

Fig. 6.2 A chameleon projecting its tongue (Image from *Wikimedia Commons*)

natural terrain with irregularities and vegetation. One apparently bio-inspired, out-of-the-box solution was the utilization of jumping as proposed and demonstrated by Bergbreiter and co-workers [226, 227]. Once completed, it should constitute a particularly effective modality of displacement in naturally irregular terrains, as evidenced by the abundance of jumping insects around us.

A similar yet unattempted biological actuation capable of supporting another new displacement modality is the *rope-catapulting*. Projection of a body part is frequently observed in nature as a means of hunting. The most notable example may be the chameleon's tongue that can be extended up to 150% of the body length in a fraction of a second as shown in Fig. 6.2 [228]. A more amazing feature is the underlying mechanism of such a dynamic action. De Groot et al. showed that the acceleration and final speed of the tongue's tip are too high for the chameleon's muscle capacity [229]. The ensuing investigation revealed that the chameleon literally *catapults* its tongue using the tongue's cartilage skeleton and the surrounding accelerator muscle as the frame and *sliding springs*.

In addition, the mucus at the tip of the tongue turned out to be 400 times more viscous than human saliva so that it can function as the adhesive for catching the prey [230]. By replicating the catapulting effect of the tongue and the stickiness of its tip in combination, we may be able to realize a new modality of displacement for small robots in which the "projection–attachment–retraction/dragging" sequence forms one dynamic cycle for movement, in a way very similar to that of the *Spiderman*.

On the individual actuator side, mechanisms based on small animals, insects in particular, are on their way to maturity while those based on plants or cellular level functionalities are newly introduced into the limelight. One famous example is the Venus flytrap (*Dionesa muscipula*) shown in Fig. 6.3. It can close its leaves within 100 ms, achieving one of the fastest actuation among plants. Forterre et al. revealed that such a fast motion is enabled through snap-buckling instability [231].

Fig. 6.3 The leaves of venus flytrap *D. muscipula* (Image from *Wikimedia Commons*)

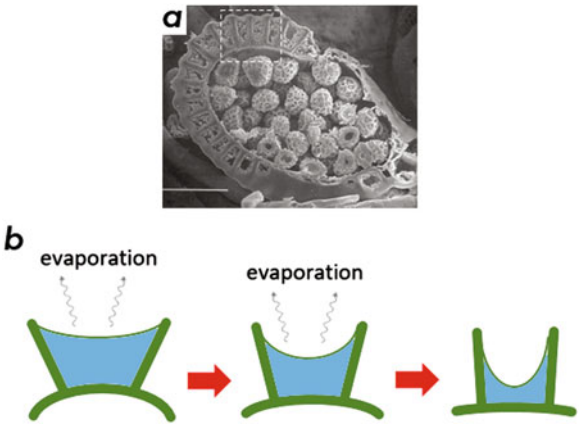

Fig. 6.4 (**a**) A scanning electron micrograph of *Pteris vittata* sporangium (scale bar: 0.1 mm). Reprinted with permission from [238]. Copyright 2006 Springer. (**b**) Schematic diagrams showing the water evaporation-inspired actuation mechanism in which the water placed between the ribs wets the device and pulls the ribs, bending the spine eventually

As mentioned briefly in the previous chapters, it did not take much time for the unique actuation mechanism to be artificially replicated with the help of soft lithography [125]. The studies on such mechanical instabilities have been particularly intense in conjunction with soft mechanics and soft MEMS [126, 127, 232–235]. Also of interest among plant-inspired actuation schemes include the osmosis-based pressure generation for driving soft robots [236] and transpiration actuation based on changes in surface tension [237] shown schematically in Fig. 6.4. These plant-inspired actuation mechanisms are slower than those based on those of animals but often exhibit self-contained operations which will be re-emphasized in the sections to follow.

Bio-Hybridization Conventionally, the biological world has been utilized either as the target of mimicry or as the source of inspiration. Along the progress in microscale soft robotics, the need for a higher-level exploitation of nature has

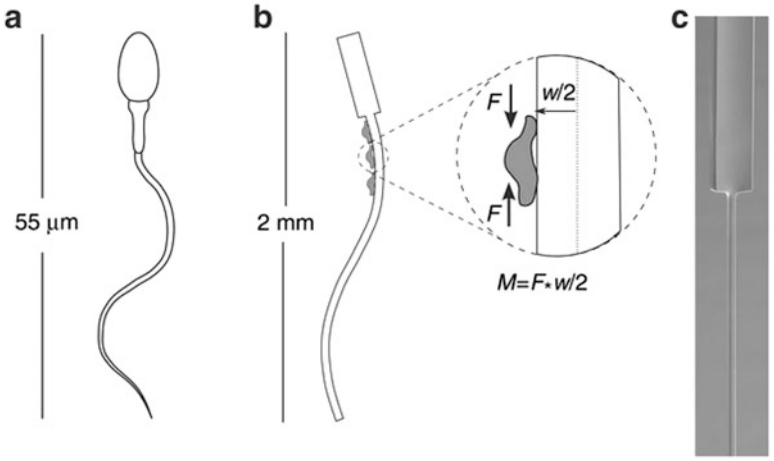

Fig. 6.5 Conceptual diagrams of (**a**) Spermatozoa and (**b**) the biohybrid swimmer utilizing a cluster of contractile cells for propulsion. (**c**) Scanning electron micrograph of a fabricated PDMS filament near the head/tail junction. Reprinted with permission from [239]. Copyright 2014 Nature

emerged, leading to the attempts to *steal* from it in the form of bio-hybridization. The most popular form of bio-hybridization in microscale soft robotics is shown in Fig. 6.5. The main body of the microscale soft robot comprises a PDMS plate, which functions as the head, and a PDMS filament [240], which functions as the flagellum for swimming. With the help of attached cardiomyocytes, the completed *bio-hybrid swimmer* can propel itself at 81 µm/s in water. This type of *bio-derived engineering* is expected to play the main role in future microscale soft robotics in collaboration with tissue engineering which has been exhibiting an equally rapid advances.

Embracing Biological Nanotechnology As the size of the microscale soft robots shrinks, they will get influenced increasingly more by various physical phenomena unique to the microscale world, such as the ever-increasing surface tension and surface-to-volume ratio. They can be either beneficial or detrimental depending on how they got utilized. The same effects have also been impacting small animals, especially the insect, from time immemorial and the consequences of the accumulated adoption can be observed in many parts of their bodies. Embracing such biological nanotechnology certainly is an essential topic in the evolution of microscale soft robotics.

Presently at the forefront in that line of research is the endeavor to control the surface characteristics through nanoscale patterning [241, 242]. For small animals, as mentioned above, the interaction between their skin and its direct environment can affect their biological functions, and hence their survival, significantly. For example, they may need hydrophobic surfaces to prevent dust particle-induced contamination of the eye surface. At the same time, they may also need oleophobic skins to repel potentially dangerous liquid-phase organic substances.

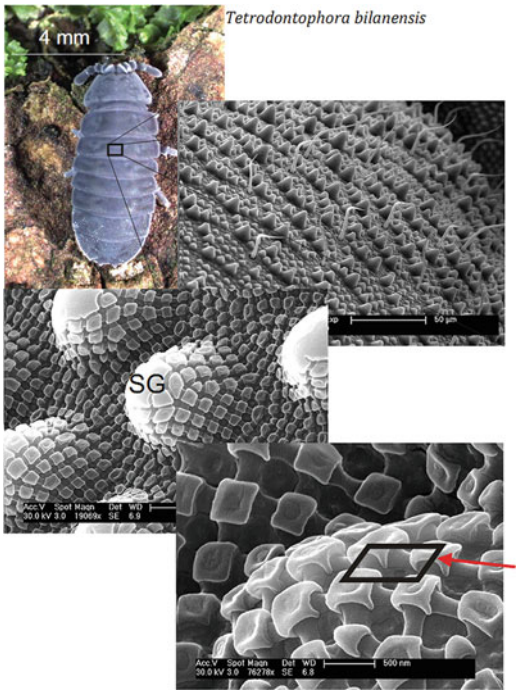

Fig. 6.6 Optical and scanning electron micrographs of *T. bilanensis* and its nanoscale textured skin structure (Images from Public Library of Science [243])

This line of research is by no means new. Replication of straightforward nanostructures, such as the humidity-repelling motheye surface consisting only of nanocones, has been already done in the early stage of the field. However, more complex structures, such as the multi-scale lotusan leaf surface or the tree-like nanopillars in the butterfly's wings which produce their structural colors, still leave rooms for further research.

One especially challenging example is the *smart skin* of the springtail (*Folsomia candida*) shown in Fig. 6.6a [243–245]. The skin is omniphobic in the sense that it repels both water and oil. Nanoscopically, as shown in Fig. 6.6a, the skin consists of closely packed nanopillars with caps larger than the nanopillar's diameter, forming its unique *overhang* architecture which turned out to be ideal for realizing the highly desired omniphobicity [243, 244]. Using a new fabrication technique called the reverse imprint lithography, Werner and co-workers successfully replicated the structure and observed similar omniphobicity [245].

This subsection can be compactly summarized by quoting Feynman's 1959 declaration "*There's plenty of room at the bottom*." The past achievements in biomimetics and bio-inspired engineering can easily give the wrong impression that most essential tasks have already been carried out. Quite to the contrary, we have been scratching only the outer surface of the whole potential to date. Beyond the realm of direct replication (bio-mimicry) and optimized adoption (bio-inspired engineering) lies the wonderful new world of bio-hybrids. Its implication on the

miniaturization and full-scale integration of microscale soft robots is significant. The pace of the progress will be set by the level of inter-disciplinary collaboration between researchers.

6.3 Agenda 2: Achieve Self-Sufficiency

Leaving robots to rely on externally supplied resources, such as power, control, and substances, can be detrimental in many aspects. Above all, doing so will harm their utility as standalone functional units by eliminating the potential for untethered operation. In addition, it will also complicate the efforts for miniaturization and full-scale integration by requiring installation of additional components for interface, delivery, and signaling.

Consequently, the future research in microscale soft robotics, at least partially, will be directed towards the realization of technologies ensuring their self-sufficiency in operation. Harvesting of ambient energy as the source of power for the robot's operation has already become a well-established topic in the field [247], thus need not be reiterated here. One point of emphasis is the inherently low resonance frequency attainable from soft MEMS devices, which will help with harvesting more energy from low-frequency movements such as human gaits and motions. The sub-kHz resonance frequency of the PDMS micropillar shown in Fig. 3.20c is a good example. The need for external control will also be minimized through the improvement in embedded autonomy as discussed above.

One relatively new aspect of self-sufficiency is the harvesting of essential substances. Water can be the representative example since it functions as the basis for many chemical reactions and also as an effective coolant. Dispensing water to microscale soft robots individually will produce severe logistical complications and surely hurt the miniaturization effort. Recently, a number of soft MEMS-based water harvesting schemes have appeared as a solution. Harvesting of water with spider silk-like thin wires has been in use for a long time. Tian et al. demonstrated that its efficiency can be improved through the use of humps [248]. Such a substance-harvesting scheme is in fact doubly promising. In addition to providing the needed substance in a standalone fashion, it can also be utilized to enable other self-sufficiency schemes. One example is the bio-inspired evaporation flow-enabled energy harvesting system shown in Fig. 6.7 [246]. Cascading the two schemes mentioned above may lead to self-sufficient power generation enabled by the morning dew.

Another important aspect of self-sufficiency is the task of maintaining the robot's structural and functional integrity along its operation. One interesting feature which is concerned both with the self-sufficiency and material/fabrication (i.e., the topic of the next subsection) aspects is the *self-healing* capability. The self-healing concept has been pursued in many different material systems but the mainstream has always been along polymeric and, in particular, elastomeric materials. The work in [249] shows one example implemented through a combined use of self-healable

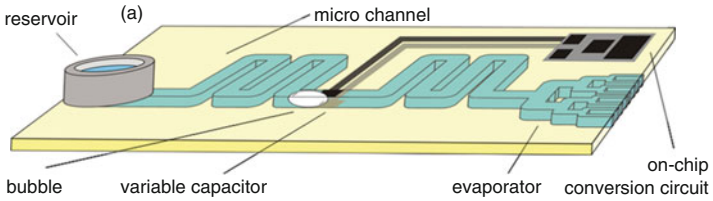

Fig. 6.7 A schematic diagram of a bio-inspired energy harvester based on evaporation flow. Reprinted with permission from [246]. Copyright 2009 American Institute of Physics

polymer (such as Riverlink^{TM}) and liquid-phase conductor (such as EGaIn^{TM}). Many other configurations exist and they are not limited to electrical connections. Optical interfaces could also be made self-healable, in fact with greater ease due to their metal-free nature. Overall healing of the elastomeric bulk through the use of microfludic network has also been demonstrated [250]. For the foreseeable future, the topic will keep attracting research interest for its wide-ranged application potential.

6.4 Agenda 3: Refine Material and Fabrication Technologies

In light of miniaturization and full-scale integration, the two agendas introduced in the previous two sections are more towards the basic concept. Their practical implementation requires backing up in materials and fabrication aspects. The topics are so vast that they defy brief surveys. However, a few salient points of thrust, with specific emphasis on microscale soft robotics, can be identified here as the future reference.

On the material side, the field of microscale soft robotics will strengthen its demand for more functional materials. In particular, materials *intrinsically* capable of actuation, sensing, and control without relying on external interventions are of special interest. The self-healing material described in the previous section also falls in the category of this intrinsically functional material in a wide sense. They may become qualified for the rank of the *intelligent material* once two or more functionalities got incorporated simultaneously.

One important trend is that the endeavor has become increasingly proactive. Instead of trying to find new materials with suitable properties, chemists and material scientists are joining forces with mechanical and biological engineers to *create* new composite structures with the desired functionalities. The microfluidics-enabled self-healing material [250] mentioned in the previous section is a good example.

On the fabrication side, the effort to find and establish microfabrication techniques narrowly focused on a limited set of elastomers, with PDMS at the top of the line, will form the mainstream. The capillary-origami technique shown in

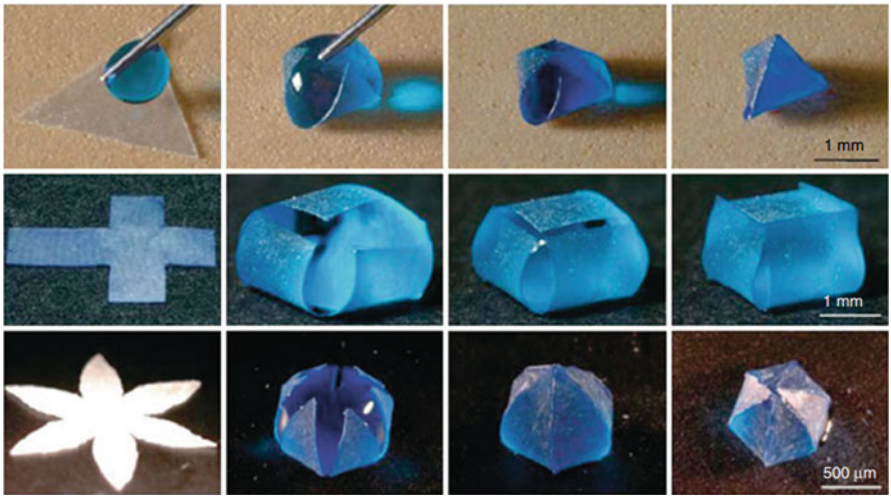

Fig. 6.8 Capillary-origami-based formation of 3D structures in pyramidal, cubic, and quasi-spherical geometries through water droplet-enabled folding of triangular, cross-like, and stellar PDMS sheets, respectively. Reprinted with permission from [251]. Copyright 2007 American Institute of Physics

Fig. 6.8 is the most prominent example since it exploits the softness of PDMS and the dominance of surface tension at microscale in combination in a highly efficient and synergistic fashion.

Conventional 3D-sculpting methods for PDMS can be roughly divided into two categories: Additive and Subtractive. The former has already been described in Chap. 3 in conjunction with the additive co-molding process that is so powerful and ubiquitous in soft MEMS. The future agenda is clear along the line: A fully fledged technique for direct 3D-printing of PDMS must be perfected. The biggest hurdle to the effort must be the slow curing rate of PDMS. On the other hand, in the subtractive fabrication side, lack of effective etching methods for PDMS may remain the biggest hurdle. Currently there is no clear solution to the problem. The adoption of water-soluble sacrificial template material seems the only bypass.

The vibrant field of soft MEMS, however, has never been in shortage of creative, *out-of-the-box* solutions. There are two notable examples. The first one is the recent thrust to write optical functionalities directly *inside* the bulk of PDMS through UV-patterning [252, 253]. In this way, gratings and volume holograms can be written in the bulk of a PDMS block in a totally embedded fashion. The second one is the so-called *solid-on-liquid deposition* method in which a relatively stiff elastomer, such as Parylene, is deposited over liquid-phase elastomer, such as uncured PDMS [254]. It has been utilized to form highly deformable active devices such as microliquid lenses and liquid prisms [255].

All of these development paths will eventually lead to the expedited accomplishment of miniaturization and higher-level integration in soft robotics, pushing it towards truly microscale soft robotics.

6.5 Target on Horizon: Embedded Intelligence

With the two objectives (i.e., miniaturization and full-scale integration) and the corresponding three agendas (i.e., getting more from nature, achieving self-sufficiency, and refining material and fabrication techniques) firmly set as described in the previous sections, identification of a short-term goal is in order. It is not a very hard task since there already exists a consensus on this *target on the horizon* among the researchers in the field. It comes under different names, such as *mechanical intelligence* or *embedded intelligence*, but basically points to the same concept which has been nicely outlined by Rus and Tolley in their highly renowned review paper *Design, fabrication and control of soft robots* [1] as:

> "For the body of a soft robot to achieve its potential, facilities for sensing, actuation, computation, power storage and communication must be **embedded** in the soft material, resulting in **smart materials**."
>
> "This tight coupling between body and brain allows us to think about soft-bodied systems as machines with **mechanical intelligence**, in which the body can be viewed as augmenting the brain with **morphological computation**"

The real-world solutions for realizing such an embedded intelligence are still under quest at this point in time. Among the functionalities to be embedded, at the forefront of practical implementation are those related to actuation and morphological changes. In particular, the efforts to learn from nature for the realization of programmable and re-configurable shape transformation materials have been very intense [124, 256–258]. Figure 6.9 is one prominent example in which hydrogel sheets are configured to transform into different shapes in response to pH changes in accordance with their material-embedded pre-programming.

As surveyed in the previous sections and chapters, however, material-embedded implementation of other functionalities, such as sensing, control, and computation, is still in its infancy with few reports of accomplishment published. For the foreseeable future, the realization of embedded intelligence will remain the forefront of soft robotics and microscale soft robotics.

The possible form of help, be it a major breakthrough in bio-mimicry, discovery of a new material system, or cross-disciplinary success beyond imagination, is still at large. With the motivations firmly recognized, however, it will eventually be accomplished as things have always been.

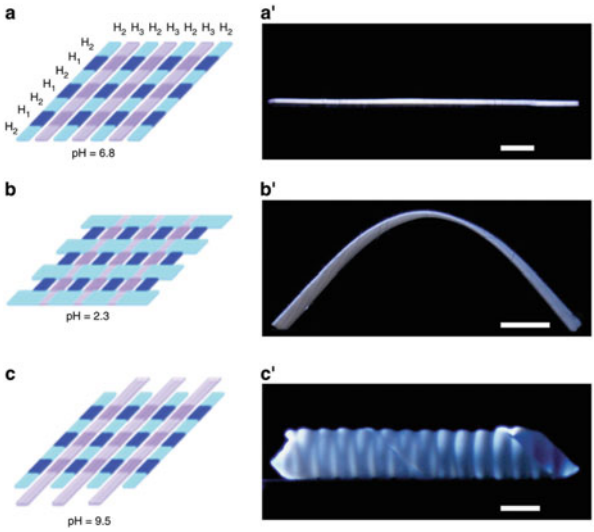

Fig. 6.9 Hydrogel sheets transforming into different shapes in accordance with their material-embedded pre-programming. Reprinted with permission from [256]. Copyright 2012 Nature

6.6 Targets over the Horizon

Finally, this section will wrap up the book by making forecasts on long-term goals in the research and applications of microscale soft robots. Above all, the downscaling in the robot's size will never be stopped. It will actually continue to the point at which the microscale soft robots become literally at micron-scale, or even at nanoscale. By the time, the distinction between tissue engineering and robotics will become very blurry and their hybridization will also become inevitable and critical. Biological cells will not only provide their functionalities to the completed microscale robots but also participate in the process of their realization. At nanoscale, the cells will be replaced by biological molecular machines such as ion pumps or kinesin motor proteins, this time obfuscating the borderline between robotics and biochemistry.

On the material side, there will be initiatives upholding green, *sustainable* robotics as well. PDMS may be bio-compatible and non-toxic but generally deemed cytotoxic to a certain degree and definitely not bio-degradable. In near future, microrobots made of dissolvable and bio-degradable materials will be developed. Particularly the latter will see their tasks extended to in vivo operations, such as the targeted drug delivery, with an emphasis on gentle self-destruction under normal biological environment.

On the utilization side, the microscale soft robots will increasingly become S^3 robots while expanding their application scope beyond biomedicine. As mentioned briefly in Chap. 4, there are many subtle and fragile micro-objects to be manipulated gently and safely. On the organic side, the S^3 robot's delicate end-effectors can contribute to palynology and forensics. On the inorganic side, they can also be

utilized as grabbers and manipulators of fragile mechanical parts and chemical substances. It is quite possible that the S^3 robots will be building microscale soft robots someday.

Throughout the past, present, and foreseeable future phases of microscale soft robotics, two aspects of its characteristics are persistently self-evident. First, it is a great promoter of convergence in both academia and industry. Second, as stated in the Preface of this book, to maximize the performance of the microscale soft robots, they need to be conceived, designed, and optimized from ground up with a proper level of attention paid to the soft and small nature of the final outcomes. These two lessons must be kept in mind of all the S^3 robot engineers.

References

1. D. Rus, M.T. Tolley, Design, fabrication and control of soft robots. Nature **521**, 467–475 (2015)
2. G.M. Whitesides, What comes next? Lab Chip **11**, 191–193 (2011)
3. C. Bergeles, G.-Z. Yang, From passive tool holders to microsurgeons: safer, smaller, smarter surgical robots. IEEE Trans. Biomed. Eng. **61**, 1565–1576 (2014)
4. S. Konishi, Small, soft and safe micro-machines for biomedical applications, in *2015 Transducers - 2015 18th International Conference on Solid-State Sensors, Actuators and Microsystems (TRANSDUCERS)* (2015), pp. 863–866
5. A. Abbott, Cell culture: biology's new dimension. Nature **424**, 870–872 (2003)
6. G. Mehta, A.Y. Hsiao, M. Ingram, G.D. Luker, S. Takayama, Opportunities and challenges for use of tumor spheroids as models to test drug delivery and efficacy. J. Control. Release **164**, 192–204 (2012)
7. A.Y. Hsiao, Y.-S. Torisawa, Y.-C. Tung, S. Sud, R.S. Taichman, K.J. Pienta, S. Takayama, Microfluidic system for formation of PC-3 prostate cancer co-culture spheroids. Biomaterials **30**, 3020–3027 (2009)
8. Q. Wang, S. Zhao, J. Choi, X. He, Y. Zhao, Polymeric micro-gripper for applying mechanical stimulation on three-dimensional cell aggregates, in *Solid-State Sensors, Actuators and Microsystems Workshop* (2014), pp. 9–12
9. S. Shimomura, Y. Teramachi, Y. Muramatsu, S. Tajima, Y. Tabata, S. Konishi, Pinching and releasing of cellular aggregate by microfingers using PDMS pneumatic balloon actuators, in *2014 IEEE 27th International Conference on Micro Electro Mechanical Systems (MEMS)* (2014), pp. 925–926
10. C. Majidi, Soft robotics: a perspective—current trends and prospects for the future. Soft Rob. **1**, 5–11 (2013)
11. M. Silva-López, A. Fender, W.N. MacPherson, J.S. Barton, J.D.C. Jones, D. Zhao, H. Dobb, D.J. Webb, L. Zhang, I. Bennion, Strain and temperature sensitivity of a single-mode polymer optical fiber. Opt. Lett. **30**, 3129–3131 (2005)
12. J. Paek, J. Kim, Microsphere-assisted fabrication of high aspect-ratio elastomeric micropillars and waveguides. Nat. Commun. **5** (2014)
13. Q. Cheng, Z. Sun, G.A. Meininger, M. Almasri, Note: mechanical study of micromachined polydimethylsiloxane elastic microposts. Rev. Sci. Instrum. **81**, 106104 (2010)
14. C.H. Lee, Y. Ma, K.-I. Jang, A. Banks, T. Pan, X. Feng, J.S. Kim, D. Kang, M.S. Raj, B.L. McGrane, B. Morey, X. Wang, R. Ghaffari, Y. Huang, J.A. Rogers, Epidermal systems: soft core/shell packages for stretchable electronics. Adv. Funct. Mater. **25**, 3697–3697 (2015)

J. (Jay) Kim, *Microscale Soft Robotics*, SpringerBriefs in Applied Sciences and Technology, DOI 10.1007/978-3-319-50286-1

15. P.G. Agache, C. Monneur, J.L. Leveque, J. De Rigal, Mechanical properties and Young's modulus of human skin in vivo. Arch. Dermatol. Res. **269**(3), 221–232 (1980)
16. E.J. Chen, J. Novakofski, W.K. Jenkins, W.D. O'Brien, Young's modulus measurements of soft tissues with application to elasticity imaging. IEEE Trans. Ultrason. Ferroelectr. Freq. Control **43**, 191–194 (1996)
17. R.F. Shepherd, F. Ilievski, W. Choi, S.A. Morin, A.A. Stokes, A.D. Mazzeo, X. Chen, M. Wang, G.M. Whitesides, Multigait soft robot. Proc. Natl. Acad. Sci. **108**, 20400–20403 (2011)
18. Y. Watanabe, M. Maeda, N. Yaji, R. Nakamura, S. Konishi, Small, soft, and safe microactuator for retinal pigment epithelium transplantation, in *IEEE 20th International Conference on Micro Electro Mechanical Systems (MEMS)* (2007), pp. 659–662
19. J. Paek, I. Cho, J. Kim, Microrobotic tentacles with spiral bending capability based on shape-engineered elastomeric microtubes. Sci. Rep. **5** (2015)
20. A. Ghanbari, V. Nock, S. Johari, R. Blaikie, X. Chen, W. Wang, A micropillar-based on-chip system for continuous force measurement of C. elegans. J. Micromech. Microeng. **22**, 095009 (2012)
21. D. Trivedi, C.D. Rahn, W.M. Kier, I.D. Walker, Soft robotics: biological inspiration, state of the art, and future research. Appl. Bionics Biomech. **5**, 99–117 (2008)
22. E. Delamarche, A. Bernard, H. Schmid, B. Michel, H. Biebuyck, Patterned delivery of immunoglobulins to surfaces using microfluidic networks. Science **276**, 779–781 (1997)
23. J. Lee, J. Kim, Elastomeric microwire-based optical gas flowmeter with stretching-enabled tunability in measurement range. Opt. Lett. **36**(19), 3789–3791 (2011)
24. R. Bogue, The development of medical microrobots: a review of progress. Ind. Robot. **35**, 294–299 (2008)
25. J.N. Lee, C. Park, G.M. Whitesides, Solvent compatibility of poly (dimethylsiloxane)-based microfluidic devices. Anal. Chem. **75**, 6544–6554 (2003)
26. F. Schneider, J. Draheim, R. Kamberger, U. Wallrabe, Process and material properties of polydimethylsiloxane (PDMS) for optical MEMS. Sensors Actuators A Phys. **151**, 95–99 (2009)
27. J. Lee, J. Kim, Fabrication of strongly anchored, high aspect ratio elastomeric microwires for mechanical and optical applications. J. Micromech. Microeng. **21**, 085016 (2011)
28. J. Kim, Joining plasmonics with microfluidics: from convenience to inevitability. Lab Chip **12**, 3611–3623 (2012)
29. A. Piruska, I. Nikcevic, S.H. Lee, C. Ahn, W.R. Heineman, P.A. Limbach, C.J. Seliskar, The autofluorescence of plastic materials and chips measured under laser irradiation. Lab Chip **5**, 1348–1354 (2005)
30. J. Paek, Q. Li, I.H. Cho, J. Kim, Minimally intrusive optical micro-strain sensing in bulk elastomer using embedded Fabry-Pérot Etalon. Micromachines **7**, 61 (2016)
31. G. Firpo, E. Angeli, L. Repetto, U. Valbusa, Permeability thickness dependence of polydimethylsiloxane (PDMS) membranes. J. Membr. Sci. **481**, 1–8 (2015)
32. T.C. Merkel, V.I. Bondar, K. Nagai, B.D. Freeman, I. Pinnau, Gas sorption, diffusion, and permeation in poly(dimethylsiloxane). J. Polym. Sci. B Polym. Phys. **38**, 415–434 (2000)
33. Y.S. Heo, L.M. Cabrera, J.W. Song, N. Futai, Y.-C. Tung, G.D. Smith, S. Takayama, Characterization and resolution of evaporation-mediated osmolality shifts that constrain microfluidic cell culture in poly(dimethylsiloxane) devices. Anal. Chem. **79**, 1126–1134 (2007)
34. D. Bartolo, G. Degré, P. Nghe, V. Studer, Microfluidic stickers. Lab Chip **8**, 274–279 (2008)
35. D. Dendukuri, D.C. Pregibon, J. Collins, T.A. Hatton, P.S. Doyle, Continuous-flow lithography for high-throughput microparticle synthesis. Nat. Mater. **5**, 365–369 (2006)
36. S.E. Chung, W. Park, S. Shin, S.A. Lee, S. Kwon, Guided and fluidic self-assembly of microstructures using railed microfluidic channels. Nat. Mater. **7**, 581–587 (2008)
37. D. Dendukuri, P. Panda, R. Haghgooie, J.M. Kim, T.A. Hatton, P.S. Doyle, Modeling of oxygen-inhibited free radical photopolymerization in a PDMS microfluidic device. Macromolecules **41**, 8547–8556 (2008)

38. H. Sasaki, H. Onoe, T. Osaki, R. Kawano, S. Takeuchi, Parylene-coating in PDMS microfluidic channels prevents the absorption of fluorescent dyes. Sensors Actuators B Chem. **150**, 478–482 (2010)
39. J. Flueckiger, V. Bazargan, B. Stoeber, K.C. Cheung, Characterization of postfabricated parylene C coatings inside PDMS microdevices. Sensors Actuators B Chem. **160**, 864–874 (2011)
40. B.J. Kim, E. Meng, Micromachining of Parylene C for bioMEMS. Polym. Adv. Technol. **27**, 564–576 (2016)
41. H. Gensler, R. Sheybani, P.-Y. Li, R.L. Mann, E. Meng, An implantable MEMS micropump system for drug delivery in small animals. Biomed. Microdevices **14**, 483–496 (2012)
42. J.B. Fortin, T.-M. Lu, Step-by-step guide to depositing Parylene, in *Chemical Vapor Deposition Polymerization* (Springer, New York, 2004), pp. 23–26. doi:10.1007/978-1-4757-3901-5_3
43. E. Meng, P.-Y. Li, Y.-C. Tai, Plasma removal of Parylene C. J. Micromech. Microeng. **18**(4), 045004 (2008)
44. B. Ratier, Y.S. Jeong, A. Moliton, P. Audebert, Vapor deposition polymerization and reactive ion beam etching of poly(p-xylylene) films for waveguide applications. Opt. Mater. **12**, 229–233 (1999)
45. N. Majid, S. Dabral, J.F. McDonald, The parylene-aluminum multilayer interconnection system for wafer scale integration and wafer scale hybrid packaging. J. Electron. Mater. **18**, 301–311 (1989)
46. R. Thakar, R. Zakeri, C.A. Morris, L.A. Baker, Rapid fabrication of nanoporous membrane arrays and single-pore membranes from parylene C. Anal. Methods **4**(12), 4353–4359 (2012). WOS:000311967200068
47. Y. Rui, J. Liu, Y. Wang, C. Yang, Parylene-based implantable Pt-black coated flexible 3-D hemispherical microelectrode arrays for improved neural interfaces. Microsyst. Technol. **17**, 437 (2011)
48. R. Wang, X. Huang, G. Liu, W. Wang, F. Dong, Z. Li, Fabrication and characterization of a parylene-based three-dimensional microelectrode array for use in retinal prosthesis. J. Microelectromech. Syst. **19**, 367–374 (2010)
49. P.-J. Chen, C.-Y. Shih, Y.-C. Tai, Design, fabrication and characterization of monolithic embedded parylene microchannels in silicon substrate. Lab Chip **6**, 803–810 (2006)
50. N. Binh-Khiem, K. Matsumoto, I. Shimoyama, Polymer thin film deposited on liquid for varifocal encapsulated liquid lenses. Appl. Phys. Lett. **93**, 124101 (2008)
51. T.Y. Chang, V.G. Yadav, S. De Leo, A. Mohedas, B. Rajalingam, C.-L. Chen, S. Selvarasah, M.R. Dokmeci, A. Khademhosseini, Cell and protein compatibility of parylene-C surfaces. Langmuir **23**, 11718–11725 (2007)
52. E.M. Schmidt, J.S. Mcintosh, M.J. Bak, Long-term implants of Parylene-C coated microelectrodes. Med. Biol. Eng. Comput. **26**(1), 96–101 (1988)
53. B.A. Weisenberg, D.L. Mooradian, Hemocompatibility of materials used in microelectromechanical systems: platelet adhesion and morphology in vitro. J. Biomed. Mater. Res. **60**, 283–291 (2002)
54. J. Lahann, Vapor-based polymer coatings for potential biomedical applications. Polym. Int. **55**, 1361–1370 (2006)
55. P.Y. Li, R. Sheybani, C.A. Gutierrez, J.T.W. Kuo, E. Meng, A parylene bellows electrochemical actuator. J. Microelectromech. Syst. **19**, 215–228 (2010)
56. N. Chou, S. Kim, A fabrication method of out-of-plane stretchable and flexible electrodes based on PDMS, in *Proceedings of the 2013 SPIE Micro/Nano Materials, Devices, and Systems*, vol. 8923 (2013), pp. 89233Q–89233Q–6
57. J.-M. Hsu, L. Rieth, S. Kammer, M. Orthner, F. Solzbacher, Effect of thermal and deposition processes on surface morphology, crystallinity, and adhesion of Parylene-C. ResearchGate **20**, 87–102 (2008)
58. K.G. Pruden, K. Sinclair, S. Beaudoin, Characterization of parylene-N and parylene-C photooxidation. J. Polym. Sci. A Polym. Chem. **41**, 1486–1496 (2003)

59. H.-S. Noh, Y. Huang, P.J. Hesketh, Parylene micromolding, a rapid and low-cost fabrication method for parylene microchannel. Sensors Actuators B Chem. **102**, 78–85 (2004)
60. E.M. Davis, N.M. Benetatos, W.F. Regnault, K.I. Winey, Y.A. Elabd, The influence of thermal history on structure and water transport in Parylene C coatings. Polymer **52**, 5378–5386 (2011)
61. H.C. Koydemir, H. Külah, C. Özgen, Solvent compatibility of Parylene C Film Layer. J. Microelectromech. Syst. **23**, 298–307 (2014)
62. S.N. Bhatia, D.E. Ingber, Microfluidic organs-on-chips. Nat. Biotech. **32**, 760–772 (2014)
63. D. Huh, B.D. Matthews, A. Mammoto, M. Montoya-Zavala, H.Y. Hsin, D.E. Ingber, reconstituting organ-level lung functions on a chip. Science **328**, 1662–1668 (2010)
64. E.T. Roche, R. Wohlfarth, J.T.B. Overvelde, N.V. Vasilyev, F.A. Pigula, D.J. Mooney, K. Bertoldi, C.J. Walsh, A bioinspired soft actuated material. Adv. Mater. **26**, 1200–1206 (2014)
65. Y. He, J. Qiu, J. Fu, J. Zhang, Y. Ren, A. Liu, Printing 3d microfluidic chips with a 3d sugar printer. Microfluid. Nanofluid. **19**, 447–456 (2015)
66. J. Lee, J. Paek, J. Kim, Sucrose-based fabrication of 3d-networked, cylindrical microfluidic channels for rapid prototyping of lab-on-a-chip and vaso-mimetic devices. Lab Chip **12**(15), 2638 (2012)
67. J.S. Miller, K.R. Stevens, M.T. Yang, B.M. Baker, D.-H.T. Nguyen, D.M. Cohen, E. Toro, A.A. Chen, P.A. Galie, X. Yu, R. Chaturvedi, S.N. Bhatia, C.S. Chen, Rapid casting of patterned vascular networks for perfusable engineered three-dimensional tissues. Nat. Mater. **11**, 768–774 (2012)
68. H.N. Chan, Y. Chen, Y. Shu, Y. Chen, Q. Tian, H. Wu, Direct, one-step molding of 3d-printed structures for convenient fabrication of truly 3d PDMS microfluidic chips. Microfluid. Nanofluid. **19**, 9–18 (2015)
69. M.M. Stanton, C. Trichet-Paredes, S. Sánchez, Applications of three-dimensional (3d) printing for microswimmers and bio-hybrid robotics. Lab Chip **15**(7), 1634–1637 (2015)
70. S. Waheed, J.M. Cabot, N.P. Macdonald, T. Lewis, R.M. Guijt, B. Paull, M.C. Breadmore, 3d printed microfluidic devices: enablers and barriers. Lab Chip **16**, 1993–2013 (2016)
71. A.A. Yazdi, A. Popma, W. Wong, T. Nguyen, Y. Pan, J. Xu, 3d printing: an emerging tool for novel microfluidics and lab-on-a-chip applications. Microfluid. Nanofluid. **20**, 50 (2016)
72. S. Große, T. Soodt, W. Schröder, Dynamic calibration technique for the micro-pillar shear-stress sensor MPS 3. Meas. Sci. Technol. **19**(10), 105201 (2008)
73. A.S. Nain, J.C. Wong, C. Amon, M. Sitti, Drawing suspended polymer micro-/nanofibers using glass micropipettes. Appl. Phys. Lett. **89**, 183105 (2006)
74. S.A. Harfenist, S.D. Cambron, E.W. Nelson, S.M. Berry, A.W. Isham, M.M. Crain, K.M. Walsh, R.S. Keynton, R.W. Cohn, Direct drawing of suspended filamentary micro- and nanostructures from liquid polymers. Nano Lett. **4**, 1931–1937 (2004)
75. X. Xing, Y. Wang, B. Li, Nanofibers drawing and nanodevices assembly in poly(trimethylene terephthalate). Opt. Express **16**, 10815–10822 (2008)
76. L.L. Lebel, B. Aissa, M.A.E. Khakani, D. Therriault, Ultraviolet-assisted direct-write fabrication of carbon nanotube/polymer nanocomposite microcoils. Adv. Mater. **22**, 592–596 (2010)
77. K. Lee, H.C. Lee, D.-S. Lee, H. Jung, Drawing lithography: three-dimensional fabrication of an ultrahigh-aspect-ratio microneedle. Adv. Mater. **22**, 483–486 (2010)
78. M. Prakash, J.W.M. Bush, Interfacial propulsion by directional adhesion. Int. J. Non Linear Mech. **46**, 607–615 (2011)
79. P.J. Hung, K. Jeong, G.L. Liu, L.P. Lee, Microfabricated suspensions for electrical connections on the tunable elastomer membrane. Appl. Phys. Lett. **85**, 6051–6053 (2004)
80. D.-H. Kim, N. Lu, R. Ma, Y.-S. Kim, R.-H. Kim, S. Wang, J. Wu, S. M. Won, H. Tao, A. Islam, K.J. Yu, T.-i. Kim, R. Chowdhury, M. Ying, L. Xu, M. Li, H.-J. Chung, H. Keum, M. McCormick, P. Liu, Y.-W. Zhang, F.G. Omenetto, Y. Huang, T. Coleman, J.A. Rogers, Epidermal electronics. Science **333**, 838–843 (2011)
81. F. Xu, Y. Zhu, Highly conductive and stretchable silver nanowire conductors. Adv. Mater. **24**, 5117–5122 (2012)

82. J. Viventi, D.-H. Kim, J.D. Moss, Y.-S. Kim, J.A. Blanco, N. Annetta, A. Hicks, J. Xiao, Y. Huang, D.J. Callans, J.A. Rogers, B. Litt, A conformal, bio-interfaced class of silicon electronics for mapping cardiac electrophysiology. Sci. Transl. Med. **2**, 24ra22–24ra22 (2010)
83. M. Dickey, R. Chiechi, R. Larsen, E. Weiss, D. Weitz, G. Whitesides, Eutectic gallium-indium (EGaIn): a liquid metal alloy for the formation of stable structures in microchannels at room temperature. Adv. Funct. Mater. **18**, 1097–1104 (2008)
84. M. Kubo, X. Li, C. Kim, M. Hashimoto, B.J. Wiley, D. Ham, and G.M. Whitesides, Stretchable microfluidic radiofrequency antennas. Adv. Mater. **22**, 2749–2752 (2010)
85. Y.L. Park, B.R. Chen, R.J. Wood, Design and fabrication of soft artificial skin using embedded microchannels and liquid conductors. IEEE Sensors J. **12**, 2711–2718 (2012)
86. J. Park, S. Wang, M. Li, C. Ahn, J.K. Hyun, D.S. Kim, D.K. Kim, J.A. Rogers, Y. Huang, S. Jeon, Three-dimensional nanonetworks for giant stretchability in dielectrics and conductors. Nat. Commun. **3**, 916 (2012)
87. J. Paek, J. Kim, Building freestanding elastomeric waveguides: exploring an emerging field. Opt. Photonics News **11**, 18–21 (2014)
88. Z.L. Sámson, K.F. MacDonald, F.D. Angelis, B. Gholipour, K. Knight, C.C. Huang, E.D. Fabrizio, D.W. Hewak, N.I. Zheludev, Metamaterial electro-optic switch of nanoscale thickness. Appl. Phys. Lett. **96**, 143105 (2010)
89. V. Lien, Y. Berdichevsky, Y.-H. Lo, A prealigned process of integrating optical waveguides with microfluidic devices. IEEE Photon. Technol. Lett. **16**, 1525–1527 (2004)
90. V. Lien, K. Zhao, Y. Berdichevsky, Y.-H. Lo, High-sensitivity cytometric detection using fluidic-photonic integrated circuits with array waveguides. IEEE J. Sel. Top. Quantum Electron. **11**, 827–834 (2005)
91. C.-S. Huang, E.Y.-B. Pun, W.-C. Wang, Fabrication of an elastomeric rib waveguide Bragg grating filter. J. Opt. Soc. Am. B **26**(6), 1256–1262 (2009)
92. Z. Cai, W. Qiu, G. Shao, W. Wang, A new fabrication method for all-PDMS waveguides. Sensors Actuators A Phys. **204**, 44–47 (2013)
93. J. Missinne, S. Kalathimekkad, B. Van Hoe, E. Bosman, J. Vanfleteren, G. Van Steenberge, Stretchable optical waveguides. Opt. Express **22**, 4168 (2014)
94. S. Aikio, J. Hiltunen, J. Hiitola-Keinänen, M. Hiltunen, V. Kontturi, S. Siitonen, J. Puustinen, P. Karioja, Disposable photonic integrated circuits for evanescent wave sensors by ultra-high volume roll-to-roll method. Opt. Express **24**, 2527 (2016)
95. D. Jandura, D. Pudis, A. Kuzma, Fabrication technology for PDMS ridge waveguide using DLW. Optik Int. J. Light Electron Opt. **127**, 2848–2851 (2016)
96. Y.M. Song, Y. Xie, V. Malyarchuk, J. Xiao, I. Jung, K.-J. Choi, Z. Liu, H. Park, C. Lu, R.-H. Kim, R. Li, K. B. Crozier, Y. Huang, J.A. Rogers, Digital cameras with designs inspired by the arthropod eye. Nature **497**, 95–99 (2013)
97. C.-C. Kim, H.-H. Lee, K.H. Oh, J.-Y. Sun, Highly stretchable, transparent ionic touch panel. Science **353**, 682–687 (2016)
98. R. Knight, U. Nehmzow, C.C. Sq, Walking robots — a survey and a research proposal. Technical Report, 2002
99. I. Gaiser, A. Andres, G. Bretthauer, H. Breitwieser, O. Ivlev, R. Wiegand, S. Schulz, *Compliant Robotics and Automation with Flexible Fluidic Actuators and Inflatable Structures*. (INTECH Open Access Publisher, Rijeka, 2012). Google-Books-ID: QjmUoAEACAAJ. Rijeka, Croatia
100. C.-P. Chou, B. Hannaford, Static and dynamic characteristics of McKibben pneumatic artificial muscles, in *Proceedings of the 1994 IEEE International Conference on Robotics and Automation*, vol.1 (1994), pp. 281–286
101. M. De Volder, A. Moers, D. Reynaerts, Fabrication and control of miniature McKibben actuators. Sensors Actuators A Phys. **166**, 111–116 (2011)
102. S. Kim, C. Laschi, B. Trimmer, Soft robotics: a bioinspired evolution in robotics. Trends Biotechnol. **31**, 287–294 (2013)
103. S.A. Morin, R.F. Shepherd, S.W. Kwok, A.A. Stokes, A. Nemiroski, G.M. Whitesides, Camouflage and display for soft machines. Science **337**, 828–832 (2012)

104. M.F. Land, D.-E. Nilsson, *Animal Eyes* (Oxford University Press, New York, 2002)
105. J. Kim, Absorption-assisted mode transformation in butterfly compound eyes. Sci. Rep. **4**, 6291 (2014)
106. J.P. Miller, S. Krueger, J.J. Heys, T. Gedeon, Quantitative characterization of the filiform mechanosensory hair array on the cricket cercus. PLoS One **6**, e27873 (2011)
107. J. Kim, K.-H. Jeong, L.P. Lee, Artificial ommatidia by self-aligned microlenses and waveguides. Opt. Lett. **30**, 5–7 (2005)
108. K.-H. Jeong, J. Kim, L.P. Lee, Biologically inspired artificial compound eyes. Science **312**, 557–561 (2006)
109. T. Shimozawa, T. Kumagai, Y. Baba, Structural scaling and functional design of the cercal wind-receptor hairs of cricket. J. Comp. Physiol. A **183**, 171–186 (1998)
110. T. Kumagai, T. Shimozawa, Y. Baba, The shape of wind-receptor hairs of cricket and cockroach. J. Comp. Physiol. A **183**, 187–192 (1998)
111. J.J. Heys, P.K. Rajaraman, T. Gedeon, J.P. Miller, A model of filiform hair distribution on the cricket cercus. PLOS One **7**, e46588 (2012)
112. K. Joshi, A. Mian, J. Miller, Biomechanical analysis of a filiform mechanosensory hair socket of crickets. J. Biomech. Eng. **138**, 081006–081006 (2016)
113. S. Große, W. Schröder, C. Brücker, Nano-newton drag sensor based on flexible micro-pillars. Meas. Sci. Technol. **17**(10), 2689 (2006)
114. C. Brücker, D. Bauer, H. Chaves, Dynamic response of micro-pillar sensors measuring fluctuating wall-shear-stress. Exp. Fluids **42**, 737–749 (2007)
115. C. Brücker, J. Spatz, W. Schröder, Feasability study of wall shear stress imaging using microstructured surfaces with flexible micropillars. Exp. Fluids **39**, 464–474 (2005)
116. B.T. Dickinson, Hair receptor sensitivity to changes in laminar boundary layer shape. Bioinspir. Biomim. **5**, 16002 (2010)
117. J. Tao, X.B. Yu, Hair flow sensors: from bio-inspiration to bio-mimicking—a review. Smart Mater. Struct. **21**(11), 113001 (2012)
118. S.N. Gorb, Insect-inspired technologies: insects as a source for biomimetics, in *Insect Biotechnology*, vol. 2, ed. by A. Vilcinskas. Biologically-Inspired Systems (Springer, Dordrecht, Netherlands, 2011), pp. 241–264. doi:10.1007/978-90-481-9641-8_13
119. C. Menon, C. Lira, Active articulation for future space applications inspired by the hydraulic system of spiders. Bioinspir. Biomim. **1**, 52–61 (2006)
120. D.A. Parry, R.H.J. Brown, The jumping mechanism of salticid spiders. J. Exp. Biol. **36**, 654–664 (1959)
121. H. Lin, G. Leisk, B. Trimmer, Soft robots in space: a perspective for soft robotics. Acta Futura **6**, 69–79 (2013)
122. H.-T. Lin, G.G. Leisk, B. Trimmer, GoQBot: a caterpillar-inspired soft-bodied rolling robot. Bioinspir. Biomim. **6**(2), 026007 (2011)
123. Z. Suo, Mechanics of stretchable electronics and soft machines. MRS Bull. **37**, 218–225 (2012)
124. R. Kempaiah, Z. Nie, From nature to synthetic systems: shape transformation in soft materials. J. Mater. Chem. B **2**, 2357–2368 (2014)
125. D.P. Holmes, A.J. Crosby, Snapping surfaces. Adv. Mater. **19**, 3589–3593 (2007)
126. J. Zhu, T. Li, S. Cai, Z. Suo, Snap-through expansion of a gas bubble in an elastomer. J. Adhes. **87**, 466–481 (2011)
127. C. Keplinger, T. Li, R. Baumgartner, Z. Suo, S. Bauer, Harnessing snap-through instability in soft dielectrics to achieve giant voltage-triggered deformation. Soft Matter **8**(2), 285–288 (2012)
128. R.V. Martinez, J.L. Branch, C.R. Fish, L. Jin, R.F. Shepherd, R.M.D. Nunes, Z. Suo, G.M. Whitesides, Robotic tentacles with three-dimensional mobility based on flexible elastomers. Adv. Mater. **25**, 205–212 (2013)
129. B. Mosadegh, P. Polygerinos, C. Keplinger, S. Wennstedt, R.F. Shepherd, U. Gupta, J. Shim, K. Bertoldi, C.J. Walsh, G.M. Whitesides, Pneumatic networks for soft robotics that actuate rapidly. Adv. Funct. Mater. **24**, 2163–2170 (2014)

130. K. Suzumori, S. Endo, T. Kanda, N. Kato, H. Suzuki, A bending pneumatic rubber actuator realizing soft-bodied manta swimming robot, in *Proceedings 2007 IEEE International Conference on Robotics and Automation* (IEEE, 2007), pp. 4975–4980
131. B. Gorissen, W. Vincentie, F. Al-Bender, D. Reynaerts, M. De Volder, Modeling and bonding-free fabrication of flexible fluidic microactuators with a bending motion. J. Micromech. Microeng. **23**, 045012 (2013)
132. M.B. Trimmer, P.R.H. Ewoldt, M. Kovac, H. Lipson, N. Lu, M. Shahinpoor, C. Majidi, At the crossroads: interdisciplinary paths to soft robots. Soft Rob. **1**, 63–69 (2013)
133. C. Laschi, M. Cianchetti, Soft robotics: new perspectives for robot bodyware and control. Front. Bioeng. Biotechnol. **2** (2014)
134. S. Fusco, M.S. Sakar, S. Kennedy, C. Peters, R. Bottani, F. Starsich, A. Mao, G.A. Sotiriou, S. Pané, S.E. Pratsinis, D. Mooney, B.J. Nelson, An integrated microrobotic platform for on-demand, targeted therapeutic interventions. Adv. Mater. **26**, 952–957 (2014)
135. A. De Greef, P. Lambert, A. Delchambre, Towards flexible medical instruments: review of flexible fluidic actuators. Precis. Eng. **33**, 311–321 (2009)
136. M. Calisti, M. Giorelli, G. Levy, B. Mazzolai, B. Hochner, C. Laschi, P. Dario, An octopus-bioinspired solution to movement and manipulation for soft robots. Bioinspir. Biomim. **6**, 036002 (2011)
137. M. Calisti, M. Giorelli, C. Laschi, A locomotion strategy for an octopus-bioinspired robot, in *Biomimetic and Biohybrid Systems*, vol. 7375, ed. by T.J. Prescott, N.F. Lepora, A. Mura, P.F.M.J. Verschure. Lecture Notes in Computer Science (Springer, Berlin/Heidelberg, 2012), pp. 337–338. doi:10.1007/978-3-642-31525-1_31
138. M. Cianchetti, M. Calisti, L. Margheri, M. Kuba, C. Laschi, Bioinspired locomotion and grasping in water: the soft eight-arm OCTOPUS robot. Bioinspir. Biomim. **10**(3), 035003 (2015)
139. M.T. Tolley, R.F. Shepherd, B. Mosadegh, K.C. Galloway, M. Wehner, M. Karpelson, R.J. Wood, G.M. Whitesides, A resilient, untethered soft robot. Soft Rob. **1**, 213–223 (2014)
140. S. Wakimoto, K. Suzumori, K. Ogura, Miniature pneumatic curling rubber actuator generating bidirectional motion with one air-supply tube. Adv. Rob. **25**, 1311–1330 (2011)
141. B. Gorissen, T. Chishiro, S. Shimomura, D. Reynaerts, M. De Volder, S. Konishi, Flexible pneumatic twisting actuators and their application to tilting micromirrors. Sensors Actuators A Phys. **216**, 426–431 (2014)
142. S. Grilli, S. Coppola, V. Vespini, F. Merola, A. Finizio, P. Ferraro, 3d lithography by rapid curing of the liquid instabilities at nanoscale. Proc. Natl. Acad. Sci. **108**, 15106–15111 (2011)
143. Y. Shapiro, A. Wolf, K. Gabor, Bi-bellows: pneumatic bending actuator. Sensors and Actuators A Phys. **167**, 484–494 (2011)
144. L. Yao, R. Niiyama, J. Ou, S. Follmer, C. Della Silva, H. Ishii, PneUI: pneumatically actuated soft composite materials for shape changing interfaces, in *Proceedings of the 26th Annual ACM Symposium on User Interface Software and Technology (UIST)* (ACM, New York, 2013), pp. 13–22
145. E.P. Popov, *Introduction to Mechanics of Solids*, 1st edn. (Prentice-Hall, Englewood Cliffs, 1968)
146. M.D. Volder, D. Reynaerts, Pneumatic and hydraulic microactuators: a review. J. Micromech. Microeng. **20**(4), 043001 (2010)
147. S. Li, T.M. Dellinger, Q. Wang, S. Szegedi, C. Liu, Pneumatically actuated elastomeric device for nanoscale surface patterning. Appl. Phys. Lett. **91**, 023109 (2007)
148. S.Z. Hua, F. Sachs, D.X. Yang, H.D. Chopra, Microfluidic actuation using electrochemically generated bubbles. Anal. Chem. **74**, 6392–6396 (2002)
149. C. Lui, S. Stelick, N. Cady, C. Batt, Low-power microfluidic electro-hydraulic pump (EHP). Lab Chip **10**, 74–79 (2010)
150. S. Peng, M. Zhang, X. Niu, W. Wen, P. Sheng, Z. Liu, J. Shi, Magnetically responsive elastic microspheres. Appl. Phys. Lett. **92**, 012108 (2008)
151. R.J. Dijkink, J.P. van der. Dennen, C.D. Ohl, A. Prosperetti, The 'acoustic scallop': a bubble-powered actuator. J. Micromech. Microeng. **16**(8), 1653 (2006)

152. L. Zheng, S. Yoshida, Y. Morimoto, H. Onoe, S. Takeuchi, Pneumatic balloon actuator with tunable bending points, in *2015 28th IEEE International Conference on Micro Electro Mechanical Systems (MEMS)* (2015), pp. 18–21
153. S. Bergbreiter, D. Mahajan, K.S.J. Pister, A reusable micromechanical energy storage/quick release system with assembled elastomers. J. Micromech. Microeng. **19**(5), 055009 (2009)
154. A.P. Gerratt, I. Penskiy, S. Bergbreiter, High power micromechanical thrusters with embedded elastomer. in *2009 PowerMEMS Conference* (2009), O6B-1
155. A.P. Gerratt, M. Tellers, S. Bergbreiter, Soft polymer MEMS, in *2011 IEEE 24th International Conference on Micro Electro Mechanical Systems (MEMS)* (2011), pp. 332–335
156. L. Ionov, Biomimetic hydrogel-based actuating systems. Adv. Funct. Mater. **23**, 4555–4570 (2013)
157. Q. Yu, J.M. Bauer, J.S. Moore, D.J. Beebe, Responsive biomimetic hydrogel valve for microfluidics. Appl. Phys. Lett. **78**, 2589–2591 (2001)
158. G.H. Kwon, J.Y. Park, J.Y. Kim, M.L. Frisk, D.J. Beebe, S.-H. Lee, Biomimetic soft multifunctional miniature aquabots. Small **4**, 2148–2153 (2008)
159. J.-C. Kuo, H.-W. Huang, S.-W. Tung, Y.-J. Yang, A hydrogel-based intravascular microgripper manipulated using magnetic fields. Sensors Actuators A Phys. **211**, 121–130 (2014)
160. C. Keplinger, J.-Y. Sun, C.C. Foo, P. Rothemund, G.M. Whitesides, Z. Suo, Stretchable, transparent, ionic conductors. Science **341**, 984–987 (2013)
161. E. Palleau, D. Morales, M.D. Dickey, O.D. Velev, Reversible patterning and actuation of hydrogels by electrically assisted ionoprinting. Nat. Commun. **4**, 2257 (2013)
162. K. Mukai, K. Asaka, T. Sugino, K. Kiyohara, I. Takeuchi, N. Terasawa, D.N. Futaba, K. Hata, T. Fukushima, T. Aida, Highly conductive sheets from millimeter-long single-walled carbon nanotubes and ionic liquids: application to fast-moving, low-voltage electromechanical actuators operable in air. Adv. Mater. **21**, 1582–1585 (2009)
163. T. Fukushima, K. Asaka, A. Kosaka, T. Aida, Fully plastic actuator through layer-by-layer casting with ionic-liquid-based bucky gel. Angew. Chem. **117**, 2462–2465 (2005)
164. W. Lu, A.G. Fadeev, B. Qi, E. Smela, B.R. Mattes, J. Ding, G.M. Spinks, J. Mazurkiewicz, D. Zhou, G.G. Wallace, D.R. MacFarlane, S.A. Forsyth, M. Forsyth, Use of ionic liquids for pi-conjugated polymer electrochemical devices. Science **297**, 983–987 (2002)
165. R. Montazami, S. Liu, Y. Liu, D. Wang, Q. Zhang, J.R. Heflin, Thickness dependence of curvature, strain, and response time in ionic electroactive polymer actuators fabricated via layer-by-layer assembly. J. Appl. Phys. **109**, 104301 (2011)
166. G.K. Knopf, Y. Otani, *Optical Nano and Micro Actuator Technology* (CRC, 2016). Google-Books-ID: ch_OBQAAQBAJ
167. Y. Takashima, S. Hatanaka, M. Otsubo, M. Nakahata, T. Kakuta, A. Hashidzume, H. Yamaguchi, A. Harada, Expansion–contraction of photoresponsive artificial muscle regulated by host–guest interactions. Nat. Commun. **3**, 1270 (2012)
168. T. Ikeda, M. Nakano, Y. Yu, O. Tsutsumi, A. Kanazawa, Anisotropic bending and unbending behavior of azobenzene liquid-crystalline gels by light exposure. Adv. Mater. **15**, 201–205 (2003)
169. H. Yu, T. Ikeda, Photocontrollable liquid-crystalline actuators. Adv. Mater. **23**, 2149–2180 (2011)
170. D. Iqbal, M.H. Samiullah, Photo-responsive shape-memory and shape-changing liquid-crystal polymer networks. Materials **6**, 116–142 (2013)
171. N. Torras, K.E. Zinoviev, C.J. Camargo, E.M. Campo, H. Campanella, J. Esteve, J.E. Marshall, E.M. Terentjev, M. Omastová, I. Krupa, P. Teplický, B. Mamojka, P. Bruns, B. Roeder, M. Vallribera, R. Malet, S. Zuffanelli, V. Soler, J. Roig, N. Walker, D. Wenn, F. Vossen, F.M.H. Crompvoets, Tactile device based on opto-mechanical actuation of liquid crystal elastomers. Sensors Actuators A Phys. **208**, 104–112 (2014)
172. Q. Zhao, J.W.C. Dunlop, X. Qiu, F. Huang, Z. Zhang, J. Heyda, J. Dzubiella, M. Antonietti, J. Yuan, An instant multi-responsive porous polymer actuator driven by solvent molecule sorption. Nat. Commun. **5**, 4293, (2014)

173. K.-U. Jeong, J.-H. Jang, C.Y. Koh, M.J. Graham, K.-Y. Jin, S.-J. Park, C. Nah, M.-H. Lee, S.Z.D. Cheng, E.L. Thomas, Colour-tunable spiral photonic actuators. J. Mater. Chem. **19**, 1956–1959 (2009)
174. V.M. Rao, G.K. Ananthasuresh, Haptic feedback for injecting biological cells using miniature compliant mechanisms, in *14th National Conference on Machines and Mechanisms (NaCoMM09)* (Durgapur, 2009), pp. 181–186
175. D.J. Cappelleri, G. Piazza, V. Kumar, Two-dimensional, vision-based uN force sensor for microrobotics, in *IEEE International Conference on Robotics and Automation (ICRA)* (2009), pp. 1016–1021
176. A. Bolopion, Z. Ni, J. Agnus, R. Benosman, S. Régnier, Stable haptic feedback based on a dynamic vision sensor for microrobotics, in *2012 IEEE/RSJ International Conference on Intelligent Robots and Systems* (2012), pp. 3203–3208
177. T. Kawahara, F. Arai, Force sensing by microrobot on a chip, in *Robotics Research*, vol. 100, ed. by H.I. Christensen, O. Khatib. Springer Tracts in Advanced Robotics (Springer International Publishing, New York, 2017), pp. 147–160. doi:10.1007/978-3-319-29363-9_9
178. H.-J. Kwon, J.-H. Kim, W.-C. Choi, Development of a flexible three-axial tactile sensor array for a robotic finger. Microsyst. Technol. **17**, 1721–1726 (2011)
179. S. Suzuki, Y. Saegusa, T. Takahashi, Development of a electric field distortion tactile sensor. ResearchGate **1**, 607–609 (2011)
180. S. Wattanasarn, K. Noda, K. Matsumoto, I. Shimoyama, 3d flexible tactile sensor using electromagnetic induction coils, in *2012 IEEE 25th International Conference on Micro Electro Mechanical Systems (MEMS)* (2012), pp. 488–491
181. J.A. Dobrzynska, M.A.M. Gijs, Flexible polyimide-based force sensor. Sensors Actuators A Phys. **173**, 127–135 (2012)
182. G. Schwartz, B.C.-K. Tee, J. Mei, A.L. Appleton, D.H. Kim, H. Wang, Z. Bao, Flexible polymer transistors with high pressure sensitivity for application in electronic skin and health monitoring. Nat. Commun. **4**, 1859 (2013)
183. J.T. Muth, D.M. Vogt, R.L. Truby, Y. Mengüç, D.B. Kolesky, R.J. Wood, J.A. Lewis, Embedded 3d printing of strain sensors within highly stretchable elastomers. Adv. Mater. **26**, 6307–6312 (2014)
184. F.M. Yaul, V. Bulovic, J.H. Lang, A flexible underwater pressure sensor array using a conductive elastomer strain gauge. J. Microelectromech. Syst. **21**, 897–907 (2012)
185. J. Kim, D.G. Seo, Y.-H. Cho, A flexible skin piloerection monitoring sensor. Appl. Phys. Lett. **104**, 253502 (2014)
186. W. Liu, F. Li, C. Stefanini, D. Chen, P. Dario, Biomimetic flexible/compliant sensors for a soft-body lamprey-like robot. Robot. Auton. Syst. **58**, 1138–1148 (2010)
187. S. Nam, S. Park, S. Yun, B.J. Park, S.K. Park, M. Choi, K.-U. Kyung, Highly flexible and transparent skin-like tactile sensor, in *Haptic Interaction*, vol. 277, ed. by H. Kajimoto, H. Ando, K.-U. Kyung. Lecture Notes in Electrical Engineering (Springer Japan, Tokyo, 2015), pp. 187–189. doi:10.1007/978-4-431-55690-9_36
188. D.P. Holmes, B. Tavakol, G. Froehlicher, H.A. Stone, Control and manipulation of microfluidic flow via elastic deformations. Soft Matter **9**, 7049–7053 (2013)
189. S. Yun, S. Park, B. Park, Y. Kim, S.K. Park, S. Nam, K.-U. Kyung, Polymer-waveguide-based flexible tactile sensor array for dynamic response. Adv. Mater. **26**, 4474–4480 (2014)
190. H. Rafii-Tari, C.J. Payne, G.-Z. Yang, Current and emerging robot-assisted endovascular catheterization technologies: a review. Ann. Biomed. Eng. **42**, 697–715 (2014)
191. K. Ikuta, H. Ichikawa, K. Suzuki, T. Yamamoto, Safety active catheter with multi-segments driven by innovative hydro-pressure micro actuators, in *IEEE The Sixteenth Annual International Conference on Micro Electro Mechanical Systems (MEMS)* (Kyoto, 2003), pp. 130–135
192. H. Okayasu, J. Okamoto, M.G. Fujie, M. Umezu, H. Iseki, Development of a hydraulic-driven flexible manipulator for neurosurgery. Int. Congr. Ser. **1256**, 607–612 (2003)
193. M. Ikeuchi, K. Ikuta, Membrane micro emboss following excimer laser ablation (MeME-X) process for pressure-driven micro active catheter, in *IEEE 21st International Conference on Micro Electro Mechanical Systems (MEMS)* (2008), pp. 62–65

194. P.E. Dupont, J. Lock, B. Itkowitz, E. Butler, Design and control of concentric-tube robots. Trans. Rob. **26**, 209–225 (2010)
195. S. Konishi, M. Nokata, O.C. Jeong, S. Kusuda, T. Sakakibara, M. Kuwayama, H. Tsutsumi, Pneumatic micro hand and miniaturized parallel link robot for micro manipulation robot system, in *Proceedings 2006 IEEE International Conference on Robotics and Automation (ICRA)* (2006), pp. 1036–1041
196. J.H. Low, M.H. Ang, C.H. Yeow, Customizable soft pneumatic finger actuators for hand orthotic and prosthetic applications, in *2015 IEEE International Conference on Rehabilitation Robotics (ICORR)* (2015), pp. 380–385
197. N. Piacentini, A.B. Verkhovsky, C. Gabella, J.-J. Meister, B. Vianay, Ultra-soft cantilevers and 3-D micro-patterned substrates for contractile bundle tension measurement in living cells. Lab Chip **14**, 2539–2547 (2014)
198. D. Desmaële, M. Boukallel, S. Régnier, Actuation means for the mechanical stimulation of living cells via microelectromechanical systems: a critical review, J. Biomech. **44**, 1433–1446 (2011)
199. D. Desmaële, M. Boukallel, S. Régnier, Micro systems for the mechanical characterization of isolated biological cells: state-of-the-art, in *Wearable and Autonomous Biomedical Devices and Systems for Smart Environment*, vol. 75, ed. by A. Lay-Ekuakille S.C. Mukhopadhyay. Lecture Notes in Electrical Engineering (Springer, Berlin/Heidelberg, 2010), pp. 155–175. doi:10.1007/978-3-642-15687-8_8
200. T. Kawahara, M. Hagiwara, Y. Yamanishi, F. Arai, Control and sensing platform of magnetically driven microtool for on-chip single cell evaluation, in *2010 International Symposium on Micro-NanoMechatronics and Human Science (MHS)* (2010), pp. 322–327
201. W. Zheng, B. Jiang, D. Wang, W. Zhang, Z. Wang, X. Jiang, A microfluidic flow-stretch chip for investigating blood vessel biomechanics. Lab Chip **12**, 3441–3450 (2012)
202. W. Meyer, S. Engelhardt, E. Novosel, B. Elling, M. Wegener, H. Krüger, Soft polymers for building up small and smallest blood supplying systems by stereolithography. J. Funct. Biomate. **3**, 257–268 (2012)
203. J.P. Beech, J.O. Tegenfeldt, Tuneable separation in elastomeric microfluidics devices. Lab Chip **8**, 657–659 (2008)
204. W. Li, T. Chen, Z. Chen, P. Fei, Z. Yu, Y. Pang, Y. Huang, Squeeze-chip: a finger-controlled microfluidic flow network device and its application to biochemical assays. Lab Chip **12**, 1587–1590 (2012)
205. M. Hitzbleck, L. Avrain, V. Smekens, R.D. Lovchik, P. Mertens, E. Delamarche, Capillary soft valves for microfluidics. Lab Chip **12**, 1972–1978 (2012)
206. K. Iwai, K.C. Shih, X. Lin, T.A. Brubaker, R.D. Sochol, L. Lin, Finger-powered microfluidic systems using multilayer soft lithography and injection molding processes. Lab Chip **14**, 3790–3799 (2014)
207. A. Chen, T. Pan, Manually operatable on-chip bistable pneumatic microstructures for microfluidic manipulations. Lab Chip **14**, 3401–3408 (2014)
208. J. Maher, R.L. Schank, G. Pfister, Elastomeric optical waveguide modulators. Appl. Phys. Lett. **29**, 293–295 (1976)
209. D. Ge, E. Lee, L. Yang, Y. Cho, M. Li, D.S. Gianola, S. Yang, A robust smart window: reversibly switching from high transparency to angle-independent structural color display. Adv. Mater. Weinheim **27**, 2489–2495 (2015)
210. B. Mosadegh, C.-H. Kuo, Y.-C. Tung, Y.-S. Torisawa, T. Bersano-Begey, H. Tavana, S. Takayama, Integrated elastomeric components for autonomous regulation of sequential and oscillatory flow switching in microfluidic devices. Nat. Phys. **6**, 433–437 (2010)
211. R. Phillips, R. Shah, Y. Browning, P. Yager, B. Lutz, Resonant fluidic circuits for sound-controlled point-ofcare diagnostics, in *15th International Conference on Miniaturized Systems for Chemistry and Life Sciences 2011 (MicroTAS 2011)* (Seattle, 2011), pp. 1203–1205
212. T. Nguyen, S. Ahrar, P. Duncan, E. Hui, Microfluidic finite state machine for autonomous control of integrated fluid networks, in Proc. Micro Total Anal. Syst. 741–743 (2011)

213. S.-J. Kim, R. Yokokawa, S. Takayama, Analyzing threshold pressure limitations in microfluidic transistors for self-regulated microfluidic circuits. Appl. Phys. Lett. **101** (2012)
214. R.R. Collino, N. Reilly-Shapiro, B. Foresman, K. Xu, M. Utz, J.P. Landers, M.R. Begley, Flow switching in microfluidic networks using passive features and frequency tuning. Lab Chip **13**, 3668–3674 (2013)
215. T. Gervais, J. El-Ali, A. Günther, K.F. Jensen, Flow-induced deformation of shallow microfluidic channels. Lab Chip **6**, 500–507 (2006)
216. E. Seker, D.C. Leslie, H. Haj-Hariri, J.P. Landers, M. Utz, M.R. Begley, Nonlinear pressure-flow relationships for passive microfluidic valves. Lab Chip **9**, 2691–2697 (2009)
217. B.K. Wunderlich, U.A. Klessinger, A.R. Bausch, Diffusive spreading of time-dependent pressures in elastic microfluidic devices. Lab Chip **10**, 1025–1029 (2010)
218. E.J. Tremblay, D. Loterie, C. Moser, Thermal phase change actuator for self-tracking solar concentration. Opt. Express **20**, A964–976 (2012)
219. V. Zagolla, E. Tremblay, C. Moser, Light induced fluidic waveguide coupling. Opt. Express **20**, A924–931 (2012)
220. V. Zagolla, E. Tremblay, C. Moser, Proof of principle demonstration of a self-tracking concentrator. Opt. Express **22**, Suppl 2, A498–510 (2014)
221. R. Dhakal, J. Kim, Elastomer-based opto-thermo-mechanical actuation for autonomous, self-powered light level control. Appl. Opt. **53**, 5712–5719 (2014)
222. M. Wehner, R.L. Truby, D.J. Fitzgerald, B. Mosadegh, G.M. Whitesides, J.A. Lewis, R.J. Wood, An integrated design and fabrication strategy for entirely soft, autonomous robots. Nature **536**, 451–455 (2016)
223. M. Wehner, M.T. Tolley, Y. Mengüç, Y.-L. Park, A. Mozeika, Y. Ding, C. Onal, R.F. Shepherd, G.M. Whitesides, R.J. Wood, Pneumatic energy sources for autonomous and wearable soft robotics. Soft Rob. **1**, 263–274 (2014)
224. A.D. Marchese, C.D. Onal, D. Rus, Autonomous soft robotic fish capable of escape maneuvers using fluidic elastomer actuators. Soft Rob. **1**, 75–87 (2014)
225. R.K. Katzschmann, A.D. Marchese, D. Rus, Hydraulic autonomous soft robotic fish for 3d swimming, in *Experimental Robotics*, vol. 109, ed. by M.A. Hsieh, O. Khatib, V. Kumar. Springer Tracts in Advanced Robotics (Springer International Publishing, New York, 2016), pp. 405–420. doi:10.1007/978-3-319-23778-7_27
226. S. Bergbreiter, K.S. Pister, Design of an autonomous jumping microrobot, in *Proceedings 2007 IEEE International Conference on Robotics and Automation* (IEEE, 2007), pp. 447–453
227. W.A. Churaman, L.J. Currano, C.J. Morris, J.E. Rajkowski, S. Bergbreiter, The first launch of an autonomous thrust-driven microrobot using nanoporous energetic silicon. J. Microelectromech. Syst. **21**(1), 198–205 (2012)
228. U.K. Müller, S. Kranenbarg, Power at the tip of the tongue. Science **304**, 217–219 (2004)
229. J.H. de Groot, J.L. van Leeuwen, Evidence for an elastic projection mechanism in the chameleon tongue. Proc. Biol. Sci. **271**, 761–770 (2004)
230. F. Brau, D. Lanterbecq, L.-N. Zghikh, V. Bels, P. Damman, Dynamics of prey prehension by chameleons through viscous adhesion. Nat. Phys. **12**, 931–935 (2016)
231. Y. Forterre, J.M. Skotheim, J. Dumais, L. Mahadevan, How the Venus flytrap snaps. Nature **433**, 421–425 (2005)
232. J. Zhu, H. Stoyanov, G. Kofod, Z. Suo, Large deformation and electromechanical instability of a dielectric elastomer tube actuator. J. Appl. Phys. **108**(7), 074113 (2010)
233. T. Li, C. Keplinger, R. Baumgartner, S. Bauer, W. Yang, Z. Suo, Giant voltage-induced deformation in dielectric elastomers near the verge of snap-through instability. J. Mech. Phys. Solids **61**, 611–628 (2013)
234. B. Tavakol, M. Bozlar, C. Punckt, G. Froehlicher, H.A. Stone, I.A. Aksay, D.P. Holmes, Buckling of dielectric elastomeric plates for soft, electrically active microfluidic pumps. Soft Matter **10**(27), 4789–4794 (2014)
235. N. Hu, R. Burgueño, Buckling-induced smart applications: recent advances and trends. Smart Mater. Struct. **24**, 063001 (2015)

236. B.R. Bruhn, T.B.H. Schroeder, S. Li, Y.N. Billeh, K.W. Wang, M. Mayer, Osmosis-based pressure generation: dynamics and application. PLoS One **9**, e91350 (2014)
237. R.T. Borno, J.D. Steinmeyer, M.M. Maharbiz, Transpiration actuation: the design, fabrication and characterization of biomimetic microactuators driven by the surface tension of water. J. Micromech. Microeng. **16**(11), 2375 (2006)
238. B. Bondada, C. Tu, L. Ma, Surface structure and anatomical aspects of Chinese brake fern (Pteris vittata; Pteridaceae). Brittonia **58**(3), 217–228 (2006)
239. B.J. Williams, S.V. Anand, J. Rajagopalan, M.T.A. Saif, A self-propelled biohybrid swimmer at low Reynolds number. Nat. Commun. **5**, 3081 (2014)
240. J. Rajagopalan, M.T.A. Saif, Fabrication of freestanding 1-D PDMS microstructures using capillary micromolding. J. Microelectromech. Syst. **22**, 992–994 (2013)
241. X.-M. Li, D. Reinhoudt, M. Crego-Calama, What do we need for a superhydrophobic surface? A review on the recent progress in the preparation of superhydrophobic surfaces. Chem. Soc. Rev. **36**, 1350–1368 (2007)
242. S. Wang, K. Liu, X. Yao, L. Jiang, Bioinspired surfaces with superwettability: new insight on theory, design, and applications. Chem. Rev. **115**, 8230–8293 (2015)
243. R. Helbig, J. Nickerl, C. Neinhuis, C. Werner, Smart skin patterns protect springtails. PLoS One **6**, e25105 (2011)
244. R. Hensel, R. Helbig, S. Aland, H.-G. Braun, A. Voigt, C. Neinhuis, C. Werner, Wetting resistance at its topographical limit: the benefit of mushroom and serif T structures. Langmuir **29**, 1100–1112 (2013)
245. R. Hensel, A. Finn, R. Helbig, H.-G. Braun, C. Neinhuis, W.-J. Fischer, C. Werner, Biologically inspired omniphobic surfaces by reverse imprint lithography. Adv. Mater. **26**, 2029–2033 (2014)
246. R.T. Borno, J.D. Steinmeyer, M.M. Maharbiz, Charge-pumping in a synthetic leaf for harvesting energy from evaporation-driven flows. Appl. Phys. Lett. **95**, 013705 (2009)
247. S.D. Moss, O.R. Payne, G.A. Hart, C. Ung, Scaling and power density metrics of electromagnetic vibration energy harvesting devices. Smart Mater. Struct. **24**(2), 023001 (2015)
248. X. Tian, Y. Chen, Y. Zheng, H. Bai, L. Jiang, Controlling water capture of bioinspired fibers with hump structures. Adv. Mater. **23**, 5486–5491 (2011)
249. E. Palleau, S. Reece, S.C. Desai, M.E. Smith, M.D. Dickey, Self-healing stretchable wires for reconfigurable circuit wiring and 3d microfluidics. Adv. Mater. Weinheim **25**, 1589–1592 (2013)
250. K.S. Toohey, N.R. Sottos, J.A. Lewis, J.S. Moore, S.R. White, Self-healing materials with microvascular networks. Nat. Mater. **6**, 581–585 (2007)
251. C. Py, P. Reverdy, L. Doppler, J. Bico, B. Roman, C. Baroud, Capillary origami. Phys. Fluids (1994-present) **19**, 091104 (2007)
252. S.-H. Cho, W.-S. Chang, K.-R. Kim, J.W. Hong, Femtosecond laser embedded grating micromachining of flexible PDMS plates. Opt. Commun. **282**, 1317–1321 (2009)
253. A. Ryabchun, M. Wegener, Y. Gritsai, O. Sakhno, Novel effective approach for the fabrication of PDMS-based elastic volume gratings. Adv. Opt. Mater. **4**, 169–176 (2016)
254. A. Homsy, E. Laux, L. Jeandupeux, J. Charmet, R. Bitterli, C. Botta, Y. Rebetez, O. Banakh, H. Keppner, Solid on liquid deposition, a review of technological solutions. Microelectron. Eng. **141**, 267–279 (2015)
255. Y. Yoshihata, A. Takei, N. Binh-Khiem, T. Kan, E. Iwase, K. Matsumoto, I. Shimoyama, Micro liquid prism, in *IEEE 22nd International Conference on Micro Electro Mechanical Systems (MEMS)* (2009), pp. 967–970
256. Z.L. Wu, M. Moshe, J. Greener, H. Therien-Aubin, Z. Nie, E. Sharon, E. Kumacheva, Three-dimensional shape transformations of hydrogel sheets induced by small-scale modulation of internal stresses. Nat. Commun. **4**, 1586 (2013)
257. M. Jamal, A.M. Zarafshar, D.H. Gracias, Differentially photo-crosslinked polymers enable self-assembling microfluidics. Nat. Commun. **2**, 527 (2011)
258. R.M. Erb, J.S. Sander, R. Grisch, A.R. Studart, Self-shaping composites with programmable bioinspired microstructures. Nat. Commun. **4**, 1712 (2013)

Index

J. (Jay) Kim, *Microscale Soft Robotics*, SpringerBriefs in Applied Sciences and Technology, DOI 10.1007/978-3-319-50286-1